2013

# The Use of Nitriding to Enhance Wear Resistance of Cast Irons and 4140 Steel

Zaidao Yang
*University of Windsor*

# The Use of Nitriding to Enhance Wear Resistance of Cast Irons and 4140 Steel

by

Zaidao Yang

A Thesis
Submitted to the Faculty of Graduate Studies
through Engineering Materials
in Partial Fulfillment of the Requirements for
the Degree of Master of Applied Science at the
University of Windsor

Windsor, Ontario, Canada

2012

The Use of Nitriding to Enhance Wear Resistance of Cast Irons and 4140 Steel

by

Zaidao Yang

APPROVED BY:

_____

Randy J. Bowers, Program Reader
Department of Mechanical, Automotive, and Materials Engineering

_____

Leo Oriet, Outside Program Reader
Industrial and Manufacturing Systems Engineering

_____

Xichen Sun, Industrial Advisor
Chrysler LLC Technology Center (CTC)

_____

Derek O. Northwood, Advisor
Department of Mechanical, Automotive, and Materials Engineering

_____

H. Hu, Chair of Defense
Department of Mechanical, Automotive, and Materials Engineering

November 05, 2012

## DECLARATION OF ORIGINALITY

I hereby certify that I am the sole author of this thesis and that no part of this thesis has been published or submitted for publication.

I certify that, to the best of my knowledge, my thesis does not infringe upon anyone's copyright nor violate any proprietary rights and that any ideas, techniques, quotations, or any other material from the work of other people included in my thesis, published or otherwise, are fully acknowledged in accordance with the standard referencing practices. Furthermore, to the extent that I have included copyrighted material that surpasses the bounds of fair dealing within the meaning of the Canada Copyright Act, I certify that I have obtained a written permission from the copyright owner(s) to include such material(s) in my thesis and have included copies of such copyright clearances to my appendix.

I declare that this is a true copy of my thesis, including any final revisions, as approved by my thesis committee and the Graduate Studies office, and that this thesis has not been submitted for a higher degree to any other University or Institution.

## ABSTRACT

This research is focused on using nitriding to enhance the wear resistance of austempered ductile iron (ADI), ductile iron (DI), and gray iron (GI), and 4140 steel. Three gas nitriding processes, namely "Gas nitriding + nitrogen cooled down to 800$^{o}$F (Blue)", "Gas nitriding + cooled down to 300$^{o}$F (Gray)", and "Gas nitriding + oil quenched (Oil)" were used for the cast irons. Three salt bath nitriding processes, namely Isonite, QP (Quench, Polish) and QPQ (Quench, Polish, Quench) were used for the 4140 steel.

This study was carried out through optical metallography, roughness measurements, microhardness, and SEM. The ball-on-disc wear tests were conducted under lubricated conditions. It was found that COF for all materials in all nitrided conditions was small ($<$0.045). The best wear performance was seen for ADI processed using the Gray and Oil gas nitriding processes. For the 4140 steel, The surface microhardness of the ISONITE specimen was around 1400HV. QP and QPQ processes produce a surface microhardness of 2000-2200HV, which suggests that they may show improved wear behaviour compared to ISONITE- treated steels.

# DEDICATION

This thesis is dedicated to Prof. Derek O Northwood and Dr. Xichen Sun. They are both my respected and beloved supervisors for my life and academic career.

ACKNOWLEDGEMENTS

Above all, I would like to present my heartfelt appreciation to my great supervisor Prof. Derek O. Northwood for funding my M.A.Sc degree, and remarkable work to help me to prepare the thesis. Also thanks are extended to Dr. Xichen Sun, my industrial advisor from Chrysler Technical Center who provided a number of supports on the experiments and on my life. He is a warm hearted and wonderful man.

I would also like to thank my committee members Dr. Derek O. Northwood, Dr. Randy J. Bowers, Dr. Leo Oriet and Dr. Xichen Sun, for their helpful discussion.

Furthermore, I would also like to thank Hao Ma, Xiangnan Zhao, and Yanda Zou for their much appreciated support in the laboratory. Thanks also to Jin Qian for microhardness testing, Ying Chen for roughness measurements, Sharon Lackie and Dr. Gang Li for SEM, and Andy Jenner and Steven Budinsky for cutting the samples.

Also thanks are extended to Rebecca Lumbreras from Oakland University for the wear testing.

In the end, to all of my dear colleagues and friends, I am glad to have come to Canada and spent this wonderful period of time with you.

## TABLE OF CONTENTS

LIST OF ABBREVIATIONS

| | |
|---|---|
| ADI | Austempered Ductile Iron |
| DI | Ductile Iron |
| GI | Gray Iron |
| BLUE | Gas nitride + nitrogen cooled down to 800$^{o}$F (blue color) |
| GRAY | Gas nitride + cooled down to 300$^{o}$F (gray color) |
| OIL | Gas nitride + oil quenched (gray color) |
| CL | Compound Layer |
| DZ | Diffusion Zone |
| WTW | Wear Track Width |
| WTD | Wear Track Depth |
| HV | Vickers Hardness |
| ASTM | American Society for Testing and Materials |
| ASM | American Society for Metals |
| AISI | American Iron and Steel Institute |
| OM | Optical Microscopy |
| MHV | Vickers Microhardness Measurements |
| SEM | Scanning Electron Microscopy |
| XRD | X-Ray Diffraction |
| EDS | Energy Dispersive X-ray Spectroscopy |

LIST OF TABLES

LIST OF FIGURES

# CHAPTER I

# INTRODUCTION

This research is focused on using nitriding to enhance the wear resistance of austempered ductile iron (ADI), ductile iron (DI), and gray iron (GI), and 4140 steel.

## 1.1 Motivation

Cast irons have played an important role in human history. They are one of the most widely used families of materials in the automotive industry. They are ferrous alloys with carbon contents higher than 2.1%, silicon and often other alloying elements. Generally, they are divided into the following basic types: White Iron, Gray Iron, Ductile Iron, and Malleable Iron.[1] They are widely used in the automotive industry for applications such as fly-wheels, cylinders, crankshafts, camshafts, gears, and rolls.[2-12]

4140 steel is a common steel that is also widely used in the automotive industry. It is a high tensile alloy steel, with around 0.4wt% C, 1wt %Cr, and 0.2wt%Mo. The normal heat treatment condition is hardened and tempered to an UTS range of 850-1000MPa. Pre-hardened and tempered 4140 can be further surface hardened by nitriding, and by flame or induction hardening. It is typically used for shafts, axles, ball studs and gears.[13]

Wear is one of the major forms of material deterioration. Wear types include: adhesive wear, abrasive wear, surface fatigue, fretting wear, erosive wear, and corrosive wear. Wear is defined as the erosion or sideways displacement of surface and near-surface material from its original position resulting from the contact with other solids, flowing liquids, flowing gas, or the mixture of them.

Nitriding is a low-temperature heat treating process that diffuses nitrogen into the surface of a metal to create a hardened surface. Compared to other case hardening

methods, it is relatively easy to control in terms of process parameters. Nitriding can improve wear resistance, corrosion resistance, fatigue resistance, surface compressive strength, friction properties, and aesthetic finish.

Because the surface properties of the cast irons and 4140 steel do not match the performance requirements of the automotive industry, research is required to improve the surface properties of these materials, especially the wear resistance. The research undertaken is a proof-of-concept study on the application of nitriding to cast irons and 4140 steel to improve wear resistance of automotive components. Three gas nitriding processes, namely "Gas nitriding + nitrogen cooled down to 800$^{o}$F (Blue)", "Gas nitriding + cooled down 300$^{o}$F (Gray)", and "Gas nitriding + oil quenched (Oil)" were used for the three types of cast iron (DI, ADI, GI); and three different salt bath nitriding processes, namely Isonite, QP and QPQ were used for the 4140 steel.

The overall concept of this study is shown in Figure 1.1, namely nitriding, wear testing, and possible application to automotive components such as ball studs and brake rotors. The ball stud is currently made from 4140 steel, while the brake rotor is made from gray iron.


Figure 1.1: Overall concept of study

## 1.2 Research scope

The scope of this research is to investigate the use of gas nitriding and salt bath nitriding techniques to improve the wear performance of cast irons and 4140 steel for potential automotive applications.

An overview of the research study is given in Figure 1.2. As with any research study, the first stage is a background (literature) review. This review examined cast irons, nitriding processes, microstructures developed, and wear. Three cast irons (DI, ADI, GI) and one steel (4140) were selected for the study. Three gas nitriding processes (Blue, Gray, Oil) were examined for the cast irons and three salt bath nitriding processes (Isonite, QP, QPQ) were used for the 4140 steel. All nitrided materials were examined using optical metallography, profilometry and microhardness to determine the nitrided case microstructure, surface roughness and through-thickness microhardness.

Wear testing was performed for all nitrided cast irons and the Isonite-treated 4140 steel. Tests were performed using a ball (ceramic)-on-disc apparatus under lubricated conditions. The coefficient of friction was continuously monitored during the wear test. The worn samples were examined by SEM and profilometry to determine wear track width and depth, and hence wear rate, as well as other features of the wear track, e.g., polishing and debris. The wear performance was related to the nitride layer parameters.

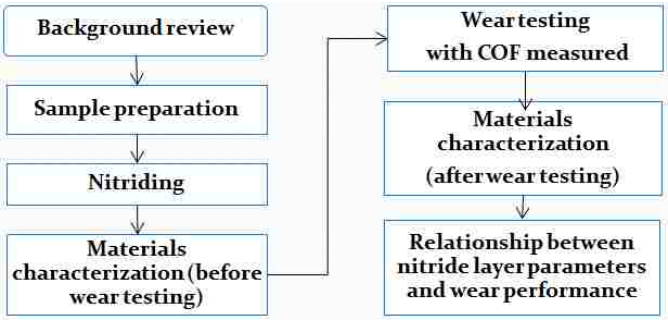


Figure 1.2: Research plan

# CHAPTER II

# REVIEW OF LITERATURE

Although this research is focussed on a specific topic, namely improving wear resistance of irons and steels through nitriding, a more general overview is given in this chapter. This overview is divided into four main sections, namely, (i) cast irons and 4140 steel, (ii) nitriding, (iii) tribology, and (iv) wear. For cast irons, their classification, chemical composition and mechanical properties are briefly explained. For nitriding, the gas nitriding, salt bath nitriding, plasma/ion nitriding and mechanisms of nitriding are discussed with some examples from our experiments. The section on tribology discusses the surface properties, friction, and lubricants. The section on wear discusses types of wear, detection and evaluation of wear, methods to improve wear resistance, and factors that affect wear behaviour such as microstructure and surface properties.

## 2.1 Cast Irons and 4140 steel

### 2.1.1 History and classification of cast irons

Cast irons are a large family of ferrous alloys with carbon contents higher than 2.1wt%, usually 3.0-4.5wt%, and silicon contents in the range 1 to 3wt%. The nature and extent of alloying and the control of heating and cooling processes can give rise to a wide range of physical and mechanical properties for the different grades of cast iron.[14] The matrix microstructure of cast irons in the as-cast condition consists of pearlite and ferrite. The graphite shape can be flake graphite, spheroidal graphite or compacted graphite. Most often, cast irons are used in the as-cast form to satisfy structural requirements.

Historically, cast irons dates back to 600 BC, where in China they were used for cooking utensils, plowshares and statuary. The earliest dated iron casting is a lion

produced in 502 BC.[10] Although they were introduced in Europe early in the 15th century AD, it was not until the 18th century that saw the mass production of cast irons and their subsequent use as important structural materials. In 1709, in England, Abraham Darby devised a method of smelting iron with coal by first coking the coal. The vastly greater amounts of cast irons that could be produced by using coke rather than charcoal eventually led to the famous Iron Bridge that spans the Severn River in England being erected in 1779. Since that time, the family of cast irons have continued to be one of the most widely used and versatile of engineering materials.[1]

The general classification of cast irons is shown in Figure 2.1[1] both by structure and by commercial name or application. The initially recognized types were White iron and Gray iron. They derived their names from the color of their respective fracture surfaces. "The carbon equivalent (CE) of cast irons also helps to distinguish the gray irons, which cool into a microstructure containing graphite, from the white irons where the carbon is present mainly as cementite."[14] Ductile iron derives its name from the fact that it exhibits good ductility in the as-cast form. By contrast, neither white nor gray iron exhibits significant ductility. Ductile iron is cast as white iron, then malleablized, i.e., heat treated to impart ductility.

With the advancements in metallography and knowledge of solidification, new classifications based on microstructural features were introduced. Thus, classification based on the shapes of matrix and graphite became one of the important methods. For instance, ferritic matrix, pearlitic matrix (DI, GI in this study), austenitic matrix, martensitic matrix and bainitic matrix(ADI in this study) were discovered, as well as flake graphite, nodular graphite, and compacted graphite.

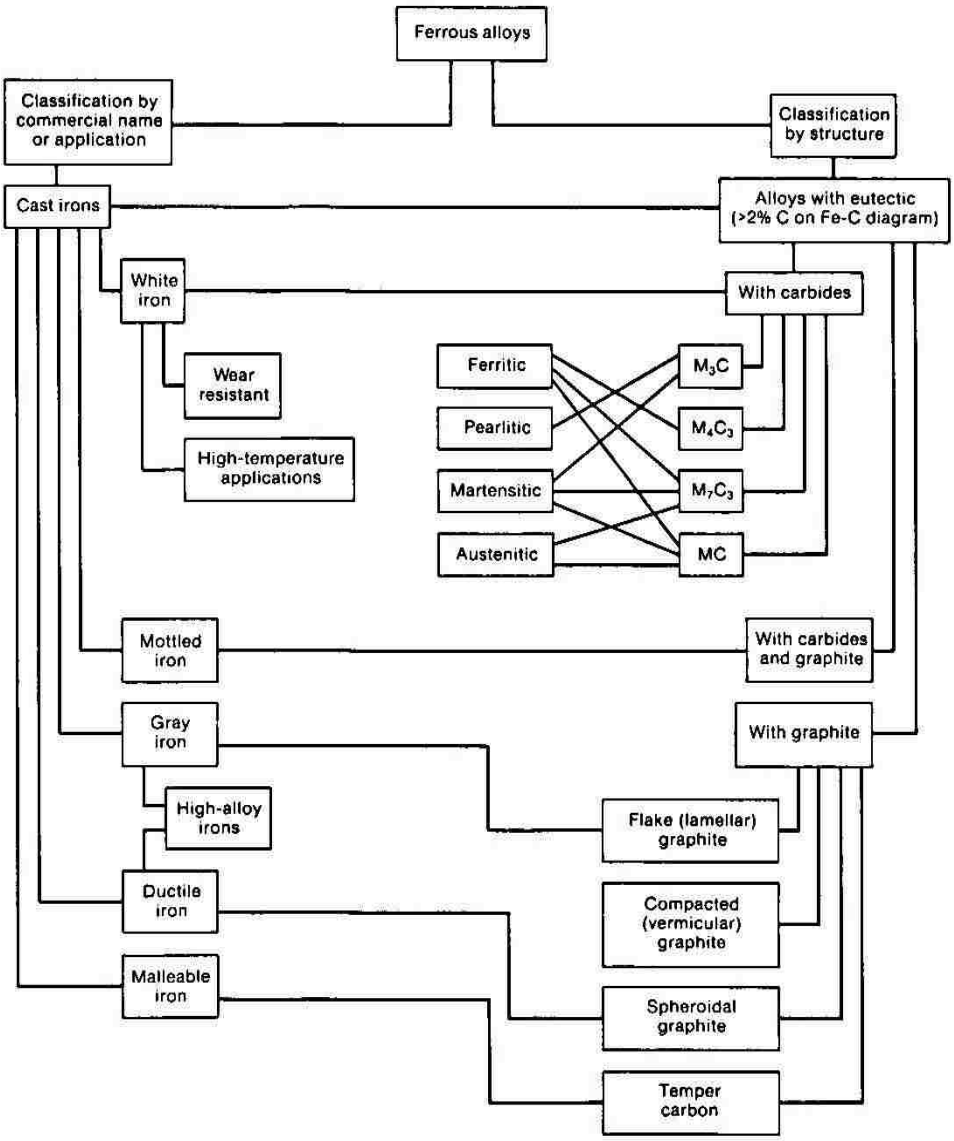


Figure 2.1 Classification of cast irons[1]

The metallurgy of cast irons is similar to that of steel when the amount of alloying elements is low. So, we can consider the cast irons as binary iron-carbon alloys, as shown in Figure 2.2.[1] We can see that the equilibrium structures are related to temperature and carbon contents. The solid curves represent the metastable system Fe-$Fe_3C$, while the dashed curves represent the stable system iron-graphite. However, if the silicon contents become appreciable, the cast irons should be considered as ternary Fe-C-Si alloys.

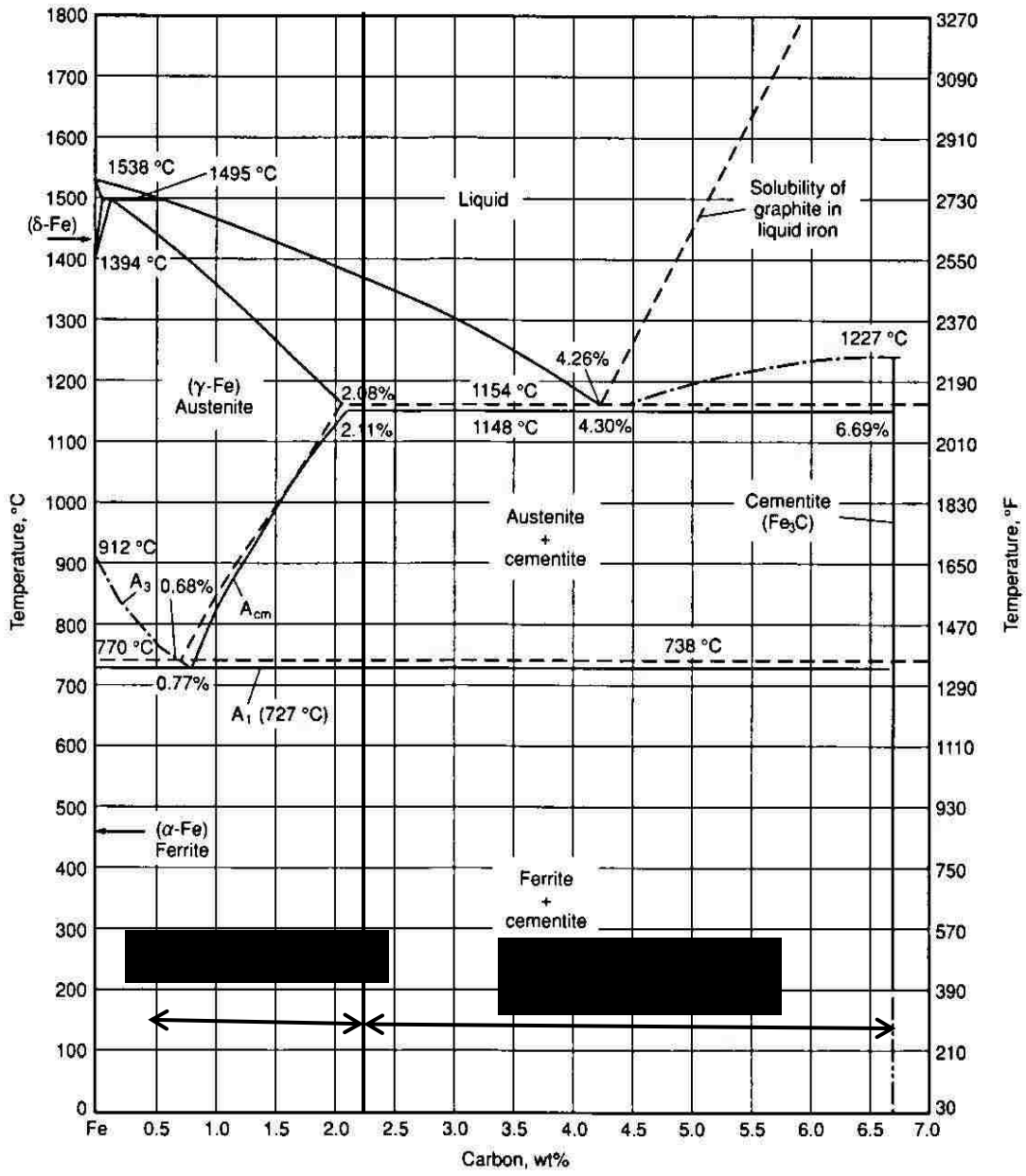


Figure 2.2: Iron-Carbon diagram [1]

Figure 2.3[1] shows the section through the Fe-Fe3C-Si ternary equilibrium diagram at 2% Si. Compared with Figure 2.2, the iron-carbon binary equilibrium diagram, we can see two new narrow zones around the γ-Fe zone. The addition of silicon decreases the stability of the metastable phase Fe3C, and increases the stability of ferrite. We can see that the α-Fe + Fe3C zone is enlarged while γ-Fe zone is constricted.

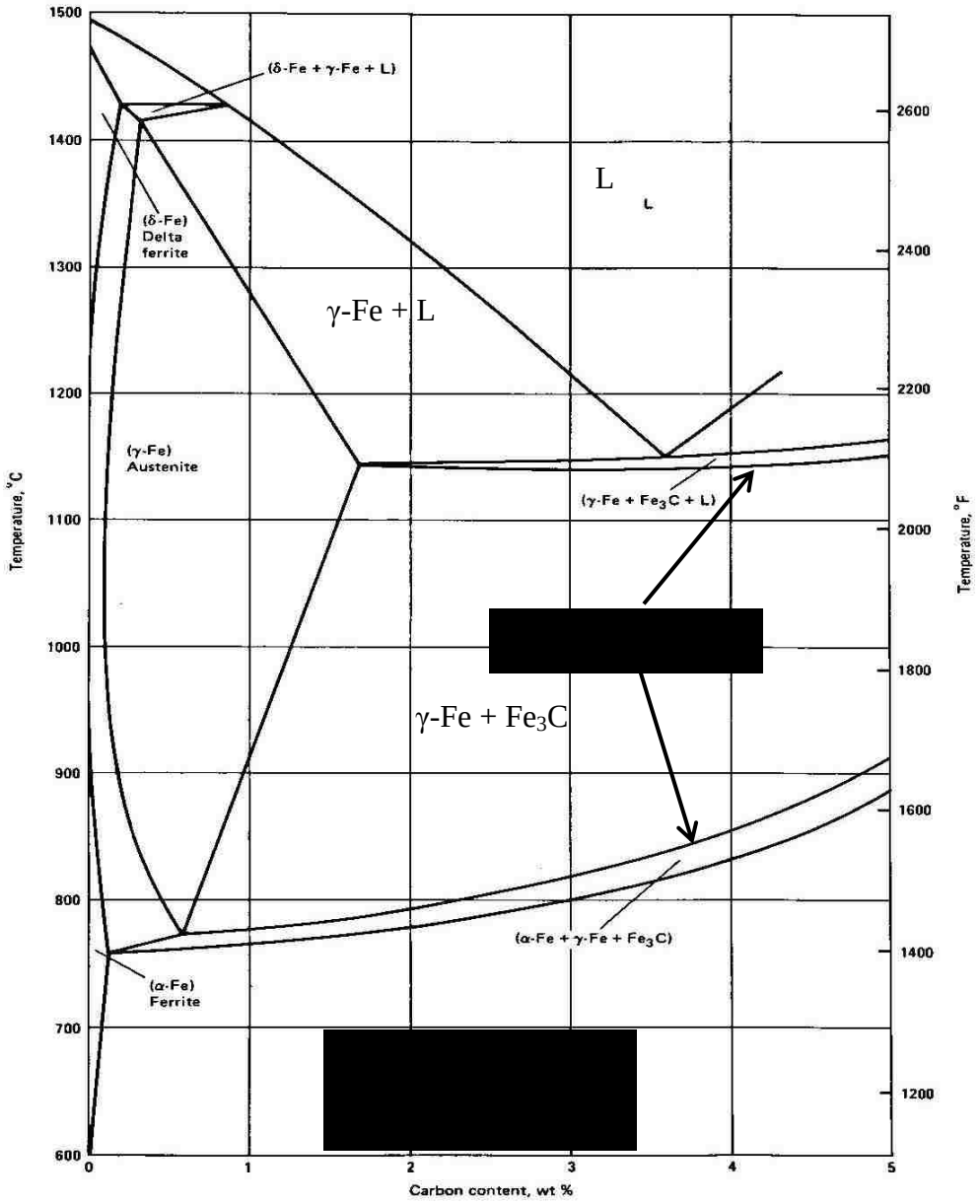


Figure 2.3: Section through the Fe-$Fe_3C$-Si ternary equilibrium diagram at 2wt% Si[1]

Figure 2.4[1] illustrates how carbon contents, basic microstructures and processing can be varied to obtain common commercial cast irons. Depending on the chemical composition and cooling rate, cast iron will solidify into gray iron, white iron, malleable iron and ductile iron.

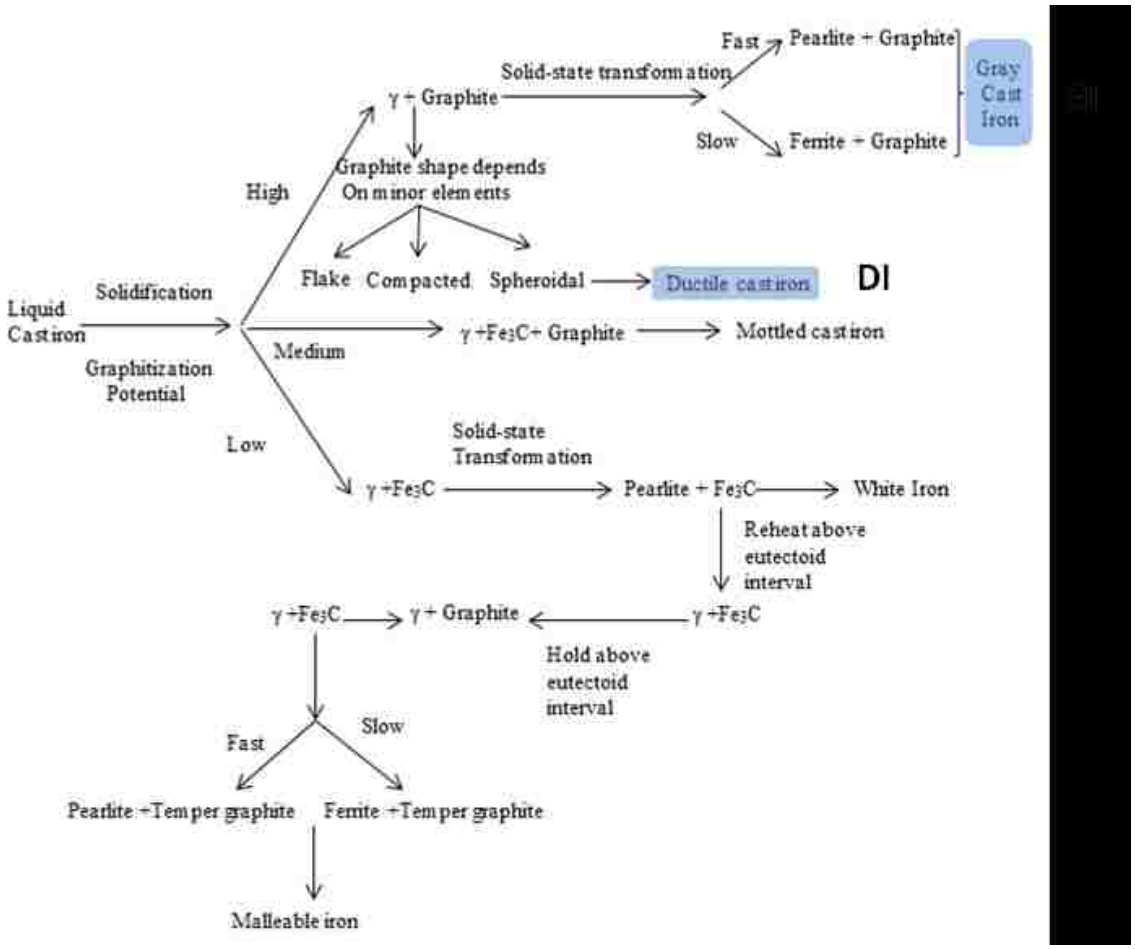


Figure 2.4: Basic microstructures and processing for obtaining common cast irons[1]

2.1.2 GI

Gray iron (GI), also called gray cast iron (GCI) is the most important casting material, comprising more than 70% of the world's total production tonnage. It has a low tensile strength, high compressive strength and poor ductility. It is widely used for many industrial applications such as machine bases, housings, fly-wheels, cylinder blocks, pipe and fittings, because of its good castability, low-cost (20%–40% less than steel), and attractive mechanical properties.[10-12]

GI is a very effective material for heavy mechanical vibration damping and can support high compressive loads. GI also exhibits high corrosion and wear resistance, so it

is also suitable for parts encountering sliding motion.[15] Moreover, graphite flakes increase the thermal conductivity.[16] However, graphite flake formation in the iron matrix can cause crack initiation on the sharp flake tip and the crack propagates along the flake edges. This makes GI very brittle. GI is usually considered to be a difficult material to be welded, because of its high carbon equivalent, inherent brittleness, and the effect of weld thermal cycle on the metallurgical structure.[17]

The carbon and silicon contents of GI are between 2.1~4.0wt% and 1.0~ 3.0wt%, respectively. The microstructure depends on both chemical composition and cooling conditions. Graphite in GI exists as flakes/lamellas dispersed into the surrounding ferrite or pearlite matrix. Foundry practice can also influence the nucleation and growth of graphite flakes. Thus, the amount of graphite and the size, shape and distribution of the graphite flakes are critical in determining the mechanical behavior of GI.[12]

Typical microstructures of GI are shown in Figures 2.5. Figure 2.5 (a), which is a sample before etching, illustrates the graphite size, shape and distribution. Figure 2.5 (b), which is an etched sample, shows the pearlite matrix and some ferrite areas.


(a) 50X, before etching (b) 500X, etched

Figure 2.5: GI optical micrographs

### 2.1.3 DI

Ductile Iron (DI) is also known as ductile cast iron (DCI), nodular cast iron, and spheroidal graphite iron. It derives its name from its good ductility in the as-cast condition. It is a family of materials with a wide range of properties, including austempered ductile iron (ADI). The common feature of DI is the spherical shape of the graphite. It is cast as white iron, and then heat-treated to improve ductility. Typical alloying elements in DI are: Carbon, Silicon, Magnesium, Manganese, Copper, Nickel and Molybdenum. Minor elements can significantly alter the graphite morphology and matrix structure. The addition of spheroidising elements, usually magnesium (Mg), results in castings that do not contain graphite flakes, but rather spheroids of graphite. A higher cooling rate requires a smaller amount of magnesium for spheroidization. The addition of sufficient nickel can help produce an austenitic matrix structure similar to that of austenitic stainless steel. Very small amounts of boron improve the hardenability of austempered ductile iron, but higher contents reduce the hardenability and toughness. [1, 18-20]

However, the use of highly reactive magnesium as a graphite nodulariser is a problem in the production of ductile iron and thus there is a need to find a safer and cheaper substitute. According to Imasogie[21] and Hernandez-Rivera[22], a calcium-magnesium (Ca-$CaC_2$-Mg) based master alloy nodulariser is effective in obtaining equivalent properties of the DI and ADI as the Mg-nodulariser, but in a safer manner.

Figure 2.6 is a schematic overview of the microstructures and ultimate tensile strengths for various types of ductile iron. [23]

| Matrix | | | | | | | |
|---|---|---|---|---|---|---|---|
| Ferritic Grade 5 | Ferritic-pearlitic Grade 3 | Pearlitic Grade 1 | Martensitic (With retained austenite) | Tempered Martensitic | ADI Grade 150 | ADI Grade 230 | Austenitic |
| 60,000 p.s.i. (414 mPa) | 80,000 p.s.i. (552 mPa) | 100,000 p.s.i. (690 mPa) | N.A.* | 115,000 p.s.i. (793 mPa) | 150,000 p.s.i. (1050 mPa) | 230,000 p.s.i. (1600 mPa) | 45,000 p.s.i. (310 mPa) |
| 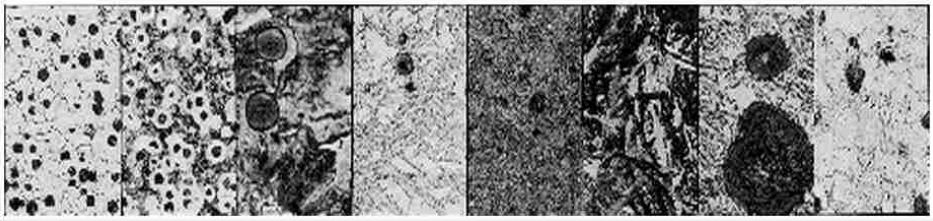 | | | | | | | |
| *Approximate ultimate tensile strength 87,000 p.s.i. (600 mPa) Hard, Brittle. (Note that the magnifications are different.) | | | | | | | |

Figure 2.6: Microstructures and ultimate tensile strengths for various types of DI[23]

The mechanical properties are determined by the size, shape and distribution of the graphite as well as the following matrix types: austenitic, ferritic, pearlitic, ferritic–pearlitic, martensitic or bainitic matrix. However, performance and reliability can be limited by various forms of wear under severe service conditions. One of the potential ways of improving wear resistance is by adding alloying elements but this invariably increases the cost.[24]

Ductile irons are widely used in manufacturing machine tool beds, cylinders, cams, and pistons. DI is regarded as a suitable replacement for steels because they have a relatively low cost, good machinability, a good combination of strength and toughness, a high fatigue resistance, good fluidity and cast-ability, and good wear resistance.[6-9]

Heat treatment often used in the processing of DI includes: stress relieving; annealing to produce a ferritic matrix; normalizing to produce a pearlitic matrix; hardening to produce tempered structures; and austempering to produce a ferritic bainite structure. It is through the austempering process that ADI can be obtained.

### 2.1.4 ADI

Austempered ductile iron (ADI) represents the top grade of the family of ductile irons. It is the result of an austempering treatment. Sometimes ADI is referred to as Bainitic Ductile Iron (BDI) because of its bainitic matrix. The bainite structure was discovered by Davenport and Bain in 1930. It exists in two forms, i.e. upper bainite and lower bainite. Upper bainite forms at higher temperature, while the lower bainite forms at a lower temperature which is still higher than the martensite start temperature. The bainitic ferrite in the retained austenite phase is called the ausferrite.[25-27] However, the bainite structure may also consist of martensite with retained austenite aggregates.[28]

The mechanical properties of ADI are determined by the following main factors: graphite morphology; bainite volume fraction; and volume fraction and distribution of martensite and carbide. ADI has excellent mechanical properties such as high strength, good wear resistance, excellent fatigue strength and good fracture toughness, attractive strength-weight ratio (10% lighter than steel) and high vibration absorption. Because of the attractive physical and mechanical properties, and significant savings in weight and cost compared with steel parts, ADI is currently being widely used in mining, automotive, agriculture and power plant applications such as crankshafts, camshafts, gears, and rolls.[2-5] The elevated toughness of the cast iron is a result of the bainitic matrix that includes austenite and ferrite formed in the process of bainitic hardening. The high content of carbon in the bainite matrix causes strain aging of the surface layers, which provides high wear resistance in the metal. Copper, molybdenum and nickel can promote formation of an austenite-ferrite matrix. For instance, a ductile cast iron containing (wt%) 3.2 C, 2.5 Si, 1.09 Ni, 0.87 Cu, 0.5 Mo and 0.16 Mn, when it is austenitized at 900 ℃ and austempered at 350 ℃ for 150 min, has the highest toughness.[29]

The heat treatment of ADI is composed of two steps, namely austenitizing and austempering. A schematic diagram of the heat treatment process for ADI is shown in Figure 2.7.[30] First, the DI is heated up to the austenitizing temperature (usually 800-950 ℃), where austenite is formed (γ-Fe). This temperature should be maintained for a period of time to dissolve the carbon from the graphite nodules into austenite. Then, the austenitized material is quenched and held at the austempering temperature (usually 250-400 ℃). This temperature is slightly higher than the martensite start temperature. Quenching should be fast enough to avoid pearlite formation. However, the duration of austempering should not be too long, otherwise high carbon austenite will decompose into ferrite and carbide, which results in embritlement of the material. This decomposition, as well as martensite formation, cannot be completely avoided resulting in a reduction in ductility and toughness of ADI. [31-34]

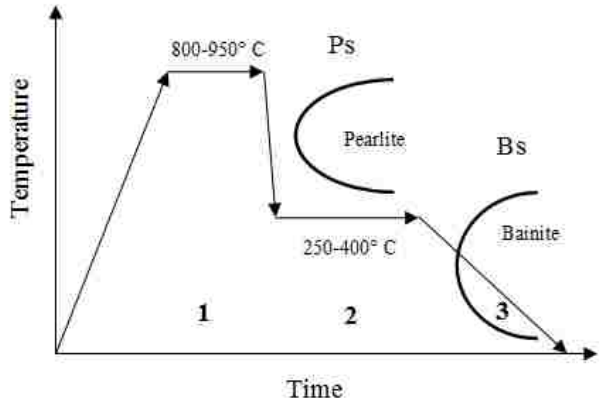


Figure 2.7 Heat treatment processes for obtaining ADI[30]

Sahin [35] showed that increasing the austempering time led to a more ductile ausferritic structure replacing the hard martensite, and in wear tests the abrasive weight loss increased with increasing austempering time. Dhanapal [2] showed that the wear resistance of cast iron treated at 250 ℃ is higher than that treated at 350 ℃. When the

duration of the isothermal austempering treatment is increased, carbon enriches the retained austenite. This promotes strain aging in the retained austenite. The decomposition of the retained austenite with segregation of cementite at long holds makes an additional contribution to the hardening of the metal. Thus, the wear resistance of the bainite-carbide iron is sensitive to the parameters of bainitic hardening and is greater when the carbide content is higher. With an increase in the austempering temperature, the acicular ferrite becomes thicker and larger, the impact toughness rises, and the hardness decreases. However, there is a complicated effect of austempering temperature on the abrasion resistance. [36]

A comparison of the microstructures of ductile iron (DI) and ADI are shown in Figures 2.8. Figure 2.8 (a) shows that ductile iron consists of ferrite, pearlite and graphite nodules with most of the ferrite surrounding the graphite nodules. However, in ADI (Figure 2.8 (b)), ferrite is in the form of feathery sheaves or laths. The laths are densely packed inside the retained austenite matrix. As well as bainitic ferrite, retained austenite and nodular graphite constitute the basic microstructure of ADI. Bainite, itself, is a mixture of ferrite lath matrix and cementite.

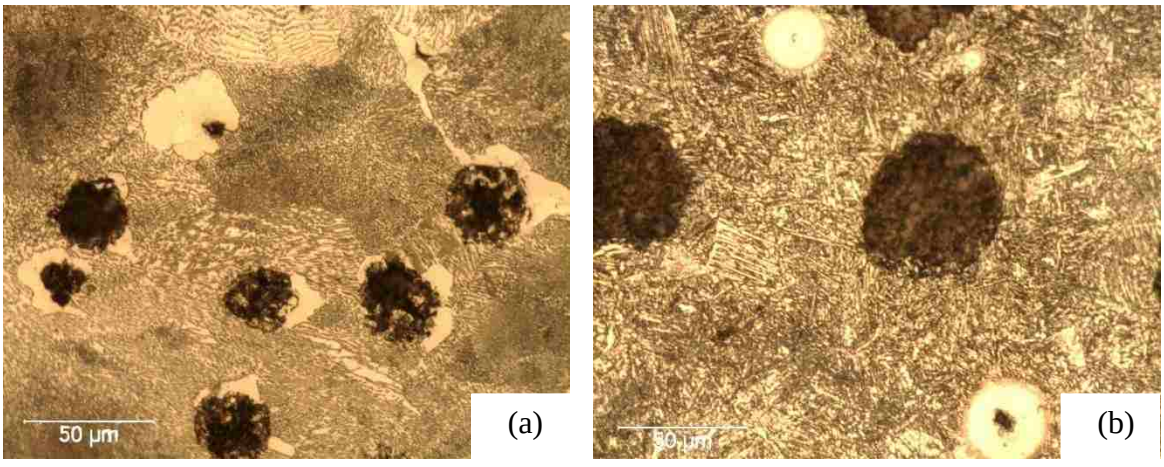


Figure 2.8: Comparison of the microstructures of (a) DI and (b) ADI (500X)

### 2.1.5 4140 Steel

4140 is a common high tensile medium carbon Cr-Mo alloy steel with 0.4wt%C, 1wt% Cr, and 0.2wt % Mo. The normal heat-treated condition is hardened and tempered to an ultimate tensile strength (UTS) in the range of 850-1000Mpa. Its dominant phase after heat-treatment is tempered martensite. It has high fatigue resistance and wear resistance, and can be used at temperatures as high as 480 ℃, which makes it suitable for critical stressed applications. Pre-hardened and tempered 4140 can be further surface hardened by nitriding, and also by flame or induction hardening. It can be used in practical applications where strength and impact toughness are required for shafts, axles, ball studs and large gears. [13, 37-39]This steel is designated as A 829 M according to ASTM standard and 42CrMo4 according to the DIN-EN 10083-1 standard.[40]

## 2.2 Nitriding

In order to improve the surface properties of the materials, different surface treatments and hard protective coatings are used. Nitriding is one of the more popular methods for surface engineering. Nitriding is predominantly used on steel, but also cast irons, aluminum and titanium. Nitrided steels are widely used due to their superior hardness and attractive surface hardness, fatigue life, and tribological properties.[41]

Figure 2.9[42] shows the general applications for nitriding in the automotive industry. Nitriding could be used to improve the wear resistance, fatigue strength, corrosion protection, aesthetic finish, and bearing characteristics of automotive parts such as camshafts, crankshafts, engine valves, link balls and clutch plates.

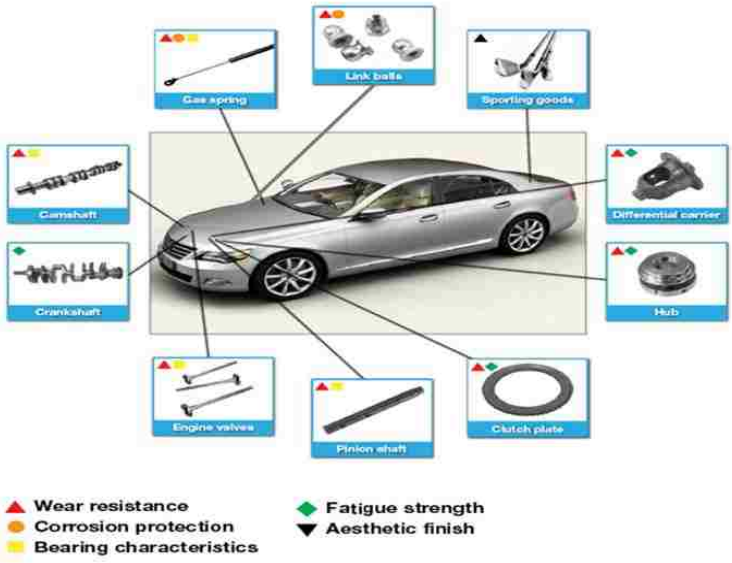


Figure 2.9: General applications of nitriding in automotive industry.[42]

However, what limits the extended use of hard, thin coatings is the load carrying capacity of the coating-substrate system. Because the hard coating is very thin, the substrate must carry most of the applied load. If the substrate does not have the capacity to carry the contact load and support the coating, plastic deformation will occur, which leads to premature failure of the coating.[43]

Nitriding is a thermochemical process which involves the introduction of nitrogen atoms into the component surface. The microstructure of a nitrided case is generally composed of a thin compound layer (CL) and diffusion zone (DZ) underneath. The compound layer at the surface generally consists of ε-$Fe_2N_{1-x}$ and γ'-$Fe_4N_{1-x}$, and diffusion zone in the subsurface region contains $\alpha$-Fe and contains needles of γ'-$Fe_4N$, owing to the long-distance diffusion of nitrogen from the surface toward the core, which generates both higher hardness and nitrogen gradients. Good corrosion resistance and wear resistance are usually ascribed to the compound layer, whereas improvement of the fatigue resistance is due to the diffusion zone.[44]

An example of a nitrided case (compound layer & diffusion zone) in 4140 steel is shown in Figure 2.10. One can clearly distinguish the compound layer, diffusion zone and the core. The top nitrided layer is usually called compound layer, because new nitride compounds form at that location. Nitrogen continues to diffuse across the compound layer, towards the core of the material. The nitrogen-rich zone between the compound layer and core is called the diffusion zone.

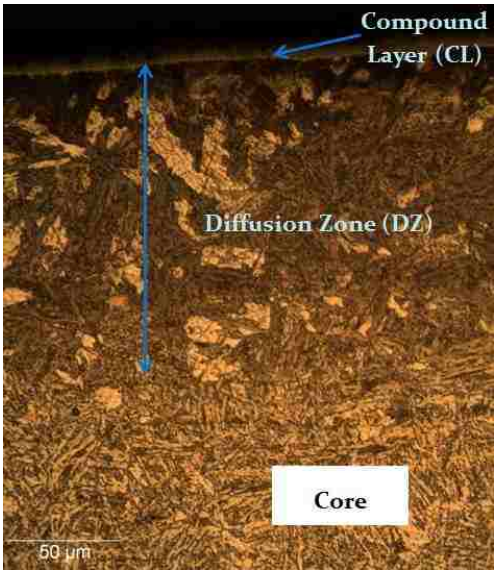


Figure 2.10: An example of nitrided case (Compound Layer & Diffusion Zone)

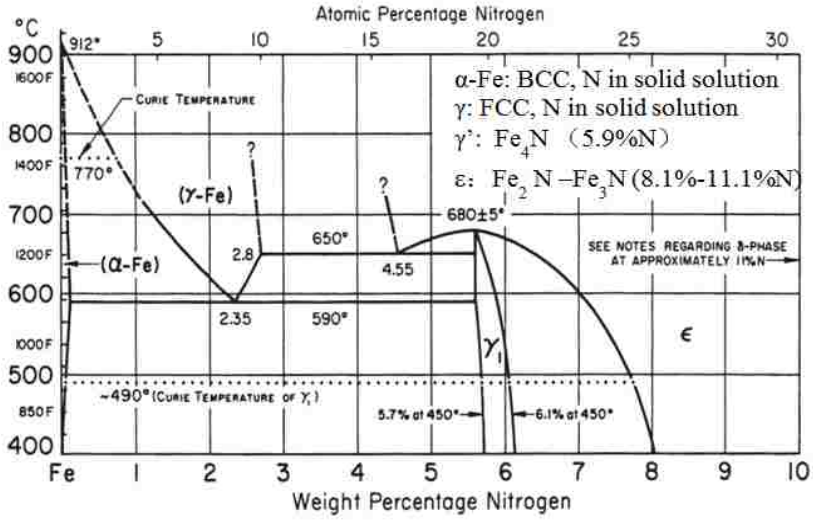


Figure 2.11: Iron-nitrogen equilibrium diagram[45]

As shown in the iron-nitrogen equilibrium diagram, Figure 2.11, ε and γ' are the nitrogen-containing phases that are formed in the nitrided case during the nitriding process. Compared with the iron-carbon diagram, the transformation temperature is lower than that for carburizing. As a result, nitriding can be conducted at a lower temperature. That is one of the advantages of nitriding over carburizing.

Figure 2.12 is a comparison of the various diffusion surface hardening techniques. It can be seen that nitriding can be conducted at a lower range of temperature, 315-550 ℃, than carburizing, carbonitriding, ferritic nitrocarburizing and boronizing. However, it is possible to use higher temperatures. For instance, Gerasimov [46] studied the hardened layer on a martensitic steel 16Kh2N3MFBAYu-Sh, an austenitic steel 12Kh18N10T, and iron after nitriding at a nitrogen pressure of 100-150 MPa and temperature of 950-1150 ℃ with 3h hold and after additional 1h tempering at 300-600 ℃. When the nitriding is applied to titanium, the processing temperature should be 650-1100 ℃ or higher.[47-50]

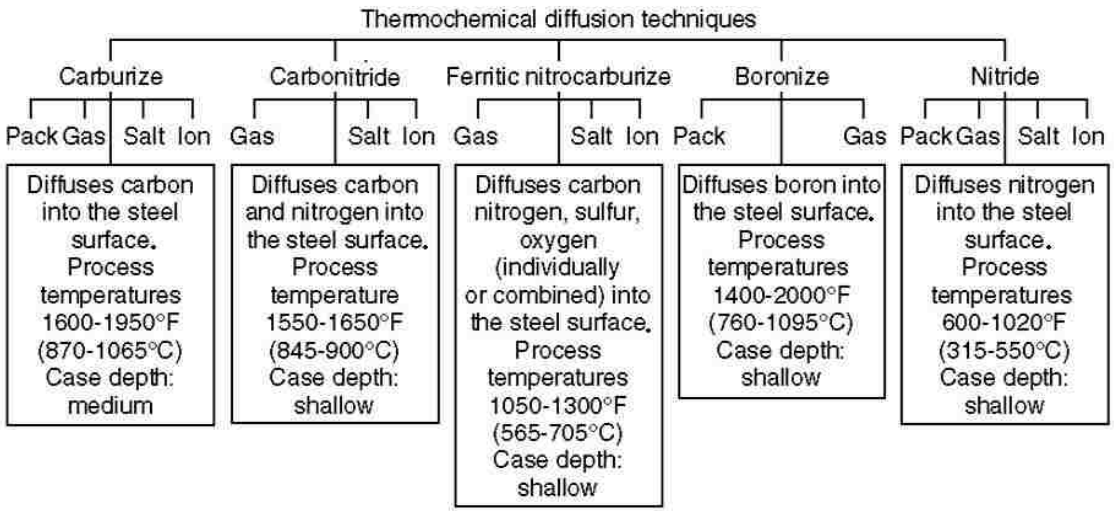


Figure 2.12: Comparison of various diffusion surface hardening techniques[45]

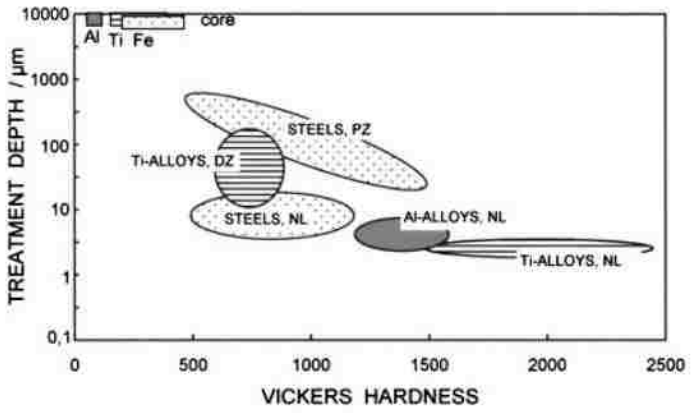


Figure 2.13: Typical thickness and hardness of nitrided layers on steels, and Ti and Al alloys: NL nitride layer; DZ diffusion zone; PZ [51]

Typical thickness and hardness of nitrided layers on steels, and Ti and Al alloys, are shown in Figure 2.13[51]. It can be seen that the hardness of nitrided layer-NL (CL in our studies) and diffusion zone (DZ & PZ in figure 2.13) increased greatly compared to the base metals (Al, Ti, Fe). Nitrided layers on steel have hardness values from 500 to 1500HV.

The three main nitriding methods are: gas nitriding, salt bath nitriding, and plasma/ion nitriding. These processes are named after the nitriding medium used.

### 2.2.1 Gas nitriding

#### 2.2.1.1 Introduction to gas nitriding

Gas nitriding provides high hardness and wear resistance due to the formation of nitrides and diffusion of the nitrogen into the material.[52] Gas nitriding has existed for over a century, though the thermodynamics and kinetics has been investigated only in the last few decades. Recent developments have led to a process that can be accurately controlled. The thickness and phase constitution of the resulting nitrided layers can be selected, and the process optimized for the particular properties required. The first study

on the subject appeared in 1876. The industrial use of gas nitriding for improving the corrosion strength of steel parts began in 1930s. Gas nitriding processes are characterized by a relatively low cost, high ecological safety, and the possibility of treating parts of any size and shape. [53]

In gas nitriding, the nitrogen-rich gas used is usually ammonia. When the ammonia flows into the heated furnace, it disassociates into nitrogen (N) and hydrogen (H). The reaction is: $2NH_3$ (g) =>$N_2$ (g) +$3H_2$ (g). The nitrogen then diffuses into the surface of the heated work piece and a nitride layer is created, as well as a diffusion zone.

2.2.1.2 Previous studies on gas nitriding

Piccilli[54] studied the main variables of a thermochemical gas nitriding process for stainless steel parts for engine components. They showed that the nitriding temperature and stress relief temperature, and the nitriding activation temperature, are relevant in the occurrence of nitriding cracks.

Studies on the gas nitriding of AISI H13 tool steel showed that nitriding time, temperature and nitrogen potential significantly affect the nitride layer formation in terms of nitrogen concentration and hardness variation as a function of nitride case depth.[55] With increasing nitriding time, the compound layer becomes thicker, and the diffusion zone containing dissolved nitrogen becomes wider.[48] In order to control the nitride layer growth, nitriding parameters such as the ammonia inlet gas flow rates, the temperature and the pressure have been investigated. [56]

Garzon[57] developed cyclic gas nitriding for duplex stainless steels. It avoids the formation of coarse grains in the austenitic case and enhances the wear resistance of the duplex stainless steels.

Vershinin[58] showed that the nitrided layer of highly dispersed particles is formed in low temperature nitriding with a globular shape and sizes from 20-100nm. The nitrided layer has maximum thickness (~3.5mm) and is characterized by low wear resistance. However, a decrease in nitrided layer thickness leads to increased wear resistance. After nitriding, the surface microhardness increased by 35%-40%, while the surface roughness was essentially unchanged. This allows for the use of nitriding as a finishing treatment.

Hussain[59] investigated the effect of retained austenite on the nitrided case when gas nitriding high-strength steel in ammonia gas atmosphere at 450 ℃. It was found that the predominant nitride phase formed was $Fe_4N$. The concentration of the nitride phase depended on the austenite content and decreased from the surface towards the core. Growth of the nitride layer decreased with an increase in the austenite content. The depth of the diffusion zone was between 30 and 90 μm.

Grain boundaries are preferential routes to enhance diffusion during nitriding. When a component is gas nitrided, a particular grain boundary orientation may prevent diffusion of nitrogen in one direction, while enhance it in another. Experimental investigations of pure iron and stainless steel demonstrated that anisotropy of grain boundaries affect the mechanical properties and diffusion involved in gas nitriding.[60]

Fare [61] found that the nitride compounds formed in the surface region of the substrate material is ε-$Fe_{2-3}N$, while as the depth increases $Fe_4N$ is the dominant phase. SEM metallography revealed that nitrided region extended more than 60 μm and the nitrided layer was free from micro-cracks and voids.

Ratajski[62] presented a complex system of design of the gas nitriding process using analytical mathematical models and artificial intelligence methods. Within this process,

the properties of nitrided layers could be predicted. For in situ visualization of the growth of the nitrided layer, computer procedures were developed.

Nathalie[63] showed that the fatigue strength improvement of 4140 steel brought by gas nitriding varies from 20% to 100%, as compared to base metal.

### 2.2.2 Salt bath nitriding

In salt bath nitriding, the medium used is a salt containing nitrogen such as a cyanide salt, or potassium nitrate. Cyanide salt baths have the same, or an even higher, nitrogen potential than ammonia. The nitriding behavior can be reasonably described by nitrogen diffusion into the work pieces. During nitriding, most nitrogen is interstitially dissolved. After nitriding, a slight oxidation has been found.[64]. Actually, it is a nitrocarburizing process, because the salts used usually also donate carbon to the workpiece surface, and the two elements generally diffuse into the workpiece surface simultaneously.[65, 66]

As with the other nitriding methods, the modified case is comprised of a compound layer and a diffusion zone from the surface towards the core. The compound layer consists of nitrides formed with the main elements and alloying elements. The diffusion zone is composed of a solid solution with N and nitride precipitates.

Salt bath nitriding has the advantages of easy operation, quick processing time, low cost, energy efficiency, and stability. However, the salts used are highly toxic when heated to a high temperature. The temperature used is typical for all nitrocarburizing processes, i.e. 580-650℃. It would seem that salt bath nitriding should have been eliminated from industrial use because of the high toxicity of the salts. However, the process is still widely used because the old toxic salts have been replaced by non-toxic salts. This process is a very active process, more intense than that of gas nitriding and

nitrocarburizing including plasma nitriding. The reactivity of the nitriding medium and the final efficiency of the process, as well as an allowance for the cost of the equipment, must be taken into account. Another advantage of salt bath nitriding is the possibility of treatment of stainless maraging steels.[66, 67]

### 2.2.3 QPQ

The QPQ surface heat treatment, namely the Quench-Polish-Quench salt bath technology, mainly consists of six steps: 1) degreasing, 2) preheating, 3) nitriding, 4) oxidizing, 5) washing and 6) oil immersion. It is a nitrocarburizing process in a cyanide-cyanate salt bath with post-oxidation in a nitrate-nitrite salt bath.[68] It is widely used for tools, molds and gears to increase their strength, wear and corrosion resistance and fatigue strength, and to obtain less distortion.[69] For example, Yu[70] reported that a 4Cr5MoSiV1 steel when treated by QPQ salt-bath nitriding at temperatures from 520 ℃ to 560 ℃ and for times from 2h to 6h showed a hardness increase of 196%, a wear resistance increase of 349%, and a corrosion resistance increase of 943%, compared to the un-nitrided condition.

QPQ is distortion-free and adaptable for all grades of steels. It has been established that a compact and integrated magnetite film ($Fe_3O_4$) can be developed through this low temperature thermo-chemical process, which can greatly improve wear resistance.[71]

An example of QPQ treatment process is shown in Figure 2.14[71]. It can be seen that the QPQ technology mainly consists nitrocarburizing and post-oxidizing processes. The three main stages: Quench, Polish and Quench are highlighted.

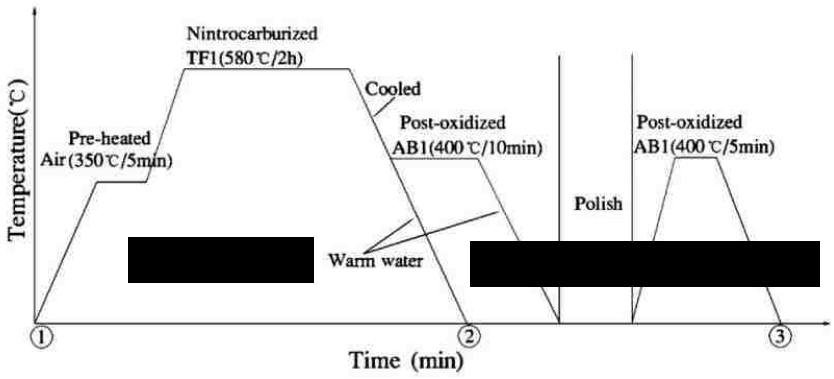


Figure 2.14: An example of QPQ treatment [71]

The literature shows that since the 1980s, QPQ surface heat treatment has been used for improving the corrosion resistance,[72, 73] but up to 1997 it had not been widely applied in mass production.[74] The process parameters should be carefully controlled. The magnetite film, developed in the post-oxidizing stage, should be generated in the porous area and should not collapse during the first post-oxidization treatment. In the second oxidizing stage, the porous area is partly eliminated, so the duration of heat treatment should be less than the first one. [75]

A new method derived from QPQ has been developed. Luo[76] developed a combined cryogenic and QPQ treatment for high speed steel. The cryogenic treatment can reduce the amount of retained austenite, and the axial ratio of martensite, thus, decreasing the martensite lattice distortion. Therefore, the impact toughness of the steel is improved.

In comparison with QPQ, QP (Quench, Polish) is similar to QPQ but without the second post-oxidization. The components treated by QP process are used directly after polishing. The surface roughness of the materials treated using QP is usually smaller than that treated using the methods without polishing. The corrosion resistance may be further improved through the second post-oxidation (QPQ).

### 2.2.4 Plasma/ion nitriding

Plasma nitriding, also referred to as plasma ion nitriding, ion nitriding or glow discharge nitriding, is a widely used surface modification treatment that improves surface hardness, fatigue strength and wear and corrosion resistance of the metallic materials. Plasma nitriding has been applied to surface modification of iron, aluminum, titanium, and their alloys for many years. It involves the diffusion of nitrogen atoms into the metal surface under plasma conditions. This produces a thin, hard case with a high compressive residual stresses at the surface. From the surface inward, the developed case is comprised of a compound layer and a diffusion zone. For iron, the compound layer consists of the ε-$Fe_{2-3}N$, γ′-$Fe_4N$ and nitrides formed with the alloying elements. The diffusion zone is composed of the Fe-N solid solution and nitride precipitates. The component in a conventional plasma nitriding process is treated as a cathode for discharge. Components with different shapes or different surface-mass ratios might undergo different ion bombardment intensities and produce different nitride layers. To create a nitrogen-containing plasma in large vacuum volumes (0.1-1$m^3$), glow and arc discharges are mainly used. [77-82] As an example of the application of plasma nitriding, Wang[83] used it to produce the hard and wear resistant layer on the surface of CoCrMo alloy.

## 2.3 Tribology

Tribology is derived from the Greek word TRIBOS meaning rubbing, so a literal translation could be the *science of rubbing*. [84] However, according to the modern wider definition, besides rubbing, the relative motion of interacting surfaces also includes rolling and sliding.

Wear and friction are the two principal constituents of tribology and our involvement with these phenomena affects nearly every aspect of our lives. Friction and wear both arise from the interaction of surfaces. We are always trying to control the friction and minimize the wear. However, life would be impossible without tribology. Wear and friction are with us all the time. It is known that during the palaeolithic period, drills were made for drilling holes to produce fire. In engineering applications, friction is employed to fulfill required functions, such as driving wheels on trains and cars, brakes and clutches. The nut and bolt only work because of the friction between them. [84]

The common distinct regimes employed to describe the fundamental principles of tribology are:[84]

a. Dry sliding;

b. Partial separation in boundary or mixed lubrication;

c. Complete separation of two surfaces by fluid-film lubrication.

Topics on tribology usually consist of lubrication, friction, wear, contact mechanics, and surface science. It is an interdisciplinary subject since the knowledge from physics, chemistry, mathematics, materials science and engineering are used simultaneously. The days of single disciplinary designs and the days of design by trial and error are gone forever. Modern products must have incorporated all the factors during their design stages that lead to a satisfactory control of friction and prevention of wear. [84]

The solutions to the tribological problems of with acceptable friction and wear are shown in Figures 2.15 (a)-(h) [84]. These are: a). The materials have intrinsically low friction and wear characteristics, although this may indicate accepting lower load carrying capacity. b). Chemical films are applied to protect the surfaces and reduce the

intimate contact. c). Lamellar solids may be used since they have low resistance to transverse shear. d). Surfaces may be separated by a continuous fluid-film, which may be liquid, vapor or gas. e). The surfaces may be separated by elastometers bonded to the two surfaces where the amplitude of transverse displacement is small f). Flexible strips may be used where the transverse force is small. g). Rolling elements such as balls, cylinders and the like are widely employed between the pair. h). The carrying of load without mechanical contact is possible by using magnetic force fields.[84]

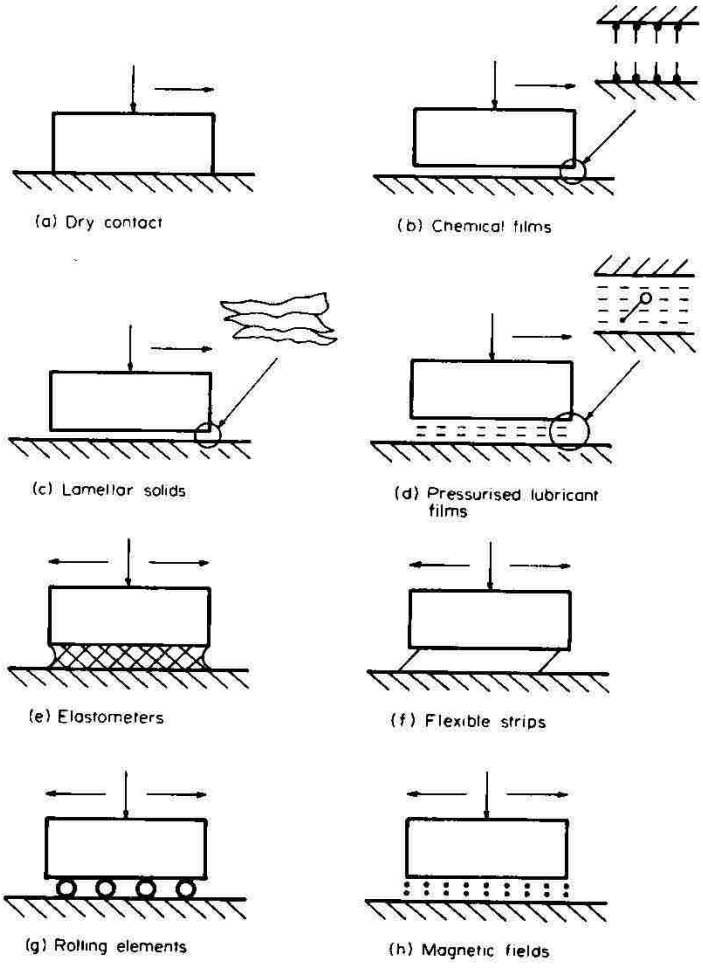


Figure 2.15: General methods for the solution of tribological problems[84]

2.3.1 Surfaces properties

A surface can be recognized as a layer that grows organically out of the solid and has properties of considerable functional significance. The surface layer of metals consists of several zones having specific physic-chemical characteristics to the bulk materials. As shown in Figure 2.16[84], for a typical surface layer, there is a zone of work hardened material on top of which is a region of amorphous or microcrystalline structure. This molecular layer is the Bielby layer that is produced by melting and surface flow during machining, which can be subsequently hardened by quenching. Usually this basic structure is covered by dust particles and molecular films deposited from the environment and contaminated by the products of chemical reaction with the atmosphere. Eventually, the surface contains atoms of gas that live within the surface but have somewhat dissimilar properties to those of the gaseous environment. [84, 85]

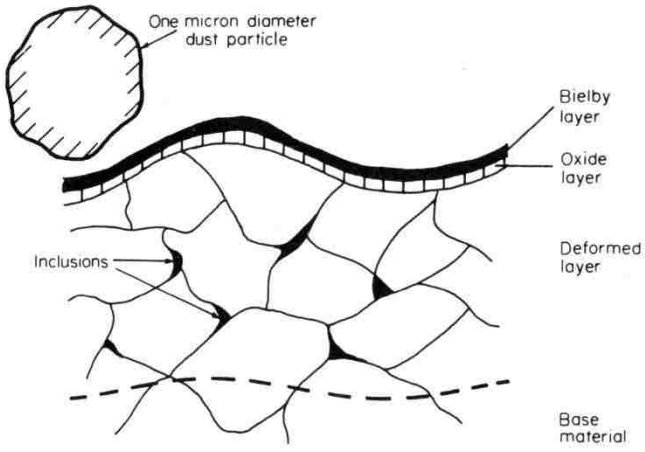


Figure 2.16: Typical surface layers[84]

In addition, solid surfaces generally contain surface irregularities irrespective of their method of formation. The geometric properties of the texture of a surface layer can be characterized by a series of irregularities, having different amplitudes and frequency of occurrence. This particular property is of fundamental importance in research on

friction, wear and lubrication. When two nominally flat surfaces are placed in contact, surface roughness causes contact to occur at discrete contact points. Deformation occurs at these points, which may be either elastic or plastic, depending on the nominal stress, material properties and surface roughness. [84, 86]

Surface imperfections at an atomic level are matched by macroscopic deviations from flatness. Almost every known surface, apart from the cleaved faces of mica is rough on a microscopic scale. Roughness means that most parts of a surface are either a peak or a valley. The typical amplitude of engineering surfaces between the peaks and valleys is below one micrometer. The profile of a surface is almost always random unless some regular features are deliberately introduced. [87] This is illustrated in Figure 2.17, which is a surface profile of a nitrided ADI from the present study.

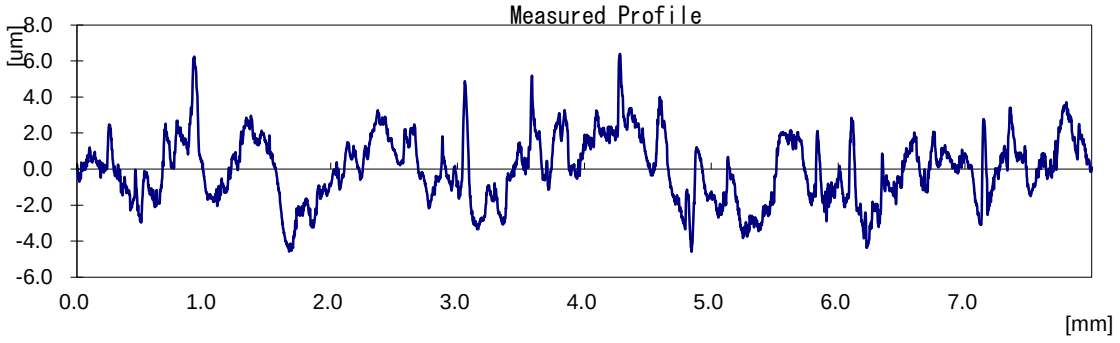


Figure 2.17: An example of surface profile of nitrided ADI

The roughness is formed by the fluctuations in the surface profile and is composed of short wavelength referred to micro-roughness, and longer wavelength roughness that is called waviness or macro-roughness. Micro-roughness is characterized by hills and valleys of different amplitudes and spacing, which are large when compared to molecular dimensions. The surface also contains undulations of very long wavelengths caused by the vibrations of the tool or workpiece during the preparation of the surface. The

distribution of the asperities over the surface is either directional or homogeneous in all directions, depending on the processing method. Surfaces produced by directional methods of processing, show a definite orientation of asperity distribution, such as planning, turning, and milling. Those prepared by non-directional methods, such as lapping and electro-polishing, exhibit an isotropic and equiprobable distribution in all directions. [84]

The geometric texture of the surfaces is controlled by the finishing process by which they are produced. Table 2.1[85] shows the common roughness values related to different machining processes.

Table 2.1: Roughness values related to different machining processes[85]

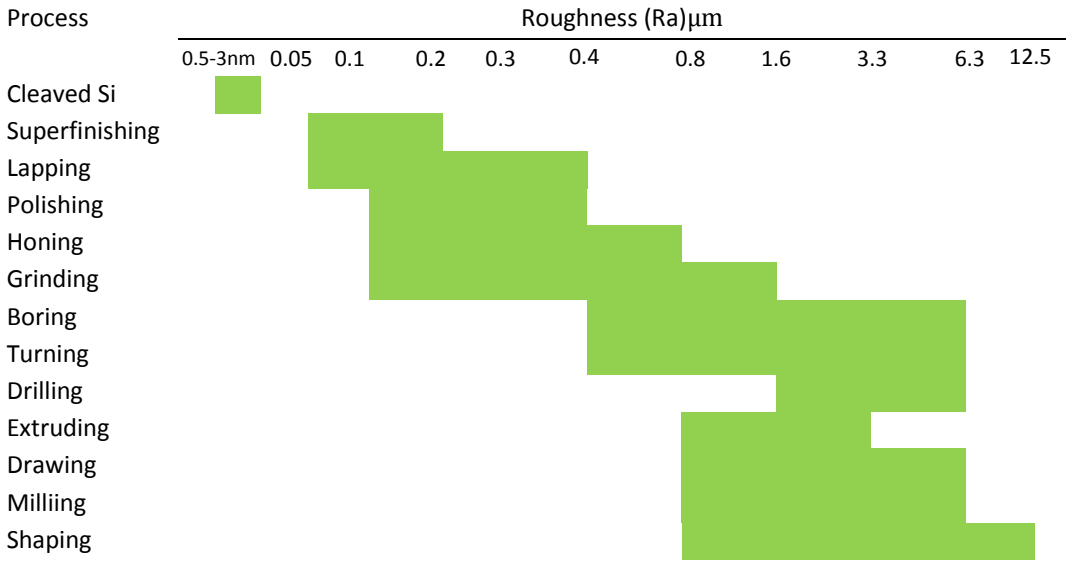


The quantitative assessment of the surface topography is very important for solving a wide variety of problems of tribology. Friction and wear primarily depend on the nature of the real area of contact between the surfaces. In turn, that is dependent on the shape, size and distribution of the asperities. [84]

The stylus method only reveals a plane property of the surface topography and is based on the nature of the ensuing single line profile. The parameters usually used to define the texture of surfaces are the center line average (CLA) roughness value, and Root Mean Square (RMS) value. The CLA value is defined as the arithmetic average value of the vertical deviation of the profile from the center line. The RMS value is defined as the square root of the arithmetic mean of the square of the deviation. In mathematical form they can be written as: [84, 85]

$$C.L.A = \frac{1}{n}\sum_{i=1}^{n}|z_i| \tag{1}$$

$$R.M.S = \left[\frac{1}{n}\sum_{i=1}^{n}(z_i)^2\right]^{1/2} \tag{2}$$

The average height of the continuous profile over length L is give as:[85]

$$Ra = \frac{1}{L}\int_0^L |z|dx \tag{3}$$

It can be seen that equation (3) has the same meaning as equation (1), but in an ideal mathematical form. When n goes to∞, the two equations are equal. In experimental conditions, equation (1) is more practical to use.

Furthermore, a 3D model of surface profile z(x, y) has been also conceived.[88]

2.3.2 Friction

In 1508, the famous artist and engineer Leonardo da Vinci postulated the concept of the coefficient of friction (COF) as the ratio of the friction force to the normal load. He had conceived a device using rolling friction around 1495. Physicist Amontons again established the significance of the coefficient of friction in 1699, which was independent

of the apparent area of contact. In 1785 physicist Coulomb further distinguished kinetic friction from static friction, which was independent of velocity.[85, 89]

Friction is the resistance to relative motion which is due to the interaction between the surfaces and experienced whenever one solid body slides over another. The resistive force is called the friction force, which is parallel to the direction of motion. Generally kinetic friction is lower than static friction. The first law of friction states that friction is independent of the apparent area of contact between the contacting bodies. The second law states that the friction force is proportional to the normal load between the bodies. These laws are often referred to as Amontons laws. The third law was introduced by Coulomb, that the kinetic friction is nearly independent of the speed of sliding. This law has a smaller range of applicability than the first two. [84]

The second law of friction enables us to define the coefficient of friction. The law states that the friction force F is proportional to the normal load $F_l$. That is:

$$F_f \propto F_l \tag{4}$$

A ratio (μ) is defined as:

$$\mu = \frac{critical\ shear\ stress\ of\ the\ interface}{yield\ pressure\ of\ the\ bulk\ metal} \tag{5}$$

Therefore

$$F_f = \mu F_l \tag{6}$$

Where μ is a constant known as Coefficient of Friction (COF). It is only a constant for a given pair of sliding materials under a given set of conditions. It varies for different materials and conditions. For example, under normal atmospheric conditions a hard steel surface rubbing against a similar surface typically would have a value of μ about 0.6. For

the same material combination rubbing under high vacuum conditions the value of μ is much higher. [84]

In considering the possible causes of friction, it is convenient to separately consider the interaction at the surfaces and the mechanism of the energy loss. When two surfaces are loaded together they can adhere over part of the contact surface and this adhesion is therefore one of the surface interaction forms causing friction. If no adhesion takes place, then the only alternative interaction which is able to result in a resistance to motion is when material is deformed and displaced to accommodate the relative motion. We need only consider two interactions of this type. The first is asperity interlocking. Motion cannot take place without deformation of the asperities. The second is the displacement type of interaction. In order for relative motion to take place, some of the material of the soft surface should be displaced. Adhesion and material displacement are two forms of surface interaction, which can cause energy losses due to both elastic and plastic deformation and fracture.[84]

As mentioned earlier, although sometimes high friction is needed to fulfill certain functions, reducing the friction is also extremely important, because of the energy it consumes and the wear failure of components it induces. Scientific effort consequently continues to be devoted to achieving lower friction. Therefore, ways of reducing friction and wear at the solid surfaces are the main aim of most studies.

### 2.3.3 Lubrication and lubricants

#### 2.3.3.1 Introduction to lubrication and lubricants

Throughout the history of tribology, a number of approaches have been tried to reduce friction. These have produced some fundamental scientific laws, the basis of

which we still use today. By means of effective lubrication, mechanical design could minimize friction and wear in devices such as engines and bearings. Lubricants can also provide a cooling effect, a cushioning effect, a cleaning action, and a sealing action. Types of lubricants are mainly animal oils, vegetable oils, mineral oils, synthetic lubricants, greases and solid lubricants. [85, 90]

Viscosity is the most important property of a hydraulic fluid, and it is a measure of the sluggishness with which a fluid moves. It can be simply described as the resistance of the lubricant to flow; more precisely it is the property of a fluid resisting to a shearing displacement. In reality, the ideal viscosity for a given hydraulic system is a compromise. Too high a viscosity will result in: 1) High resistance to flow, which causes a sluggish operation. 2) Increases power consumption due to frictional losses. 3) Increased pressure drop through valves and lines. 4) High temperatures caused by friction. However, if the viscosity is too low, the result is: a) Increased leakage losses past seals. b) Excessive wear due to break down of the oil film between moving parts. [89]

Mechanisms for reduction of friction and wear with soft coatings, adherent molecular and lubricant surface layers were elucidated by Bowden and Tabor in 1950.[85, 89] Applying a thin film boundary lubricant has little beneficial effect if the damage is caused by the presence of abrasive particles, but is extremely effective if the damage is caused by adhesion. [91]

Bhushan[86] studied the phenomena of tribology at the atomic scale with an understanding of the molecular mechanisms of tribology in thin films and at surfaces. Schematic illustrations of different types of dynamic thin-film structures that can arise during lubricated sliding are shown in Figure 2.18[86]. The upper one is dynamic phase

diagram representation of friction force or rate of energy dissipation, as a function of temperature or sliding velocity. Under certain favorable conditions involving surface-grafted chain molecules, the entangled molecules at the interface may undergo shear-induced ordering and become aligned when they disentangle. At the same time the friction force drops significantly.

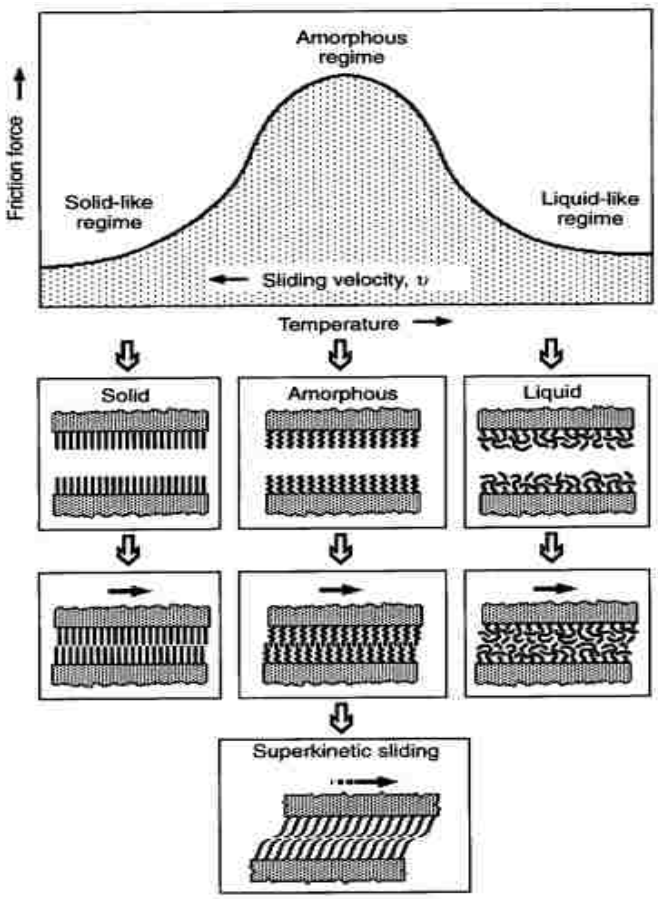


Figure 2.18: Schematic illustrations of different types of dynamic thin-film structures that can arise during lubricated sliding.[86]

The Stribeck curve is shown in Figure 2.19, where the coefficient of friction μ is plotted against λs, which is originally devised by Stribeck. The frictional contact of clean surfaces is represented by point A in Figure 2.19. When sliding surfaces are separated by lubricant films with only few molecules in thickness, the friction is influenced both by

the nature of the underlying surface and by the chemical constitution of the lubricant. This type of lubrication is called Boundary lubrication, or oiliness lubrication. At point B the surface roughness equals the film thickness, from where the partial or mixed lubrication regime BC starts. In this case, the load is supported by both a coherent flowing oil film and the regime AB type contact, or alternatively by the thin micro-scale films formed between the distorted surfaces. Regime BC represents a design failure in some ways, because the coherent lubricant film is not present everywhere. As in regime AB, the surfaces wear in regime BC, perhaps producing debris. In regime CD, a coherent elastohydrodynamic lubricant (EHL) film is produced. It is characterized by a film thickness of a couple of micrometers or less, requiring quite smooth surfaces. In this zone, the values of λs are large enough, for the surface features could not influence the lubricant film thickness much. In this regime the high pressures encountered cause the surfaces to distort elastically and the viscosity of lubricant to increase. Modern manufacturing methods and design improvements have increased this zone at the expense of zone BC. Interestingly, Dowson points out that it has also been choice of nature for the EHL regime of lubrication to occur in the synovial joints of creatures from elephants to shrews. The next regime, beyond D, covers the hydrodynamic and externally pressurized types of bearing. In certain cases, when elastic surface deformation exerts a strong influence on fluid-film behavior increasing speeds or reducing loads in zone CD can cause a reduction in elastic distortion of the surfaces that were previously in EHL contact, making them also candidates for the zone beyond D. [85, 89]

$$* \lambda s = \frac{film\ thickness}{roughness\ height} \tag{7}$$

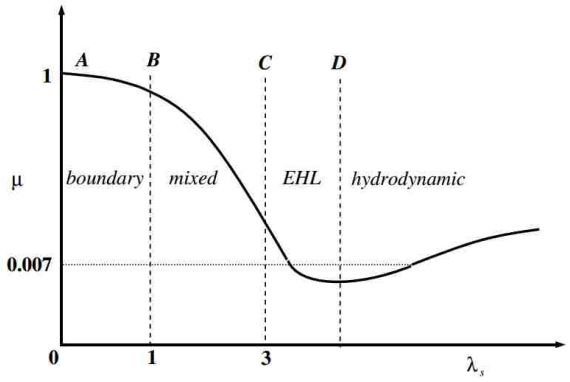


Figure 2.19: Stribeck curve (not to scale)[85]

Tallow was used to lubricate chariot wheels before 1400BC. Greases and vegetable oils were used later. Significant advances in the development of lubricants did not occur until the establishment of the modern petroleum industry, with the opening of the Drake well in 1859, Pennsylvania. Commercial use has proceeded since about 1930 in step with increasing demands in automobiles, aerospace units, and high speed and high pressure hydraulic equipment. Air, water, gasoline, refrigerant gases, solvents, and various fluids processed in individual machines began to be used as lubricants on a broadening scale in fluid-film bearings from 1950 as improved designs and mating materials were developed on a customized basis. Surface active lubricants tend to lower the life of the component as compared to straight mineral oils.[89]

The solid lubricants for tribological applications traditionally include lamellar materials such as graphite, boron nitride, and $MoS_2$, $WS_2$. Perry[92] introduced pyrophyllite as a new candidate solid lubricants. Their very low friction behavior is typically attributed to their structure which consists of strong covalent bonds within the layers and weak van der Waals interactions between the layers. Along with this lamellar structure, these materials also have low energies on the basal plane which allows for an easy shearing and low friction along the planes at the interface.

2.3.3.2 Mineral oil

Mineral oils produced by refining petroleum crude oil are the starting ingredients for over 95% of all lubricants now in production. These oils consist essentially of hydrocarbons ranging from approximately 250 (with a skeleton of about 18 carbon atoms) with low viscosity up to 1000 for very high viscosity lubricants in molecular weight. Typical molecular structures involved are n-paraffin, isoparaffin, cycloparaffin, aromatic hydrocarbon and mixed aliphatic and aromatic ring. For a given molecular size, paraffins have relatively low density, low viscosity, and higher freezing temperatures (pour points). Aromatics, involving six-member unsaturated carbon rings, introduce relatively higher viscosity, more rapid change in viscosity with temperature, and dark-colored, insoluble oxidation products. They are the source of sludge and varnish that accompany their oxidation in high temperature service. The first step in producing mineral lubricating oil is distillation of crude petroleum to remove lower-boiling gasoline, fuel oil, and kerosene, while dividing lubrication oil fractions into several grades by their boiling point ranges. Subsequent refining steps remove straight chain paraffins, undesirable aromatics, and sulfur and nitrogen contaminants. Colorless base oils of unusual purity and stability are produced by catalytic hydrocracking in an ongoing shift from solvent refining. [89]

There is no doubt that oil an attractive lubricant as its fluidity enables it to penetrate readily to all parts of the bearings where sliding is likely to occur. Oil is preferable under heavily loaded, high speed or high temperatures conditions as it acts as a heat transfer medium and serves to prevent the temperature from rising excessively. With grease lubrication no heat balance can be obtained. Operating speed is usually the main factor in determining the adoption of oil as a lubrication medium. Other conditions in which oil is found to be the most suitable lubricant are in light machines or precision instruments. [89]

A mineral oil was used in the ball-on-disc wear tests in the present study.

### 2.3.4 Wear

#### 2.3.4.1 Introduction to wear

Wear is the loss of material from the surface by transfer to another surface from its original position or the creation of wear debris, performed by the contact with other solids, flowing liquids, flowing gas, or the mixture of them. It is probably one of the major forms of material deterioration, often limiting both the life and the performance of the moving components. It is also one of the most commonly encountered problems in industry which requires frequent replacement of components. Wear types are adhesive wear, abrasive wear, surface fatigue, fretting wear, erosive wear, and corrosive wear. Wear is affected by a variety of conditions, such as the type of lubrication, loading, speed, temperature, materials, surface finish, and hardness. Consequently, the visible manifestations of wear may be the result of a combination of primary forms. It may be difficult to recognize the various damages types. However one type of damage is usually predominant. [4, 91]

#### 2.3.4.2 Wear types

Generally adhesive wear refers to unwanted displacement and attachment, of wear debris and material compounds. Adhesive wear occurs when adhesive forces hold two surfaces together though they are separated by a measurable distance, and where very small amounts of contaminant prevent adhesion. However, tangential relative motion at the contacts and cold welding of the junctions can take place. Continued relative motion causes the junctions to be sheared and new junctions formed. If shear takes place at the position of the interface, wear is zero. If shear takes place away from the interface then

material is transferred from one surface to the other surface. With further rubbing some of the transferred material may be detached to form loose wear particles. In this case, the amount of wear is proportional to the load and distance of travel, but inversely proportional to the hardness and yield stress of the soft material surface being worn. [84]

Galling is one severe form of adhesive wear, in which material transfer from one surface to the other during sliding. It is the main wear mechanism for the sheet material transfer process. Galling is not thoroughly understood and different initiation mechanisms have been proposed that are related to adhesion, surface defects, microstructure, efficiency of lubrication and temperature.[93]

Studies of the abrasive wear resistance of iron alloys have been carried out for more than a century. Abrasive wear occurs when hard particles or a rough surface runs against a soft surface. In this type of wear, relatively hard asperities and wear particles trapped at the contact interface, removing material as cutting tools by a combination of microscopic plowing and micro-cutting processes. Abrasive wear may also degrade the efficacy of machine tools and grinding/polishing components. Insight into material removal by abrasive wear over a wide range of length scales is therefore essential for optimizing surface machining and improving the operation efficiency and longevity of mechanical elements possessing contact interfaces. However, it is beneficial in surface micromachining and chemical–mechanical polishing. [88, 94]

Abrasive wear involves hard asperities on one surface, moving across a softer surface under applied load, penetrate and remove material from the softer surface, leaving a groove. In the dominant view, abrasive particles or asperities are rigidly attached to the second body. The abrasive particles are loose and free to roll. [95]

Fatigue wear occurs when the surfaces run over each other opposing asperities are deformed and ultimately fatigued off. This type of wear damage occurs under contact interaction between sliding, rolling, or slippage elements, and simultaneously transmits a cyclic load. The shear stresses that initiate failure under these conditions reach a maximum value at some distance below the surface and develop cracks at the subsurface where there are microstructural discontinuities such as oxide inclusion particles. The coating fracture is often caused by the contact fatigue, which occurs in sliding contact of surfaces with rough surfaces. Rolling contact fatigue wear is characterized by the formation of large wear fragments after a critical number of revolutions.[84, 96, 97]

Corrosive wear occurs when rubbing takes place in a corrosive environment, either gaseous, or liquid, such as oxygen, moisture and other active chemicals in the lubricant. Surface reactions take place and the reaction products are produced on one or both surfaces. These reaction products are commonly poorly adhere to the surfaces, and they tend to be rubbed off during further relative motion. Then this process is repeated. Thus this type of wear requires both corrosion and rubbing.[84]

Fretting occurs between two surfaces loaded together, having oscillatory relative motion of small amplitude. It can be found in a variety of vehicles, especially in aircraft, such as turbine blades and disks.[98]

Delamination wear takes its name from the fact that wear debris consists of flakes. In this type of wear deformation of subsurface layers occurs during sliding, as well as subsurface crack generation and crack propagation processes. Coating delamination is the primary wear mechanism and often result in catastrophic failures. In certain cases, the delamination could be realized by the way that cracks initiate from the furrow wall

formed by the micro-cutting of oxide particles in the delaminated zone, and propagate parallel to the worn surface to cause the delamination. [99-101]

Pitting is the result of the fatigue failure of metal surface. Repeated application of relatively low stress may result in numerous pi-like cavities in the surfaces of metals. Cracks may initiate at the surface or a subsurface location. Spalling is generally considered to be a special type of pitting, which results when several pits join or when a crack runs parallel to the surface, rather than running to it, for some distance. Consequently, spalling defects are typically rather large. The latter type of spalling is often associated with the surface hardened parts and occurs near the interface of core and case. This type of wear occurs because the shear strength of the subsurface material is inadequate to withstand the shear stress to which it is subjected. For this reason, a spalling condition is often rectified by increasing the case depth or the core hardness. Water contaminated lubricants can also accelerate the propagation of surface cracks. The mechanism is probably a form of corrosion fatigue.[91]

2.3.4.3 Wear detection and evaluation

One of the most difficult and challenging problems in wear studies is the quantitative assessment of wear damage. There are numerous methods of quantifying wear and the technique selected depends on the component and the design application.

The quantification of wear damage techniques are based on mass or geometric measurements. Thus, it may be expressed as a weight loss or as a dimensional change. These methods suffer from the fact that the changes are very often quite small requiring very sophisticated techniques or prolonged testing to identify. One widely used technique is gravimetric wear measurement which calculates the wear mass/volume loss.[102]

However, when the mass loss or addition of specimen is lower than the accuracy of the weight balance, typically 0.01 mg, the gravimetric wear measurement is not valuable. Another technique consists in weighing the wear area, but in which, adhesive particles cannot be accurately measured. The techniques most generally applied to study changes in surface topography are optical and electron microscopy, interferometry, and profilometry, Atomic force microscope (AFM), and Raman spectroscopy [103]. Many studies involve microscopic observations of the test samples after the wear test, with optical microscope or scanning electron microscopes(SEM) (sometimes coupled with energy dispersive spectrometry (EDS), to study the wear morphologies. [104, 105]

Microscopy is essentially qualitative and multiple beam interferometry can be applied only to very smooth surfaces. Optical microscopy, while essentially qualitative, allows a specimen to be evaluated without subjecting tit to additional strain or damage.

In nano-tribological researches the surface-force apparatus (SFA), the scanning tunneling microscope (STM), the atomic-force and friction-force microscopes (AFM and FFM), as well as the quartz microbalance technique are widely used at the molecular scale.[86] AFM is a fundamental and powerful tool to characterize the surface properties on nano-scale.

2D or 3D profilometry measurements with stylus or optical devices can quantify the wear depth and volume, and assess the development of the local wear damage on the sample surface. The roughness parameters calculated from profiles or topographies may be used to evaluate wear development. [106, 107]

Analysis of wear debris can also be conducted. It is usually conducted on samples of the lubricant which are extracted from the system. The lubricants can then be analyzed

spectographically for the metallic elements present. In addition, particle analysis can also be conducted to determine volume, size and distribution of particles contained in the lubricant. This type of ferrographic oil analysis has been used to evaluate wear in such components as diesel engines, gears and bearings. The effect of wear debris on the antifriction and anti-wear properties of oils results from the fact that they change the pattern of physical processes in the oil film between the surfaces in contact, which govern the tribological behavior of the friction unit. [84, 108]

2.3.4.4 Previous relevant studies

Although the scientific literature available in this area is quite extensive, the effect of different nitriding methods on the wear resistance of DI, ADI, GI and 4140 steel had not been compared.

2.3.4.4.1 Literature on wear behavior of cast irons and steels

Nie etal[109] studied on the sliding wear behaviour of electrolytic plasma nitrided (EPN) cast iron G3500 and cast steel S0050A. The tribological properties of nitrided materials were evaluated through a pin-on-disc test both with and without lubricants. They found that the EPN treatment significantly improved hardness and wear resistance of both the cast iron and cast steel.

Riahi and Alpas [110] produced the first dry sliding wear map for gray cast iron, where wear was classified into ultra-mild, mild and severe wear. In ultra-mild wear, a compacted oxide film covered the contacting surfaces. Mild wear was defined as oxidative wear. Severe wear appears when oxide layer did not stably form due to delamination of tribo-oxides. They also attributed the excellent wear resistance of gray cast iron during dry sliding under low loading conditions to the graphite flakes and the

formation of a graphite film. The pearlitic structure of the matrix, and ASTM A type graphite flakes provide the best wear resistance for gray iron in engine cylinder applications.

The erosion wear of Ni-Cr cast iron was studied by Xie etal[111]. Results show that after oil quench at 960 ℃ and temper at 250 ℃, the alloy carbide $(Fe, Cr)_3C$ works as a wear resistant skeleton to distribute wear uniformly in the matrix. The erosion wear mechanism was selective wear.

The wear characteristics of a ductile iron and a carbon steel were studied at 25 ℃-400 ℃ by Wei etal[112]. Results showed that oxidative wear played an important role in the wear process. During sliding, especially at a higher sliding velocity and normal load, oxidation is intensified and tribo-oxides form on the worn surfaces. The development of oxidative wear markedly affects the wear behavior and mechanisms of Fe-C alloys.

The abrasion resistance of ferritic steels AISI 439 and 444 steels were found to be moderately better than those of austenitic steel AISI 304 and low-carbon steel SAE 1010 in the abrasion test. The presence of Cr and Ti carbides present in the microstructure could explain the better wear resistance of the ferritic AISI 439 and 444. The wear resistance of the low carbon 1010 steel is the lowest among the steels because of the low hardness of the ferritic-pearlitic microstructure.[113]

Ingot cast AISI D2 and advanced PM cold-work tool steels were evaluated with respect to galling resistance. Wear tests were performed at different contact pressures under lubricated conditions. It was found that the nitrogen alloyed PM tool steels has best galling resistance.[93]

2.3.4.4.2 Methods to improve wear resistance

1. Surface modification methods

Tribological properties of ductile iron can be greatly improved by local surface reinforcement. Through the formation of carbides, a hard transition or functional gradient zone is formed which carries the load, maintains low friction and improves the wear resistance. If austempered at 350℃, the wear resistance of ductile iron will become comparable or even better than a reference Hadfield grade steel, i.e. a wear-resistant steel. [114].

Thermal spray and WC-Co based coatings are widely used in areas subjected to abrasive wear.[115] The wear behavior of thermal sprayed iron-based-alloy-coatings were studied by means of the Pin-on-Disc test with two counterparts made of stainless steel and ceramic.[116] Multi-component white cast iron was applied by High Velocity Oxygen Fuel (HVOF) thermal spray process. The effects of substrate type, substrate pre-heating and heat treatment of coating on mass loss were determined. Heat-treated coatings had a mass loss 3 times lower than for as-sprayed coatings. In the heat-treated coating, the lower mass loss is due to sintering. [117] A NiCrBSiFeC powder was sprayed on a AISI 1020 steel using a HVOF technique. The thickness of the coating was approximately 0.5 mm. The microhardness was improved from175 HV to1075HV and the coatings exhibited 3 to 6 times improved wear resistance as compared with the base material.[118]

Electron brush-plating technique was used to make a coating to improve wear resistance of Cr12MoV die steel. The results indicate that the wear-resistance of the die steel can be improved respectively by 6.4 and 3.9 times.[119]

The hybrid method of PEO and hot-dipping aluminum was employed to deposit composite ceramic coatings on Q235 steel. The results revealed that metallurgical bonding can be observed between the substrate and the ceramic coatings. The hardness of the ceramic coatings is about HV1300, which is 10 times higher than that of the Q235 steel substrate, which gives rise to the better wear resistance of the ceramic coatings. [120]

Siva [121] and Akhbarizadeh [122] found that the wear resistance of 100Cr6 bearing steel and D2 tool steel could be improved using a deep cryogenic treatment (DCT).

Pack chromising treatment is an environmentally friendly alternative to hard chromium to form wear and corrosion resistant surface layers. AISI 1060 steel pack chromised for 9 h at 1050 ℃ shows equivalent wear resistance and corrosion properties, compared with that exhibited by the hard chrome.[123]

Chang [124] treated AISI H13 steel with oxynitriding, CrN coating, and a combination of CrN and oxynitriding to investigate wear resistance. All treated specimens showed a higher wear resistance (very shallow wear), while the untreated specimen showed obvious traces of ploughing cracks. The lowest measured coefficient of friction (0.28) was for CrN coated with oxynitriding.

The effect of induction hardening and boronising treatment on the wear behaviour of GGG-70 cast iron was investigated by Calik[125]. The pin-on-disc wear tests showed that the boronising improved the wear performance of the cast iron compared to the induction hardened one, as a result of increased surface hardness.

2. Coatings and coating methods

Hardened surface layers fabricated on substrates are introduced in many cases to fulfill the basic structural requirements of acceptable wear resistance. Gurevich [126]

developed a relatively simple process for coating of porous powder steel parts with a dense layer of white cast iron. The wear resistance of coatings in conditions of abrasive wear was comparable to that of high-Cr cast iron.

Composite diamond-DLC coated nanoprobe tips for wear resistance and adhesion reduction was studied by Gou etal [103]. Results showed that the composite diamond-DLC deposition reduced the adhesion and wear of the probe.

The WC and high-Cr cast iron layer on the surface of ZG30 steel were obtained by infiltration casting process. The maximum hardness of the alloyed layer surface is 820Hv. When the content of WC is 15%, the penetrating layer has the highest wear resistance which is 18.8 times as high as the matrix.[127]

Fan etal [128] investigated the wear resistance and high-temperature oxidation of a hot dipped Al-Si-Y coating on SCH12 heat resistant cast steel using a high-temperature pin-on-disc tribometer at 650 ℃. The coated specimen had significantly improved high-temperature wear resistance and equivalent oxidation resistance compared with the original SCH12 steel specimen.

Recent research has placed emphasis on nitride coatings to improve wear resistance. A CrN coating is characterized by its fine grain and low-stress structure. TiN coatings are widely used for wear protection on tools and machine parts.[129, 130] Coating with ternary nitrides Cr-Al-N and Cr–Si–N can enhance performance as manifested by the coefficient of friction, wear rate, hardness and toughness.[131, 132] Cr and CrN multilayer coatings show excellent bonding between the constituent layers, which results in high adhesion, and good wear and corrosive resistance. [133]

Techniques to obtain these nitride coatings are dc, pulsed dc and modulated pulse power magnetron sputtering (dcMS, PMS and MPP) by sputtering using a Cr metal target[134] a pulsed DC balanced magnetron sputtering system[135]; modified ion beam enhanced magnetron sputtering and by lateral rotating cathode arc on stainless steel substrate;[136] AC reactive magnetron sputtering;[137] and dual RF magnetron sputtering system[138]. The process parameters will affect the microstructure, hardness and wear properties of the coatings.

The $CO_2$ laser surface alloying technique was used to form wear resistant layers on a medium carbon steel with spherical WC powder. The effects of WC particle size on the abrasive wear resistance were investigated and WC powder of 88-100 μm diameter produced the best wear resistance.[139]

Singh etal [140] examined NbN coatings deposited on steel substrates by reactive DC magnetron sputtering. The coated steels showed higher hardness, better adhesion and a low coefficient of friction.

Dry sliding wear tests were conducted on AISI 316 austenitic stainless steel plasma coated with NiCrBSiCFe alloy powder. Uniform lamellar microstructure with fewer amounts of pores which shows better wear resistance was obtained. The wear rate at $250^{o}$C was higher due to material softening and adhesion by intermolecular bonding. The worn debris generated during sliding at $350^{o}$C turned into oxides which behave like a protective and lubricative film.[141]

The effect of Ni-WC composite overlays deposited by plasma transfer arc welding was studied by Liyanage etal [142]. The Ni-WC overlays produced using these dilute alloys generally performed better in ASTM G65 wear tests, due to the increased fraction

of retained WC phase, and the reduced fraction of secondary brittle carbide phases when the Ni-alloy contained no Cr.

2.3.4.4.3. Factors that affect wear behaviour

The literature also shows that a number of factors can affect the wear performance.

Sliding wear resistance of the nanostructured bainitic microstructure increases as the austempering temperature decreases from 260 ℃ to 220 ℃. The higher wear resistance of the austempered sample, at the decreased temperature, is attributed to the increased hardness and acceptable toughness, caused by the decreased lath thickness of bainitic ferrite and the lower amount of retained austenite.[143]

The effect of graphite nodule characteristics such as nodule count, nodule size and nodularity on the wear performance of ductile iron has been studied. Abedi etal [144] researched the effect of nodule count on the sliding wear performance of a ferritic-pearlitic ductile iron. Results showed that the oxidative wear mechanism is operative at lower loads, while adhesive wear, which is associated with delamination, was predominant at the higher loads. At the lower loads, the samples with the high nodule count exhibit a lower wear rate. At the higher applied loads, wear performance deteriorates with increasing nodule count.

Porosity was observed to be beneficial for wear resistance by entrapping the wear debris and preventing the formation of large abrasive agglomerates. Pore filling superficially reinforced the material, and diminished plastic deformation and particle detachment around the pores.[106] In the present study, similar mechanisms could be expected because the graphite nodules can be treated as pores.

The tribological behavior of PM steels is dependent on the wear conditions. Results showed that for small mean pore sizes (10 μm) and a porosity lower than 9%, the wear resistance increased with decreasing porosity and an abrasive wear mechanism dominated. For a large mean pore size (12-18 μm) and a porosity higher than 21%, the wear resistance decreased significantly with increasing porosity and pore size.[145]

Koszela etal [146] carried out block-on-ring to explore the effect of oil pockets of spherical shape on the wear resistance and wear intensity. The block samples were made from bronze B101. The rotated rings were made from 42CrMo4 steel. The tested assembly was lubricated by a mineral oil, L-AN 46. It was found that sliding pairs with textured specimens were not superior to a system with a turned block with regard to abrasive wear resistance.

Zhong etal [147] studied on wear performance of a NbC particle-reinforced iron matrix composite at different NbC particle volume fraction values. The composite was fabricated by compounding gray cast iron with niobium wires through an in situ technique comprised of an infiltration casting process and a subsequent heat treatment. Results showed that the wear resistance of the bulk composite increased with increasing NbC volume fraction.

# CHAPTER III

# EXPERIMENTAL DETAILS

## 3.1 Overview

In the present research, austempered ductile iron (ADI), ductile iron (DI), and gray iron (GI) were treated using Gas nitriding + nitrogen cooled down to 800$^{o}$F (Blue)", "Gas nitriding + cooled down to 300$^{o}$F (Gray)", and "Gas nitriding + oil quenched (Oil)". After the samples were nitrided, the nitrided layer was characterized using optical microscopy, Vickers microhardness testing, and scanning electron microscopy (SEM). Wear tests were carried out to comparatively investigate the effects of these nitriding methods on the wear behavior of these cast irons under lubricated conditions. 4140 steel was heat treated using Isonite, QP or QPQ salt bath nitriding processes, and wear testing of the Isonited 4140 steel samples were performed.

All the wear tests were done using a ball-on-disc test apparatus. Experimental investigations consisted of sample preparation, original material characterization, and nitriding, nitrided materials characterization, including microstructure observation through optical metallography, roughness testing, and microhardness.

To evaluate the wear resistance, the wear track width and depth were measured by Scanning Electron Microscopy (SEM), White Light Interferometry and roughness two-dimensional profilometry tester, and then compared with the compound layer thickness and diffusion zone depth. Along with the SEM examination, the chemical composition at specific locations were determined by energy dispersive spectroscopy (EDS). As mentioned previously, Vickers microhardness and surface roughness were also measured to assist in the analysis of the wear behaviour of the samples.

## 3.2 Sample preparation

### 3.2.1 Materials

The chemical composition (wt%) of the cast irons in the as-cast condition as determined by optical emission spectroscopy is shown in Table 3.1. The chemical composition (wt%) of the 4140 steel is given in Table 3.2.

Table 3.1 Chemical composition (wt%) of cast irons in as-cast condition

| Element | GI | DI | ADI |
|---|---|---|---|
| C | 3.30 | 4.72 | 3.76 |
| Mn | 0.40 | 0.26 | 0.24 |
| P | 0.057 | 0.008 | 0.28 |
| S | 0.053 | 0.009 | 0.0005 |
| Si | 2.21 | 2.47 | 2.51 |
| Cr | 0.04 | 0.04 | 0.03 |
| Ni | 0.03 | 0.07 | 1.61 |
| Mo | 0.01 | 0.01 | 0.11 |
| Cu | 0.50 | 0.39 | 0.78 |
| Al | 0.007 | 0.013 | 0.17 |
| V | 0.007 | 0.019 | 0.009 |
| Cb | 0.004 | 0.004 | 0.001 |
| Ti | 0.005 | 0.011 | 0.005 |
| Co | 0.016 | 0.029 | 0.023 |
| Sn | 0.045 | 0.051 | 0.002 |
| B | ND | ND | ND |
| Mg | ND | 0.079 | 0.0057 |
| W | 0.003 | 0.003 | 0.011 |

*ND = None Detected

Table 3.2: Chemical composition (wt%) of 4140 steel

| Element | C | Mn | P | S | Si | Cr | Mo |
|---|---|---|---|---|---|---|---|
| 4140 Steel | 0.40 | 0.87 | 0.035 | 0.04 | 0.87 | 0.90 | 0.20 |

The microstructural features such as nodularity, nodule roundness and pearlite level of DI and ADI, as provided by the supplier, are given in Table 3.3. Despite the difference in chemistry, DI and ADI exhibit similar characteristics. The graphite morphology will be discussed further in section 4.2 based on micrographs of unetched (polished) samples.

Table 3.3: Nodularity, nodule roundness and pearlite level of DI and ADI

| Material | Nodularity (no flakes) | Pearlite level | Roundness |
|---|---|---|---|
| DI | 100% | 90% | 100% |
| ADI | 100% | 90% | 100% |

The microstructural characteristics of GI, again as provided by supplier, are given in Table 3.4.

Table 3.4: The microstructural characteristics of GI

| Material | Type | Size | Pearlite level | Pearlite spacing | Carbide level |
|---|---|---|---|---|---|
| GI | A | Class 3 (A=23 mm) | 95% | Coarse | Trace carbide |

3.2.2 Geometry of nitrided samples

The samples were prepared with different shapes. The diameter of the samples of DI and ADI are both 76mm, with the thickness 8mm and 14 mm, respectively. The dimensions of the samples of GI and 4140 steel are 54mm ×54mm ×11 mm and 54mm ×54mm ×14mm, respectively. Detailed drawings are given in Figures 3.1(a)-(d).

The differences in these dimensions are considered to have little effect on the wear properties of the nitrided materials, because the nitrided zone is very thin (generally, the sum of compound layer and diffusion zone is always less than 1mm), and all wear tests are conducted on the same flat surface (no corner or edge effects)

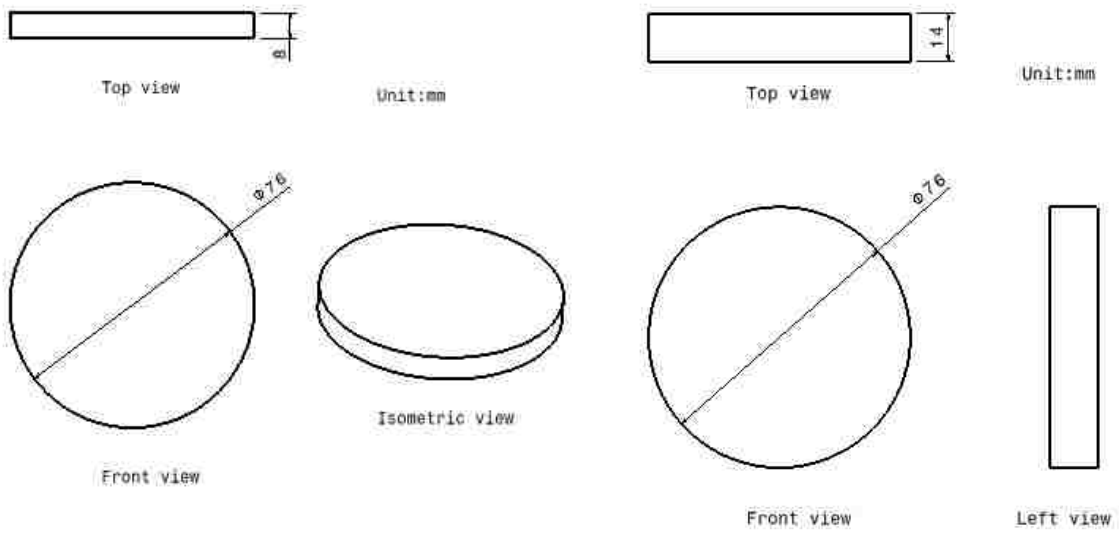


(a) The dimensions of DI samples (b) The dimensions of ADI samples

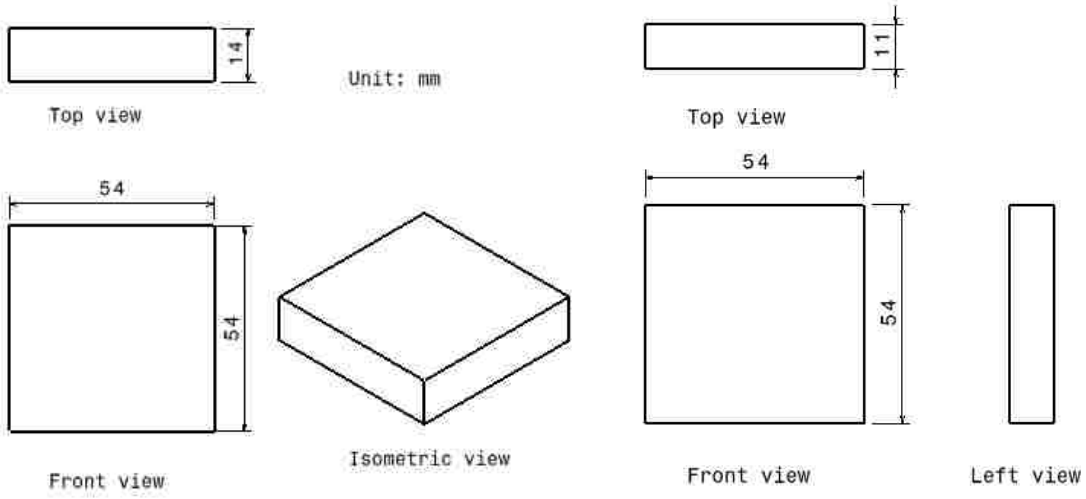


(c) The dimensions of GI samples (d) Dimensions of 4140 steel samples

Figure 3.1: The dimensions of the samples for nitriding

Figure 3.2 illustrates the sectioning of the samples of the DI, ADI, GI and 4140 steel samples for material characterization. They were sectioned using wire-cut EDM (electrical discharge machining), to ensure the least damage to the specimen, in particular to the thin nitrided layer.

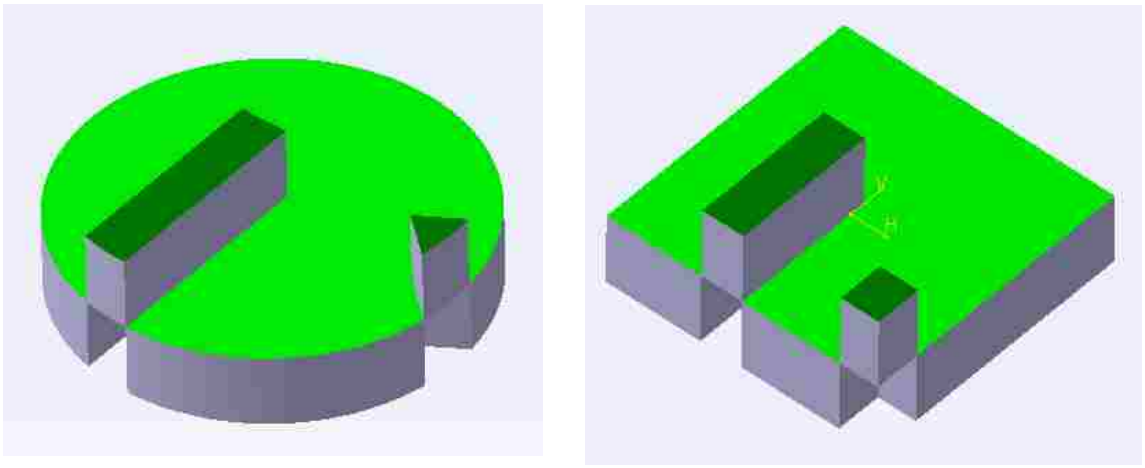

(a) The sectioning of DI and ADI samples for material characterization

(b) The sectioning of the GI and 4140 steel sample for material characterization

Figure 3.2: Sectioning methods used for the samples of the DI, ADI, GI, and 4140 steel for material characterization

3.3 Nitriding methods

The nitriding processes designed for DI, ADI and GI are given at Table 3.5. They are: “Gas nitride + nitrogen cooled down 800F (blue color)”, “Gas nitride + cooled down 300F (gray color)”, “Gas nitride + oil quenched (gray color)”.

Table 3.5: Nitriding methods and parameters for cast irons

| Material | Gas nitride + nitrogen cooled down $800^{o}$F (Blue) | Gas nitride + cooled down $300^{o}$F (Gray) | Gas nitride + oil quenched (Oil) |
|---|---|---|---|
| DI | √ | √ | √ |
| ADI | √ | √ | √ |
| GI | √ | √ | √ |

The nitriding processes for the 4140 steel are given in Table 3.6.They are all salt bath nitriding processes. QP stands for Quench-Polish. It is composed of three main steps, namely, (i) salt bath nitriding at around 580$^{o}$C for 90 minutes; (ii) quench in cooling bath for 10 minutes, and (iii) polish through tumble blast for 3 minutes. QPQ stands for Quench-Polish-Quench. A second Quench (Post-oxidation at around 400 $^{o}$C) is introduced after QP, followed by a cool down to room temperature.

Table 3.6: Nitriding treatments for 4140 steel

| Material | Isonited | QP | QPQ |
|---|---|---|---|
| 4140 | √ | √ | √ |

## 3.4 Wear testing

All the wear tests were done under lubricated conditions using a ball-on-disc test apparatus. Figure 3.3 is a schematic illustration of the apparatus. All tests were performed according to ASTM G190-06[148] and ASTM G133-05(2010) [149] standards.

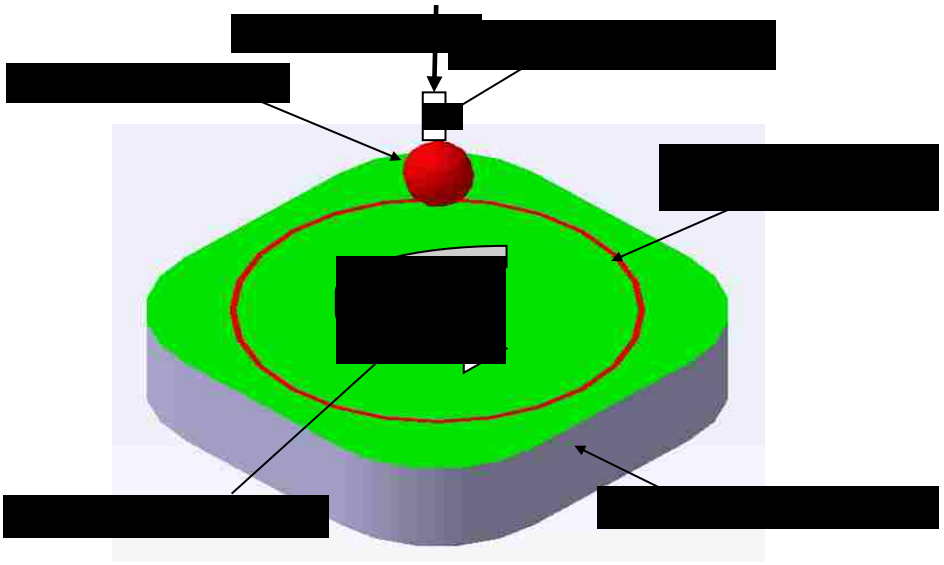

Figure 3.3: Schematic illustration of ball on disc wear test apparatus

They were carried out on a ball on disk wear test apparatus under lubricated condition with constant load of 10 lbs for 1 hour. The rotation speed is constant, 1.67m/s (700 rpm, wear track radius 22.75mm). The lubricant is 4ml light mineral oil. The coefficient of friction was recorded during the test. As the counterface in the wear test, the properties of ceramic ball are key to the wear behavior of the test materials. Detailed information of its characteristics are given in Table 3.7[150]. It should be emphasized that a "new" ceramic ball is used for each wear test.

Table 3.7: Characteristics of ceramic ball[150]

| | |
|---|---|
| Material | Nonporous High-Alumina Ceramics |
| Diameter | 5/16" |
| Diameter Tolerance | ±.0001" |
| Sphericity | 0.000025" |
| Hardness | 1700 Vickers |
| Grade | 25 |
| Operating Temperature Range | Up to +2000 °F |
| Flexural Strength | 47,000 psi (324 MPa) |
| Compressive Strength | 300,000 psi (2068MPa) |
| Porosity | Nonporous |
| Performance Characteristic | Poor temperature insulator, Poor electrical insulator |
| Color | Opaque White |
| Tolerance | Standard |
| Notes | Machine using diamond grinding wheel. |

To evaluate the wear resistance, the wear track width and depth were measured by White Light Interferometry, SEM and Roughness two-dimensional profilometry tester, and compared with the compound layer thickness and diffusion zone depth. At the same

time the chemical composition at specific locations alone the wear track were examined using energy dispersive spectroscopy (EDS).

3.5 Optical metallography

To reveal microstructures of the samples prepared for optical micrographs observation, the samples were prepared according to ASTM E768-99(2010)[151]. After sectioning, they were mounted in plastic, ground on a series of SiC papers (240, 400, 600, 1200 grit), polished with 1.0μm and 0.5μm $Al_2O_3$ powder on a Buehler polisher, and then etched by 4% nital solution for around 5s. All of the surfaces to be examined were polished to a mirror finish and then cleaned with water and 95% ethanol liquid before and after etching. The optical microscope used in the present study is shown in Figure 3.4. All sections examined were cross-sections perpendicular to large flat surface.

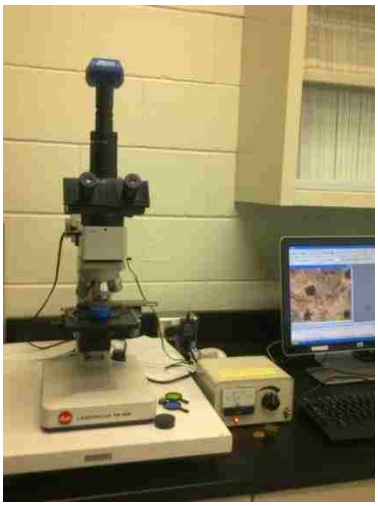

Figure 3.4: Optical microscope

3.6 Microhardness

A CSM Micro-Hardness Tester (MHT) was used to measure the microhardness of the compound layer, diffusion zone and the nitrided surface. The load used was 0.025N. This tester is ideally suited to the characterization of hard coatings, thick soft coatings

and bulk materials. It provides accurate and reproducible values for the hardness of a variety of materials and coatings of greatly varying thickness and hardness values. It was equipped with the automated optical microscope and high resolution camera, a PC software package for data acquisition, storage and analysis. With the high resolution camera we can do the indentation on the specific desired points or phase, such as the compound layer and the pearlite or bainite phase in the matrix. Figure 3.5 shows an example of the load curve that used to calculate the microhardness. Curve #1 corresponds to the loading process. Curve #2 is the unloading process. #3 is shows the shape of the square indent. The Vickers Diamond Pyramid microhardness value is the applied load (kgf) divided by the surface area of the indentation ($mm^2$) (ASTM E384-11[152]):

$$\mathrm{HV} = 1.854\frac{P}{\mathrm{d}^2} \qquad (6)$$

Where HV=Vickers hardness; P=Load in kgf; d=Arithmetic mean of the two diagonals in mm.

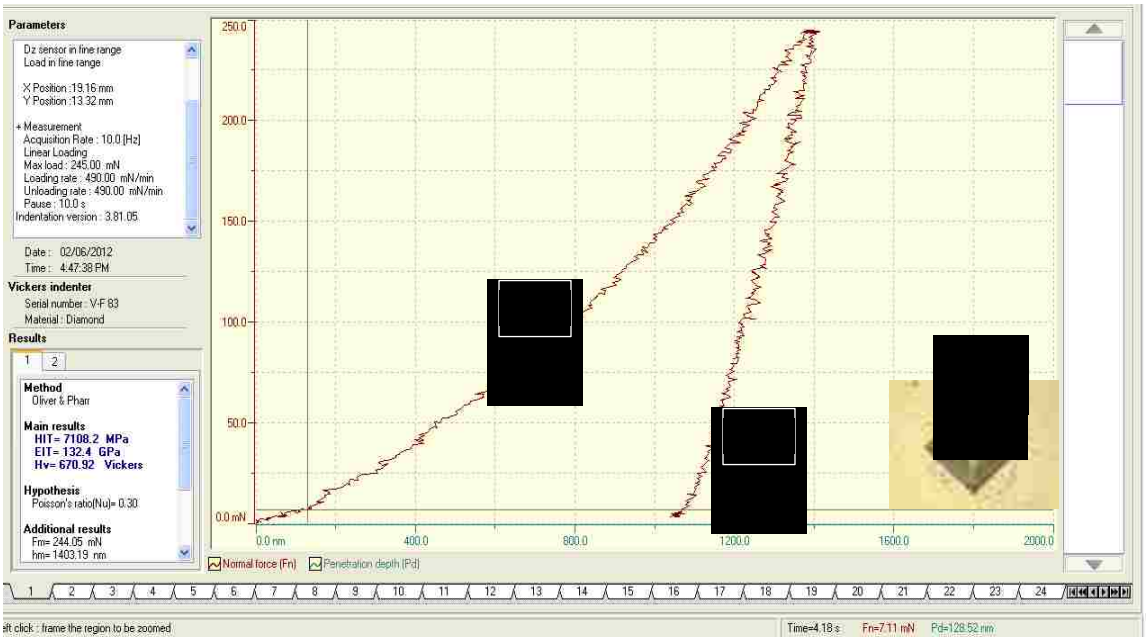


Figure 3.5: An example of the load curve in the measurement of microhardness

3.7 Surface roughness

Many methods are available for the measurement of the micro or macro geometrical features of surfaces, such as optical methods using reflection, interference or electron microscopy, and mechanical methods like oblique sectioning and profilometry. The optical methods have advantages of providing a three dimensional characterization of the surface. The best known profilometry method to obtain surface profiles is the stylus method. As the name indicates, a fine diamond stylus traverses the surface and its vertical movements are recorded by electrical systems.[84]

In this study, surface topographies of the nitrided surface layer were characterized by a two-dimensional profilometry tester (Mitutoyo SJ201), according to ASTM B946-11[153]. This profilometer, Figure 3.6, provides a representative length of the surface and a high resolution in a perpendicular plane. The major disadvantage of this instrumentation is that it is restricted to a single line sample which might not be representative of the whole surface if the surface has anisotropic characteristics. Nevertheless, it can still provide a useful measurement of the parameters required for roughness characterization.

Figure 3.6: The profilometer used for roughness measurement

3.8 Scanning Electron Microscopy (SEM)

A FEI Quanta 200 FEG SEM equipped with an energy dispersive X-ray spectroscopy (EDS) system was used to characterize the wear track and debris and to help identity the wear mechanisms. The system is designed with a single window user interface allowing for straightforward and flexible analysis. This interface allow a quick switch between the SEM image mode and EDS analysis mode. EDS was used to quantitatively determine the composition at selected locations on the wear tracks. The SEM and EDS systems are shown in Figure 3.7, and Figure 3.8 shows the user interfaces of EDS coupled to the SEM.


Figure 3.7: SEM system used in this study

Figure 3.8: The user interfaces of EDS coupled with SEM

# CHAPTER IV

# EXPERIMENTAL RESULTS AND ANALYSIS

## 4.1 Overview

In this chapter, results are presented for the microstructure of the cast irons and 4140 steel, measurements of the compound layer thickness and diffusion zone depth, surface roughness, surface and through thickness microhardness of the nitrided layer and diffusion zone, and wear testing and characterization of worn materials. The wear performance is then correlated to the microstructure and mechanical properties.

## 4.2 Optical metallography

### 4.2.1 Unetched cast irons

The graphite nodule count, nodule size and nodularity (for DI and ADI) of ductile iron and the graphite flakes of GI may affect the wear properties to a different extent. To observe the graphite shape, size, count and nodularity and graphite content, the polished surface of the cast irons were observed directly without etching.

From Figure 4.1 to Figure 4.3, the difference of graphite shapes can be seen clearly. The graphite shapes of DI and ADI are both nodules, while the graphite of GI is flake. They are all distributed in a random fashion.

The area fractions (graphite content) were obtained from the black and white pictures on the right side, which were processed by Image J, according to ASTM A247 - 10[154] and ASTM E1245 - 03(2008)[155]. It is found that the graphite contents based on 50X pictures are always higher than those based on 100X pictures. Probably the reason for this phenomenon is that the graphite edge was colored black at the lower magnification. Generally, there was good agreement with the data from supplier on the nodularity (100%), and roundness (100%).


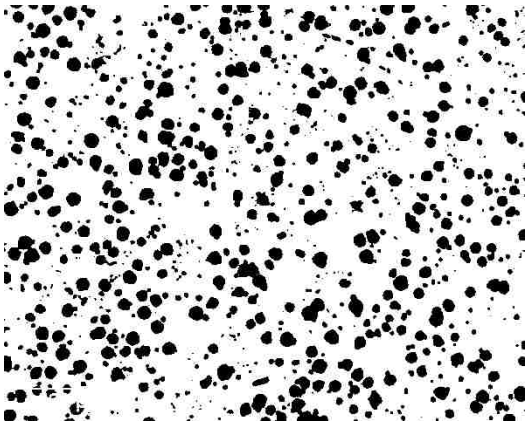

(a) Optical micrograph (b) After Image J software processing

Figure 4.1: Metallography of unetched samples-DI, 50X (Graphite content: 20.6)


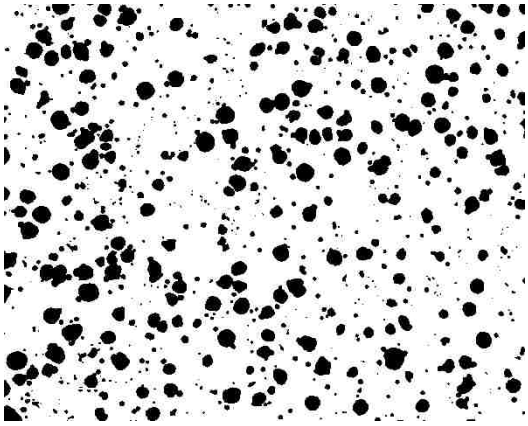

(a) Optical micrograph (b) After Image J software processing

Figure 4.2: Metallography of unetched samples-ADI, 50X (Graphite content: 18.3)


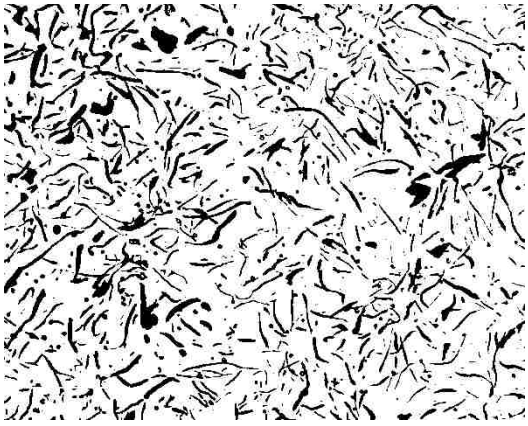

(a) Optical micrograph (b) After Image J software processing

Figure 4.3: Metallography of unetched samples-GI, 50X (Graphite content: 19.6)

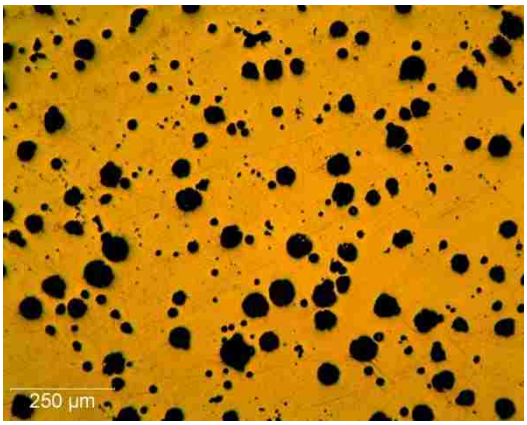


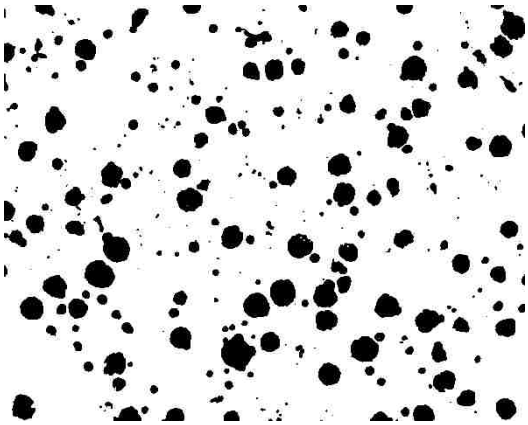

(a) Optical micrograph (b) After Image J software processing

Figure 4.4: Metallography of unetched samples-DI, 100X (Graphite content: 14.7 )

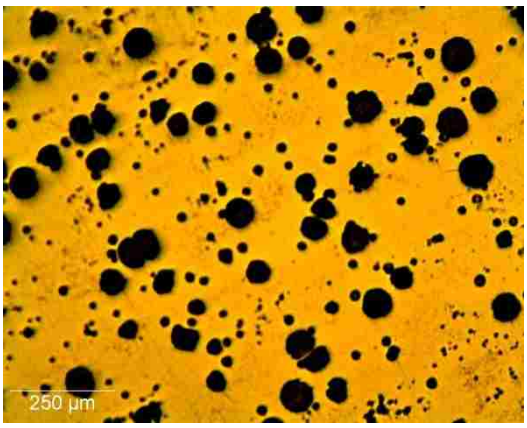


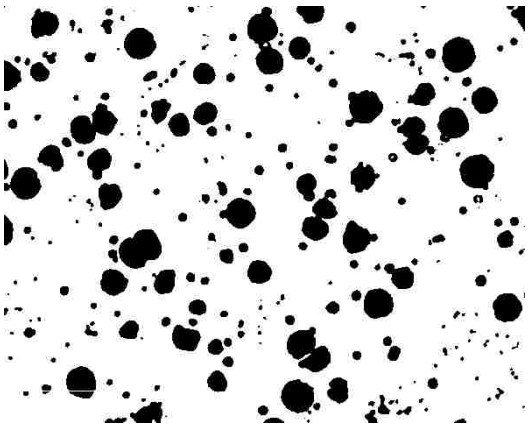

(a) Optical micrograph (b) After Image J software processing

Figure 4.5: Metallography of unetched samples-ADI, 100X (Graphite content: 16.8 )


(a) Optical micrograph (b) After Image J software processing

Figure 4.6: Metallography of unetched samples-GI, 100X (Graphite content: 15.2)

A summary of the measured graphite fractions is given in Table 4.1 for both magnifications used, i.e. 50X and 100X. The data obtained at 100X magnification are plotted in Figure 4.7.

Table 4.1: Graphite contents of DI, ADI, and GI.

| Nitriding Process | Material | Graphite content (%) | | |
|---|---|---|---|---|
| | | 50X | 100X | |
| Blue | DI | 20.61 | 13.49 | 14.91 ±1.24 |
| | | 18.90 | 14.73 | |
| | | 18.43 | 16.52 | |
| | GI | 19.57 | 15.33 | 14.81 ±0.67 |
| | | 21.40 | 15.23 | |
| | | 21.18 | 13.86 | |
| | ADI | 18.29 | 14.52 | 16.11 ±1.12 |
| | | 17.28 | 16.82 | |
| | | 21.49 | 16.98 | |
| Gray | DI | 21.44 | 15.14 | 15.24 ±0.76 |
| | | 20.61 | 16.21 | |
| | | 24.19 | 14.36 | |
| | GI | 24.52 | 20.17 | 19.11 ±1.12 |
| | | 25.84 | 19.77 | |
| | | 26.59 | 17.40 | |
| | ADI | 22.45 | 14.52 | 16.35 ±1.49 |
| | | 22.59 | 18.16 | |
| | | 22.08 | 16.37 | |
| Oil | DI | 18.33 | 13.91 | 14.53 ±0.47 |
| | | 17.38 | 15.06 | |
| | | 19.96 | 14.62 | |
| | GI | 30.08 | 15.66 | 16.55 ± 1.15 |
| | | 28.05 | 15.81 | |
| | | 27.71 | 18.17 | |
| | ADI | 21.66 | 14.52 | 16.16 ±1.16 |
| | | 23.29 | 16.98 | |
| | | 20.97 | 16.98 | |

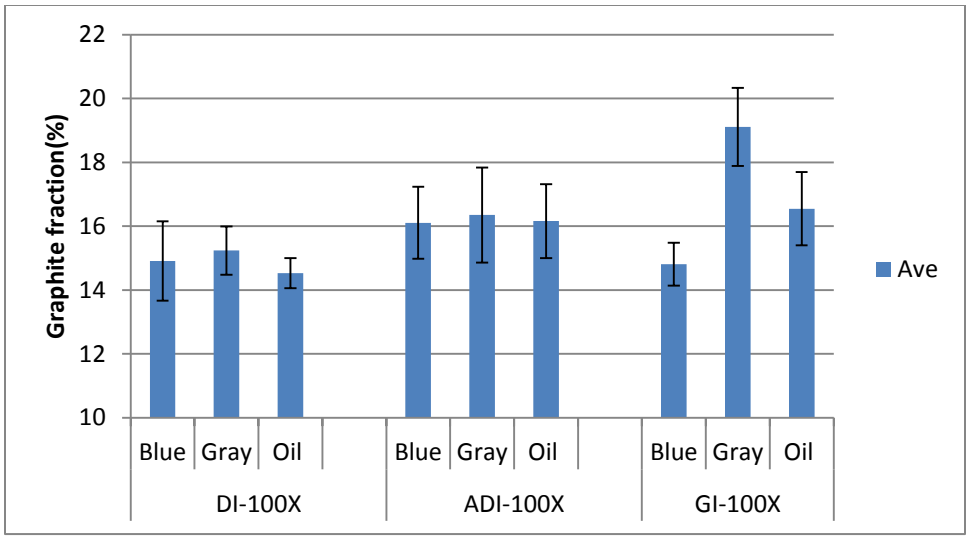


Figure 4.7: Graphite contents of cast irons obtained from 100X magnification optical images

There are a number of points to note from the data for graphite fraction. The first is the similar value for all three cast irons, being around 15%, with the exception of one of GI material (Gray nitriding), which was around 19%. Secondly, there was little or no effect of type of nitriding treatment on the graphite fraction. This is as expected since significant carbon dissolution from graphite would only occur at temperatures in the austenite phase region which is not the case for the nitriding treatments used.

4.2.2 Metallography of core material of cast irons and 4140 steel

Optical micrographs of the core materials are shown in Figures 4.8 to 4.11. The microstructure of DI, Figure 4.8, primarily consists of a pearlite matrix and graphite nodules with surrounding ferrite. The microstructure of ADI, Figures 4.9, consists of an ausferrite matrix and graphite nodules. The microstructure of GI, Figure 4.10 consists of a pearlite matrix and graphite flakes.

The macrostructure of the 4140 steel, Figure 4.11, consists of tempered martensite with a small amount of retained austenite. 4140 steel is a high tensile alloy steel, which is

normally hardened and tempered to a UTS range of 850 to 1000 MPa. This high strength is mainly attributed to the tempered martensite structure.

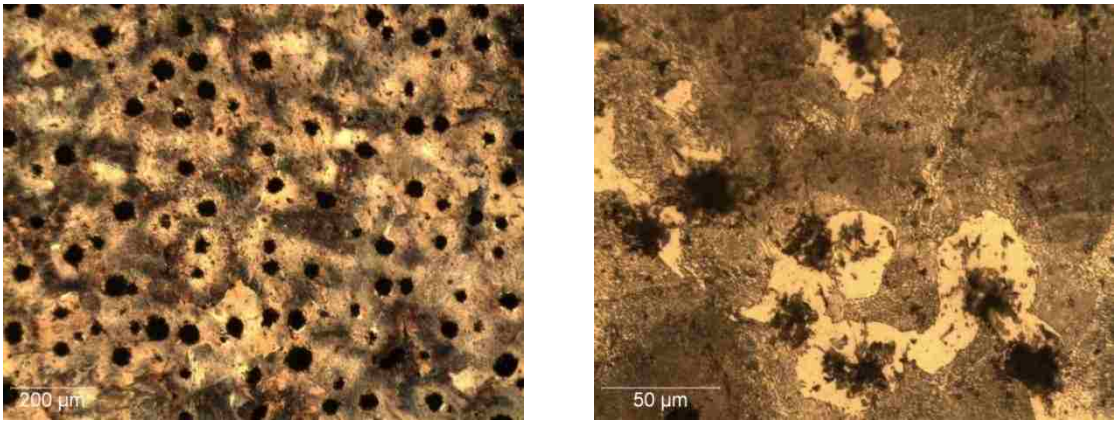


Figure 4.8: Microstructure of DI showing a pearlite matrix and graphite nodules surrounded by ferrite (white phase)

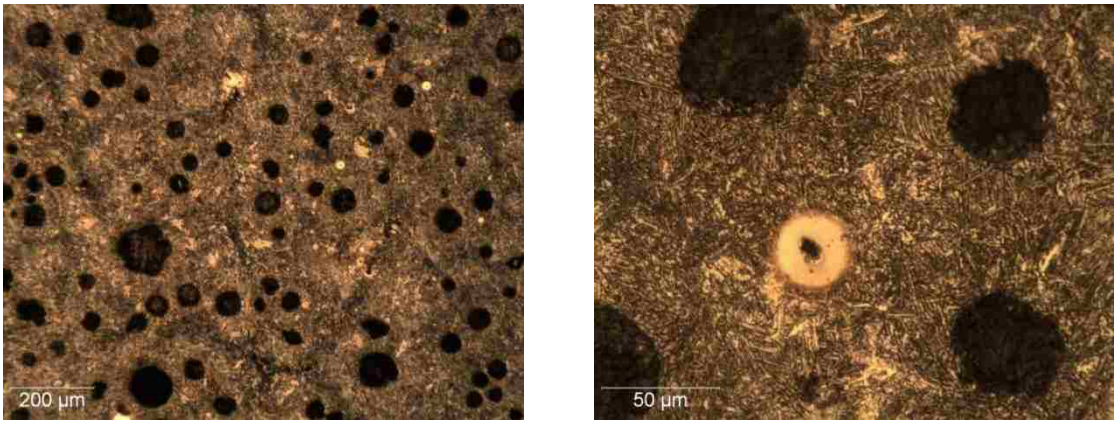


Figure 4.9: Microstructure of ADI showing an ausferrite matrix and graphite nodules

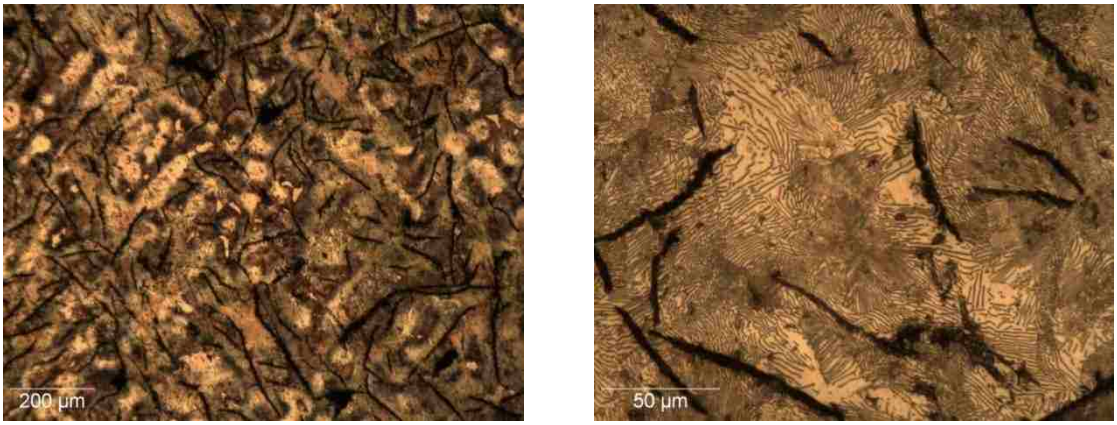


Figure 4.10: Microstructure of GI showing a pearlite matrix and graphite flakes

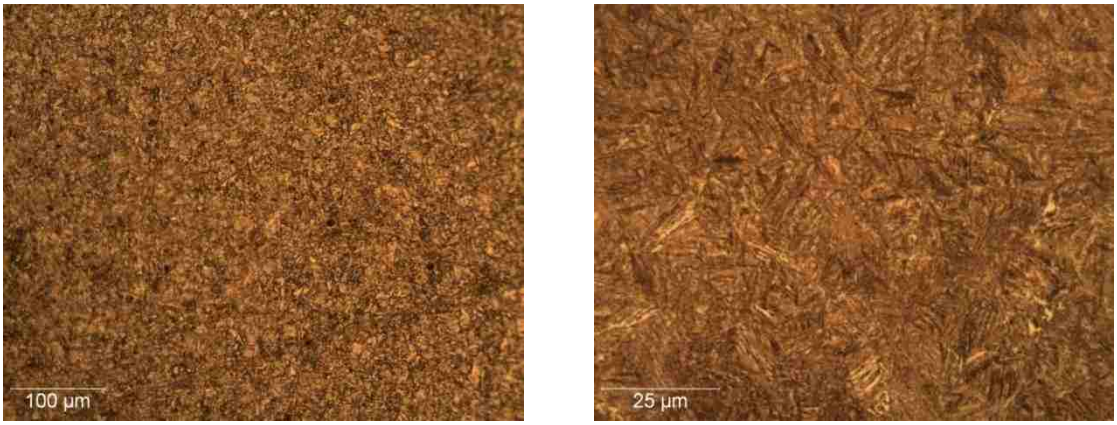


Figure 4.11: Microstructure of 4140 steel showing tempered martensite with a small amount of retained austenite

4.2.3 Metallography of nitrided layer

Optical micrographs of the three cast iron samples treated using the three gas nitriding processes were examined on optical microscopy, are presented in Figures 4.12 to 4.14. The microstructure of the nitrided case is generally composed of a thin compound layer (CL) with a diffusion zone (DZ) underneath. Good wear resistance is usually ascribed to this compound layer and the hardened diffusion zone.[44] The micrographs presented in Figure 4.12 to 4.14 were chosen to be representative of the nitrided layer across the sample surfaces. The thickness of the compound layer varies with type of cast iron and with nitriding process. The morphology also varies with material and process.

The nitrided layers on DI, Figure 4.12, are relatively thin but with little variability. The nitrided layers on ADI, Figures 4.13, show more variability in thickness. ADI treated using the Gray process is the thickest. In DI and ADI, the compound layers could envelope the graphite nodules. The morphology of the CL of GI is different from that for DI and ADI. For GI treated by either the Blue or Gray processes, the incorporation of the graphite flakes into the compound layer produces a very uneven surface, Figure 4.14. Data for the CL thickness and DZ depth are presented in the Appendix.

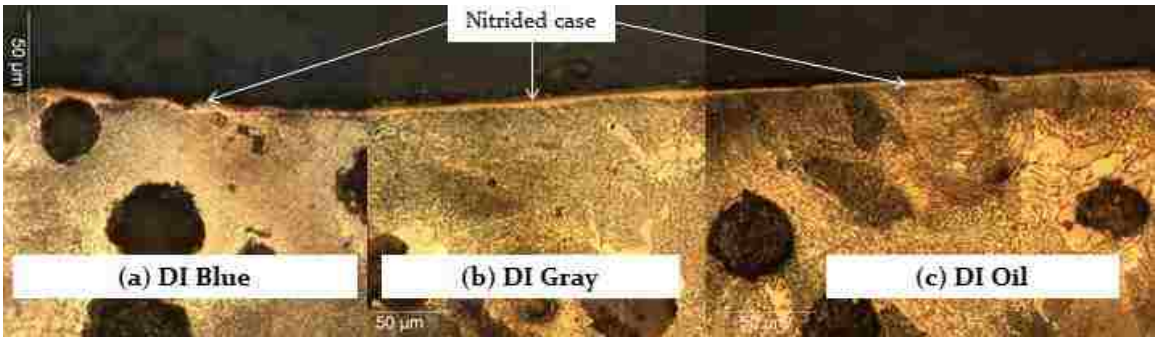


Figure 4.12: Microstructures of DI treated by Blue, Gray and Oil processes

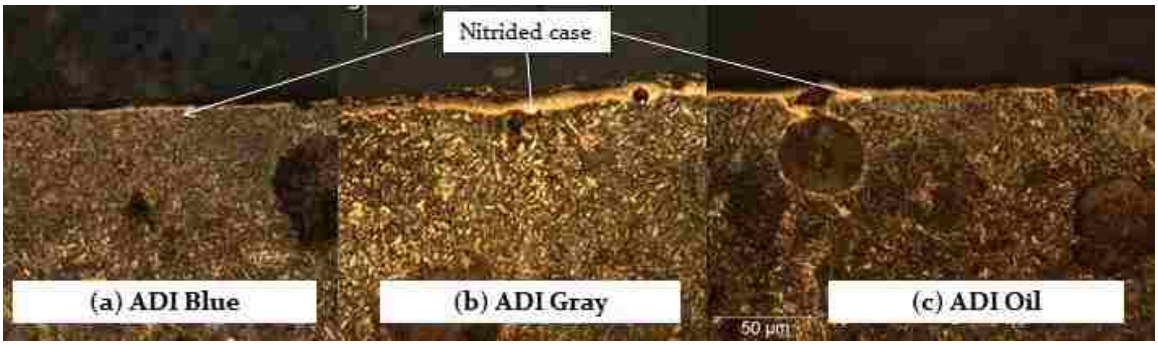


Figure 4.13: Microstructures of ADI treated by Blue, Gray and Oil processes

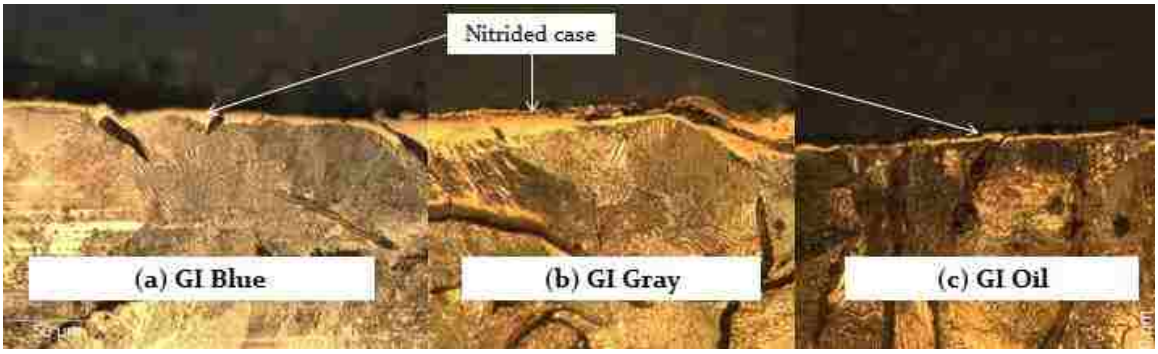


Figure 4.14: Microstructures of GI treated by Blue, Gray and Oil processes

Figure 4.15 presents the cross-sectioned micrographs for the 4140 steel treated using the Isonite, QP and QPQ processes. In Figure 4.15 (a) for the Isonite process, in addition to the compound layer, we can see larger ferrite grains which were generated in the salt bath nitriding process. This type of structure was not found for the QP, Figure 4.15 (b), or QPQ, (Figure 4.15 (c)) samples. Rather, the grain size in the diffusion zone is smaller

than in the core. The nitrided case for the QP is compact and even in thickness, Figure 4.15 (b). This is attributed to the polishing operation. The QPQ sample, Figure 4.15 (c) is similar to the QP sample except for slight differences in the appearance of the nitrided case due to the post-oxidizing operation.

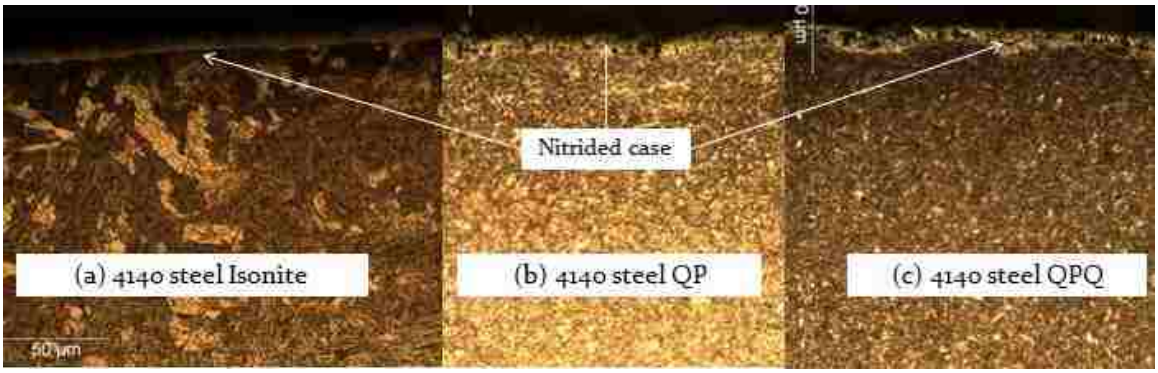


Figure 4.15: Microstructures of 4140 steel treated by (a) Isonite, (b) QP and (c) QPQ processes

Figure 4.16 is a schematic diagram showing the phases present at both the nitriding temperature, Figure 4.16 (a), and room temperature, Figure 4.16 (c), and the nitrogen distribution from the surface to the core. This diagram was developed using the iron-nitrogen equilibrium phase diagram, Figure 2.11, and the observations in the present study. ε-nitride and γ'-nitride are the hard phases that formed in the nitrided case during the nitriding process. The Fe-N phase diagram shows γ'-nitride to have a composition of $Fe_4N$, i.e. ~6 wt%N. ε-nitride exists over a composition range corresponding to $Fe_2N$ to $Fe_3N$, i.e. 8.1-11.1 wt%N. At room temperature we see that the compound layer generally consists of ε-nitride together with γ'-nitride. The diffusion zone contains γ'-nitride and α-Fe (N). α-Fe (N) represents α-Fe with nitrogen in interstitial solid solution. The N-content decreases through the diffusion zone into the core.

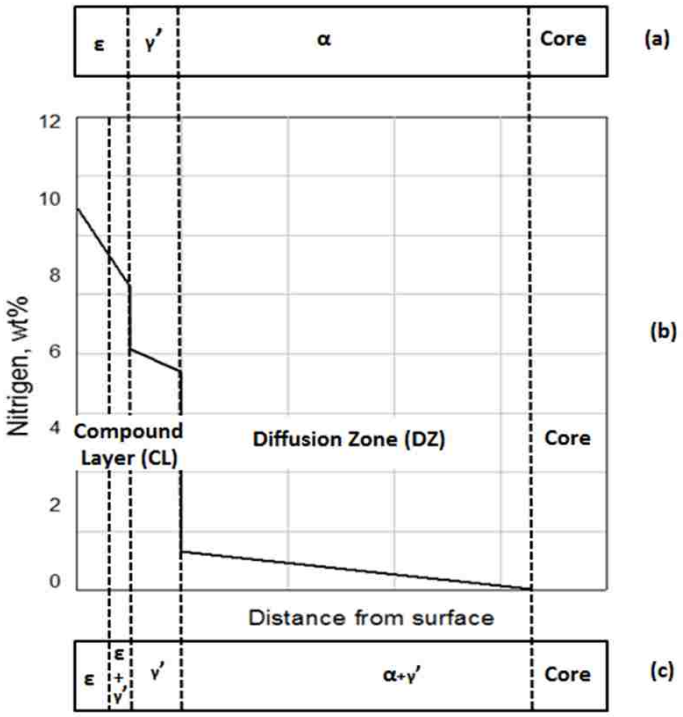


Figure 4.16: Microstructure and nitrogen distribution

(a) During nitriding; (b) Nitrogen distribution; (c) Microstructure at room temperature.

## 4.3 Compound layer thickness and diffusion zone depth

### 4.3.1 CL thickness and diffusion zone depth of cast irons

The compound layer thicknesses and diffusion zone depths of DI, ADI and GI were determined using the cross-sectional optical micrographs, as presented in section 4.2. As will be seen, and as suggested in Figure 4.16, there is a relationship between the compound layer thickness and the diffusion zone depth.

Figures 4.17 and 4.18 present the results of the CL thickness and the DZ depth measurements, respectively. From Figure 4.17, it can be seen that GI processed using Gray nitriding has thickest compound layer, while ADI processed using Blue nitriding has the thinnest compound layer. In general, the greatest variability in CL thickness was shown by GI.

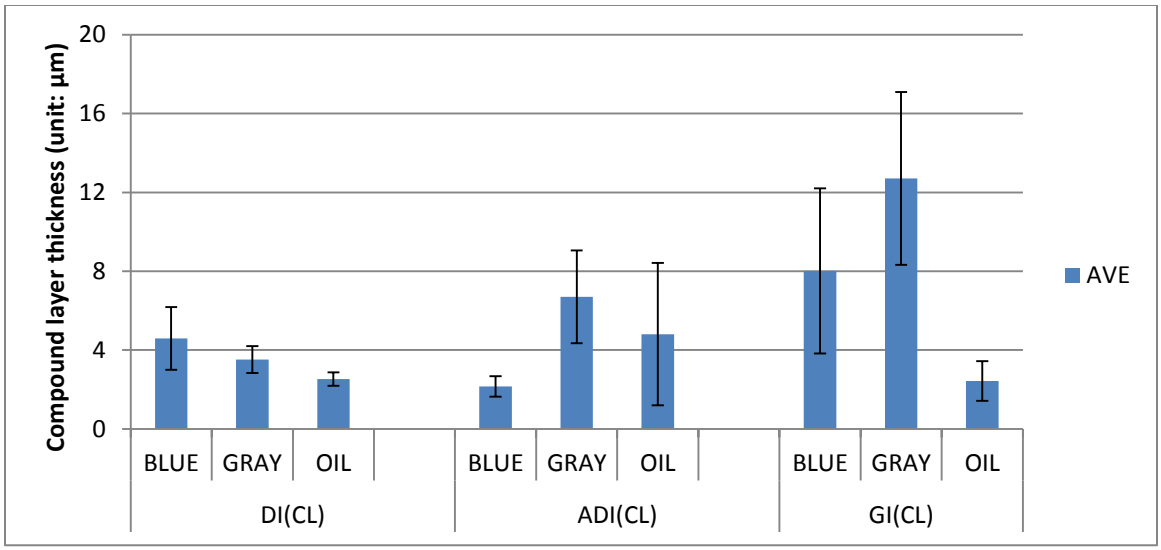


Figure 4.17: CL thickness of DI, ADI and GI treated using the Blue, Gray and Oil gas nitriding processes

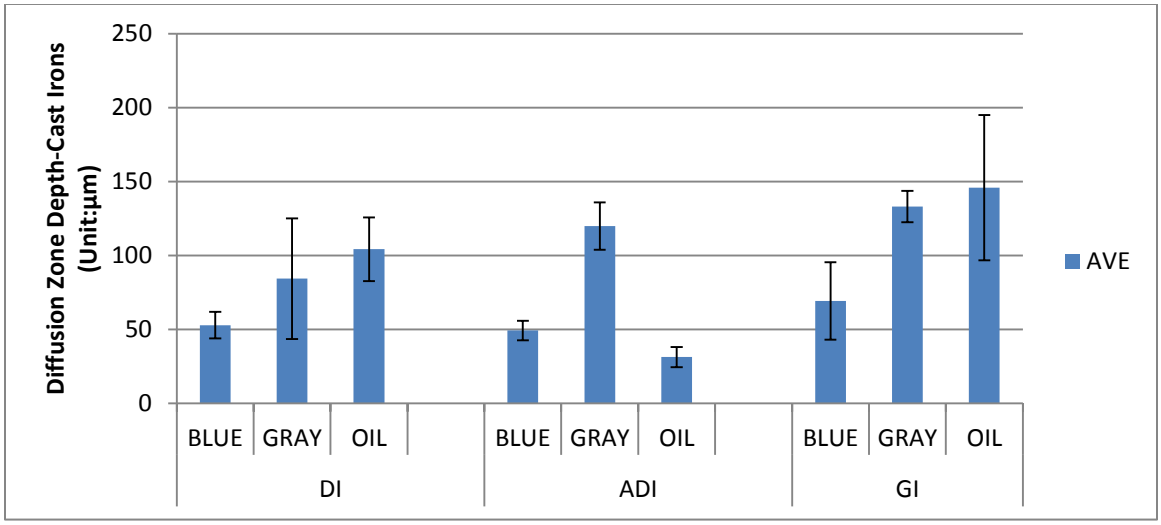


Figure 4.18: DZ depth of DI, ADI and GI treated using the Blue, Gray and Oil gas nitriding processes

From Figure 4.18, it can be seen that the diffusion zone depth largest for Gray Iron, which is same trend as for the compound layer. ADI generally has the smallest diffusion zone depth. Thus, the nitriding process that produced the highest compound layer thickness also produces larger diffusion zone depths.

To identify which cast irons have the highest capacity to be nitrided, and which nitriding treatment is the most effective in generating the compound layer, the data in Figures 4.17 and 4.18 are re-presented in terms of nitriding process or material in Figures 4.19 and 4.20, for the compound layer thickness and in Figures 4.21 and 4.22 for the diffusion zone depth.

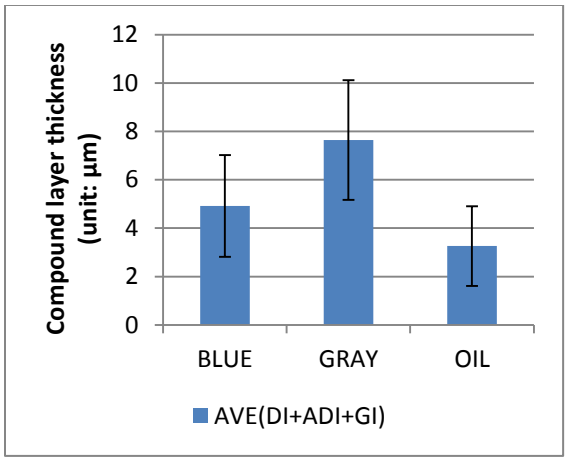


Figure 4.19: Compound layer thickness in terms of nitriding process

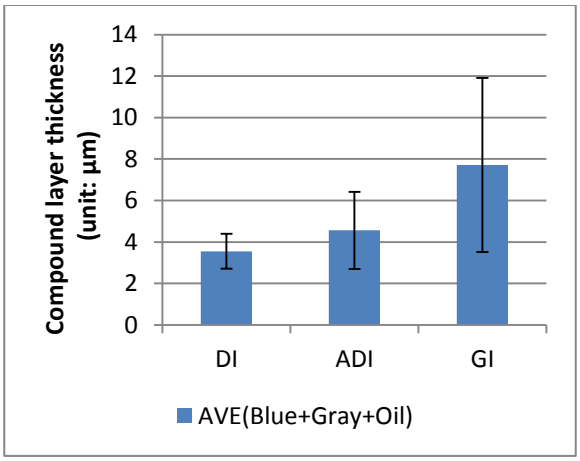


Figure 4.20: Compound layer thickness in terms of material

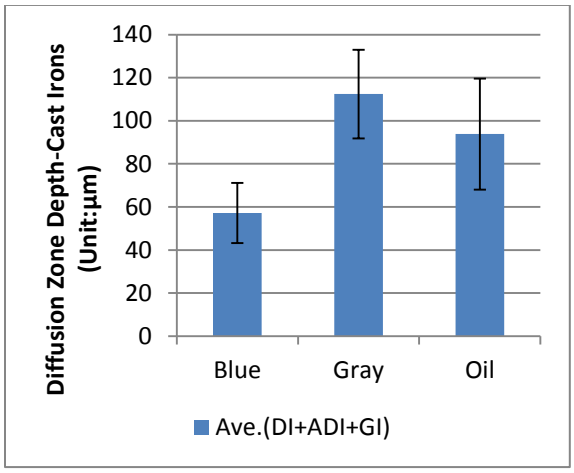


Figure 4.21: Diffusion zone depth in terms of nitriding process

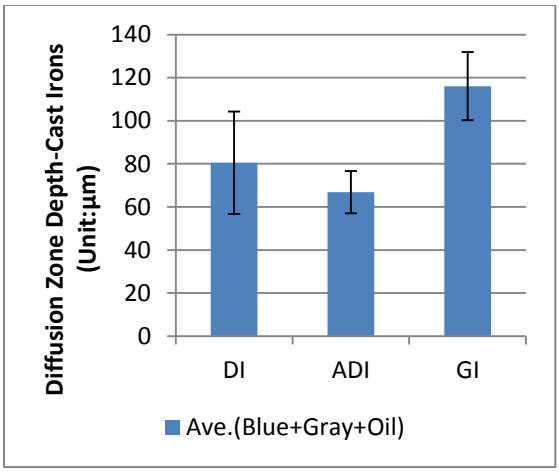


Figure 4.22: Diffusion zone depth in terms of material

It can be seen that the Gray gas nitriding process produced the thickest compound layer, followed by Blue, and then Oil. GI has the thickest compound layer on average, but the greatest variability in thickness, followed by ADI, and then DI. The Oil quench from gas nitriding produced the thinnest compound layer, and DI has thinnest compound layer.

Figure 4.21 shows that the Gray nitriding process gave the highest diffusion zone depth, followed by Oil nitriding and then Blue nitriding. Figure 4.22 shows that GI has the highest DZ depth and ADI has the lowest DZ depth. Further data on the DZ depth as determined by microhardness will be presented in section 4.4.

### 4.3.2 CL thickness and DZ depth for 4140 Steel

The compound layer thickness and diffusion zone depths in terms of salt bath nitriding process are given in Figures 4.23 and 4.24, respectively. The compound layer thickness is similar for Isonite, QP and QPQ: see Figure 4.23. However, there are significant differences in diffusion zone depth: see Figure 4.24. Processes such as QP and QPQ which involve processing subsequent to the salt bath nitriding, have thicker diffusion zones (2-3X) than Isonite.

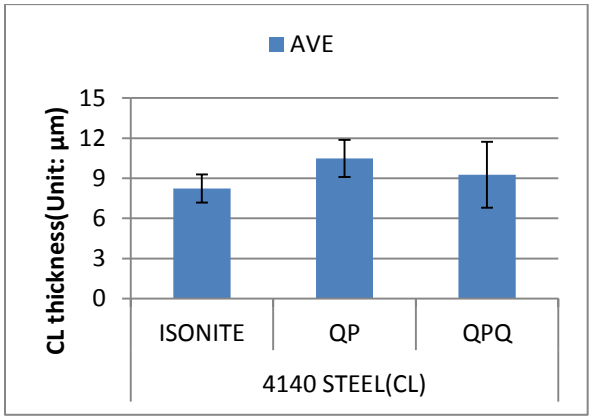


Figure 4.23: CL thickness in terms of salt bath nitriding treatment for 4140 steel

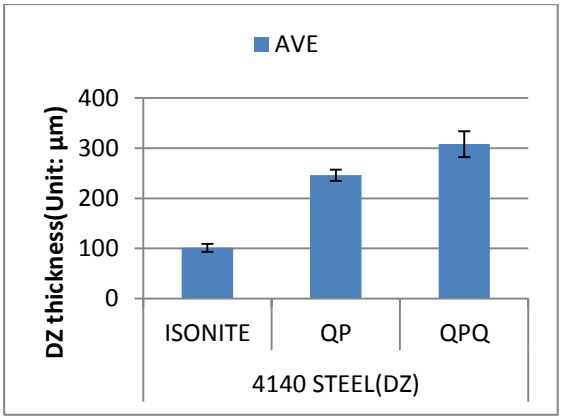


Figure 4.24: DZ depth in terms of salt bath nitriding treatment for 4140 steel

## 4.4 Surface roughness

The surface roughness results are given in Table 4.2 and plotted in Figure 4.25. It can be seen from Figure 4.25 that ADI treated using the Oil nitriding has lowest surface roughness, while GI treated using the Blue process has the highest surface roughness. GI treated using the Gray nitriding process showed the highest variability in roughness and a relatively high roughness value. In general, it can be seen that ADI has the lowest surface roughness. Figures 4.26 and 4.27 graphically illustrate these trends.

Table 4.2: Surface Roughness after heat treatment (Ra: μm)

| No. | DI | | | ADI | | | GI | | |
|---|---|---|---|---|---|---|---|---|---|
| | BLUE | GRAY | OIL | BLUE | GRAY | OIL | BLUE | GRAY | OIL |
| No. 1 | 1.39 | 1.83 | 1.91 | 1.29 | 1.33 | 0.86 | 2.28 | 1.19 | 1.22 |
| No. 2 | 2.08 | 1.33 | 2.48 | 1.04 | 1.27 | 1.11 | 2.24 | 2.36 | 1.74 |
| No.3 | 2.05 | 1.50 | 1.73 | 0.97 | 1.24 | 0.81 | 2.33 | 2.54 | 1.33 |
| Ave. | 1.84 | 1.55 | 2.04 | 1.10 | 1.28 | 0.93 | 2.28 | 2.03 | 1.43 |
| Std. | 0.32 | 0.21 | 0.32 | 0.14 | 0.04 | 0.13 | 0.04 | 0.60 | 0.22 |

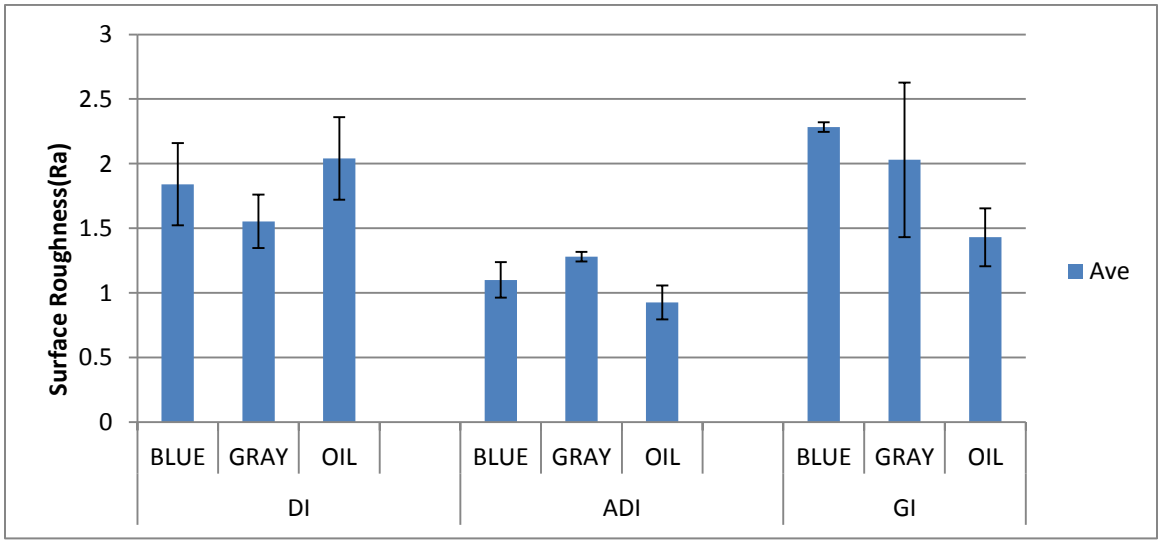


Figure 4.25: Surface roughness (Ra: μm) after nitriding

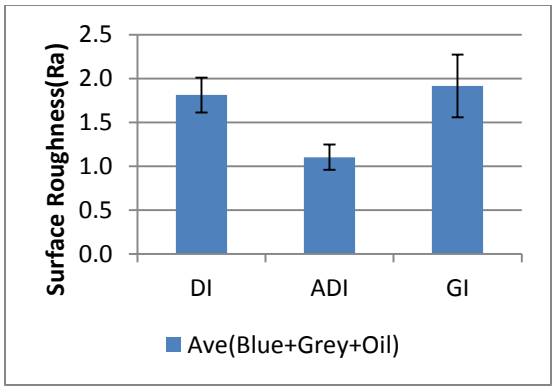


Figure 4.26: Surface roughness in terms of type of cast iron

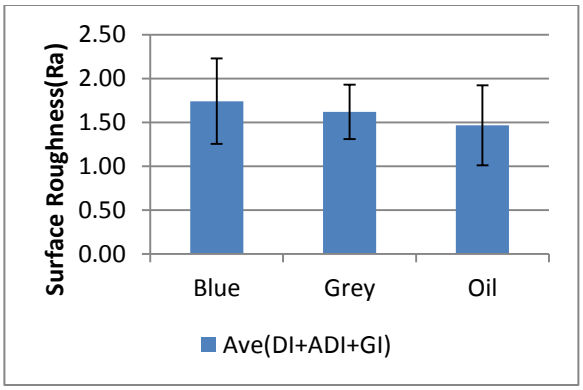


Figure 4.27: Surface roughness of cast irons in terms of gas nitriding treatment

Surface profiles can be considered to be comprised of a certain number of peaks of varying heights and an equal number of valleys of varying depths. The apparatus used in this study was a two dimensional profilometer.

Figure 4.28 (a) shows a specific example of 2-D surface profile for DI treated using the Oil nitriding process. The trace looks very jagged because the length dimension in the X-direction is around 1000 times of the length dimension in Y-direction (unit for the X-axis is mm, while the unit of the Y-axis is μm). However, if one enlarges a portion of the scan, expanding the X-axis (Figure 4.28 (b)), it can be seen that the slopes of the peaks and valleys are more gentle.

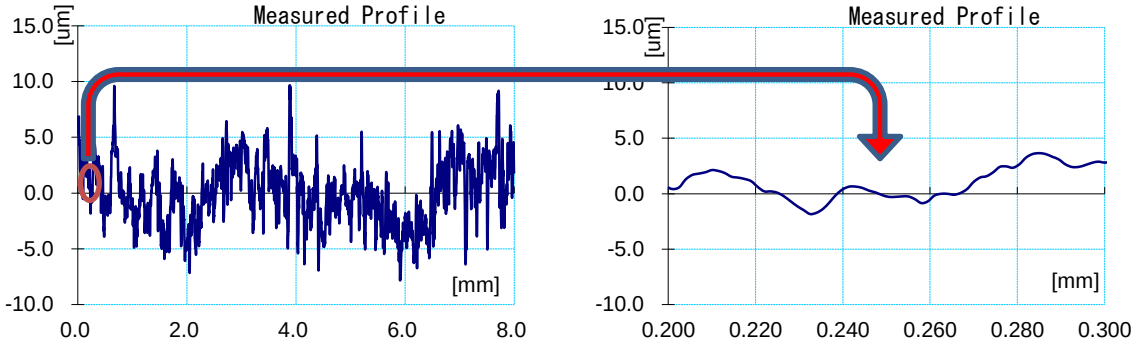


(a) (b)

Figure 4.28: Surface roughness of DI treated by Oil

Also, the peak on a profilometer trace may be different from an actual “peak” on the real surface, because the stylus will register a “peak” even when it only traverses a shoulder of an actual “peak”. Thus, the number of true “peaks” is considerably less than the number of “peaks” that are recorded. This distinction can easily be shown by taking a series of line profiles in the same direction with each traverse slightly displaced from its neighbor. In this way, the information in each of the line traces can be consolidated to produce a true 3-D contour map of the surface and thereby clearly identifies the actual “peaks” and “valleys”.

To gauge the 3-D topography of a nitrided surface, we have taken an alternative approach which involves image analysis of SEM images. Such an approach is shown in Figure 4.29 for DI nitrided using Oil process, i.e. the same material as for the profilometry traces in Figure 4.28. The SEM image is shown on the left and the 3-D topography obtained by an image analysis software, namely Image Pro Premier, is on the right. The area shown is approximately 7μm×7μm. The peaks and valleys are better identified than in surface profilometry.

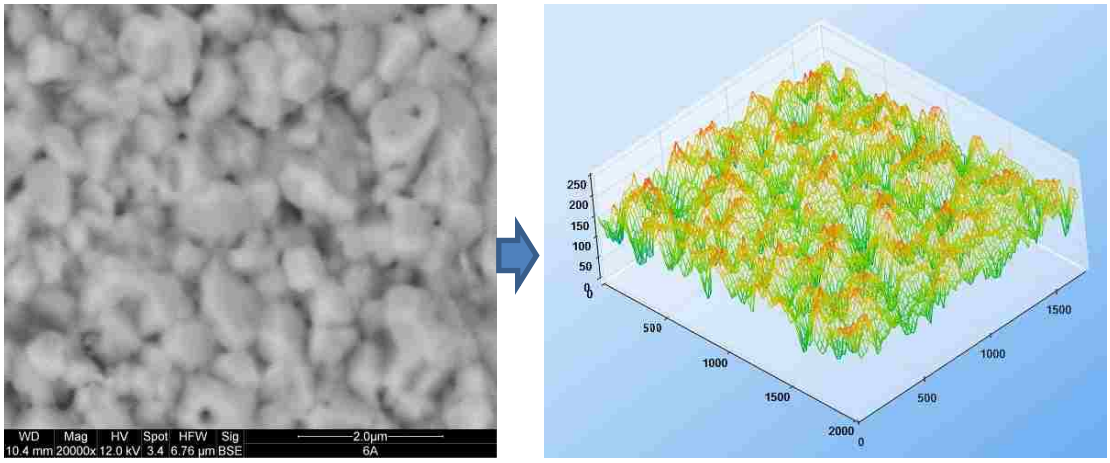


Figure: 4.29: 3-D surface profile of DI treated by Oil, (left: SEM, right: processed by image analysis software: Image Pro Premier)

## 4.5 Microhardness

The microhardness measurements are presented in two sections, namely measurements of the nitrided layer surface hardness and measurements of cross-sections to help define the hardness of compound layer (CL) and diffusion zone (DZ).

### 4.5.1 Microhardness measurements of nitrided surface

It should be noted that measuring the microhardness of the nitrided layer is not an easy task because the thickness of the layer is of comparable dimensions to the indenter. The hardness is also influenced by the specific surface topography and phase content of the area of indent, particularly whether such an area contains graphite, a soft phase. 10 indentations were made on each specimen and the highest values are given in Table 4.3 and Figure 4.30.

The highest microhardness (2251HV) was measured for ADI treated using Oil quenching after gas nitriding. However, ADI treated using Blue and Gray processes and DI treated using Blue, Gray and Oil processes, have a high microhardness (2000 ±250HV). These high hardness levels should result in better wear performance. However, the microhardness for GI, no matter what nitriding treatment was applied, is very much lower, i.e. around 1000HV, except for the Oil quench processing. This lower hardness is attributed to the graphite flakes which are incorporated into the compound layer (see for example Figure 4.14). The results are shown in Table 4.3 and plotted in Figure 4.30.

Table 4.3: Maximum values for surface microhardness of nitrided cast irons

| | DI | | | ADI | | | GI | | |
|---|---|---|---|---|---|---|---|---|---|
| | BLUE | GRAY | OIL | BLUE | GRAY | OIL | BLUE | GRAY | OIL |
| HV | 2071 | 1913 | 2136 | 1767 | 1879 | 2251 | 1072 | 1017 | 1612 |

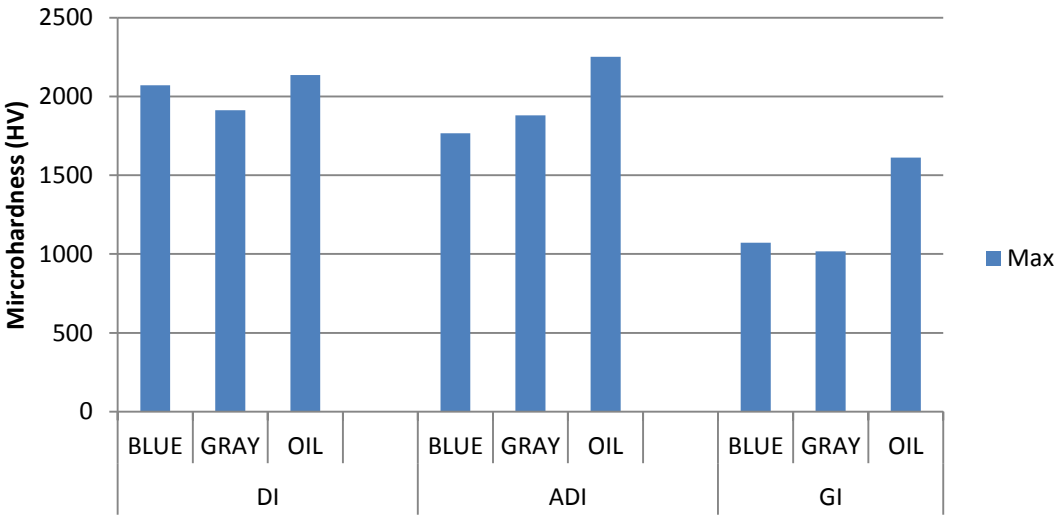


Figure 4.30: Maximum value of surface microhardness of nitrided cast irons

For 4140 steel, the results are plotted in Figure 4.31, and the maximum values of the nitrided surface microhardness are given in Table 4.4. It can be seen that the QP process produced the highest surface microhardness, followed by QPQ, and then Isonite. The reason for this may be that the Quench and Polish processes increased the microhardness, due to layer compaction during the polish. However the second Quench process, a post-oxidation treatment, produced defects in the ceramic microstructure, thus reducing the surface microhardness of 4140 steel.

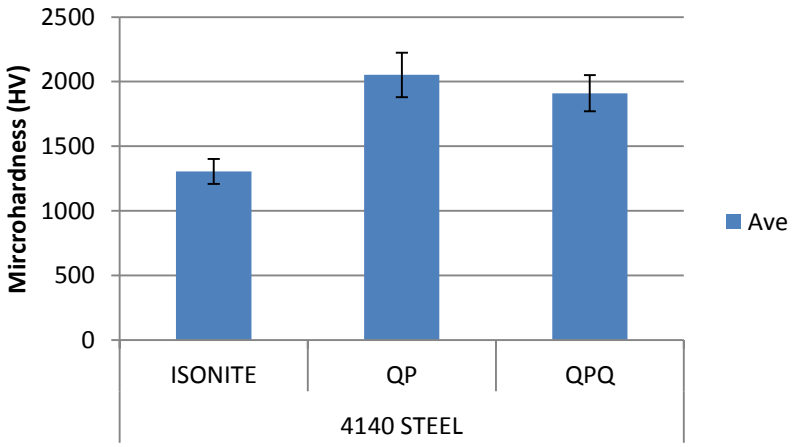


Figure 4.31: Surface microhardness of 4140 steel nitrided surface

Table 4.4: Maximum values for surface microhardness of nitrided 4140 steel

| 4140 STEEL | Surface Microhardness (HV) | | |
|---|---|---|---|
| | ISONITE | QP | QPQ |
| Max | 1401 | 2225 | 2050 |

4.5.2 Microhardness of cross-sections

As noted previously, these measurements were made to help to define the boundaries of the compound layer and diffusion zone.

Figure 4.32 (a)-(d) show the through-thickness microhardness distributions for DI, ADI, GI and 4140 steel as plotted using Origin Pro software. A similar microhardness gradient is seen for all materials in all heat treated conditions. The microhardness of the compound layer is not reflected in these plots but rather the nitrogen distributions in the diffusion zone. This is discussed in more detail in section 4.4.3.

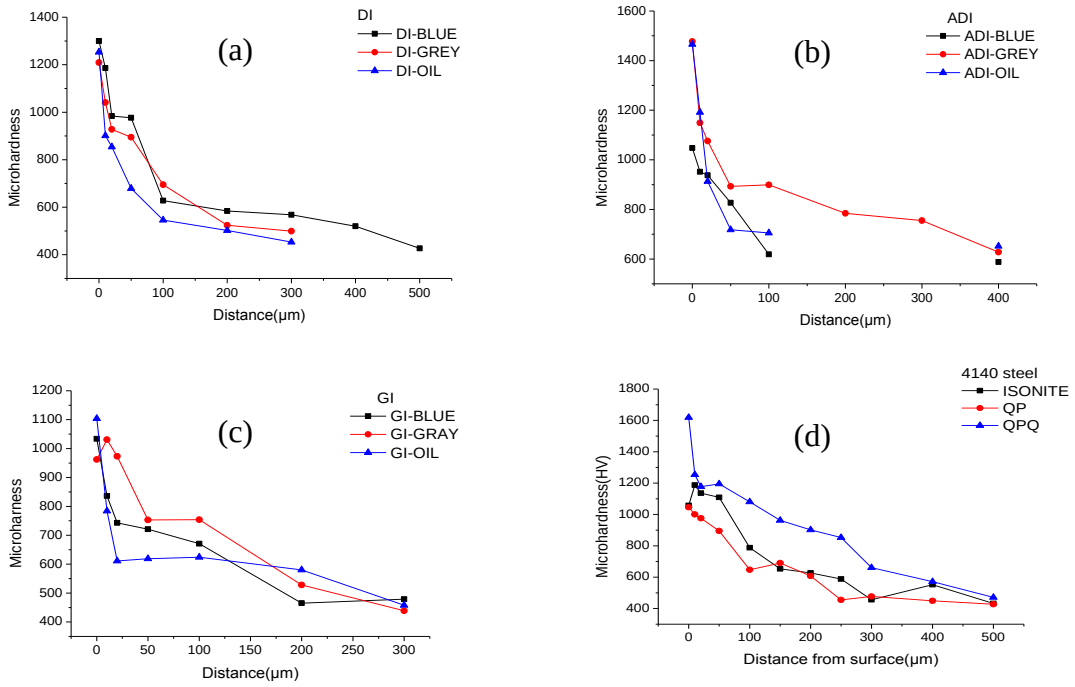


Figure 4.32: Comparisons of microhardness of cross-sections

4.5.3 Relationship between microhardness and microstructure

Two measures were used to gauge the extent of the diffusion zone namely microhardness and metallography. The results are illustrated in Figures 4.33 to 4.36 for DI, ADI, GI and 4140 steel. It can be readily seen that the diffusion zone depth measured by metallography (dashed line in plots) is always smaller than that determined by microhardness. It is suggested that this is due, at least in part because nitrogen in solution in α-Fe is not visible using optical metallography but can produce a hardness increase.

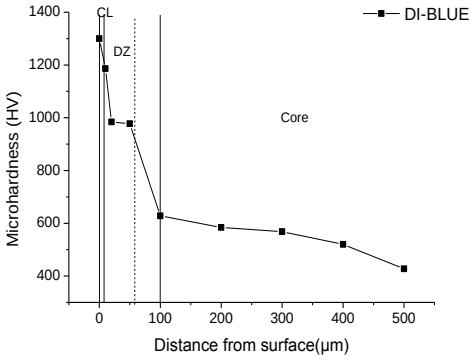


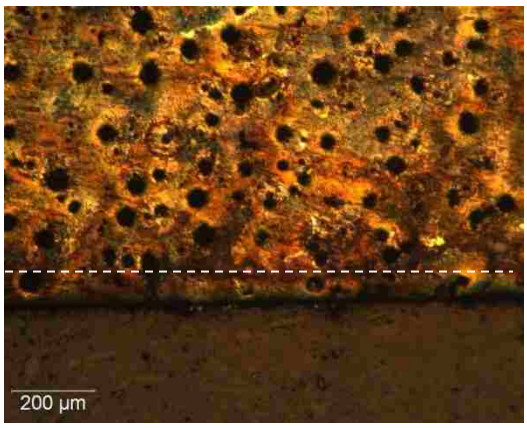


Microhardness gradient-DI-BLUE DI-BLUE(100X)

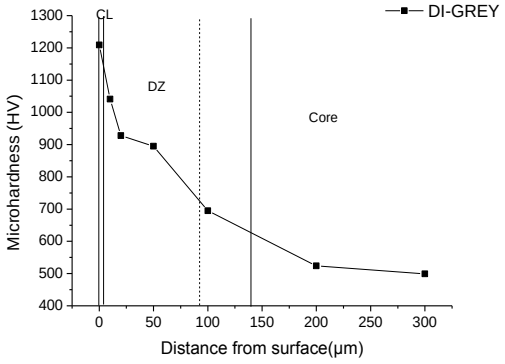


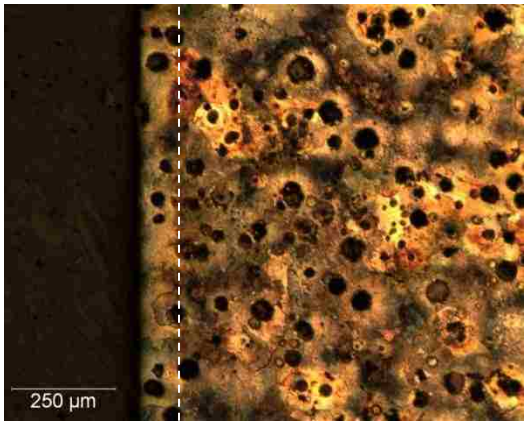


Microhardness gradient-DI-GRAY DI-GRAY(100X)

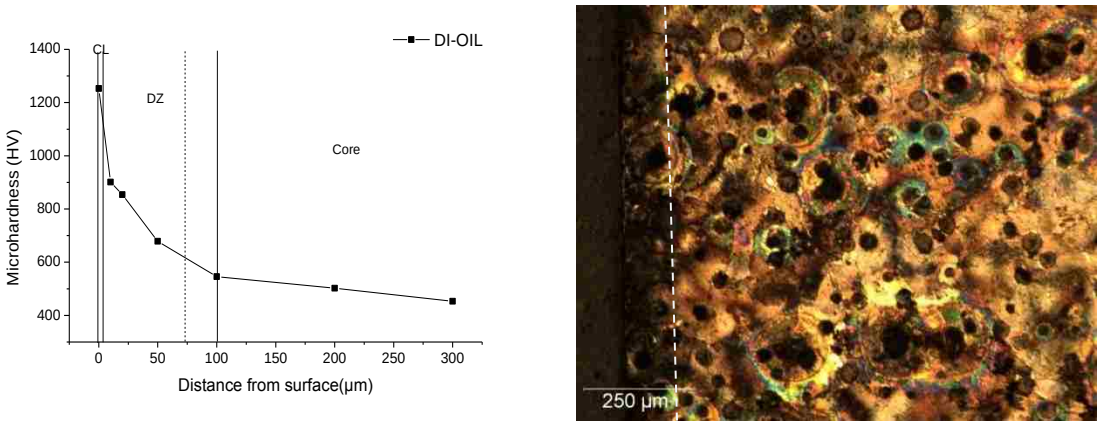


Microhardness gradient-DI-OIL　　DI-OIL(100X)

Figure 4.33 Relationship between microhardness and nitrided layer metallography-DI

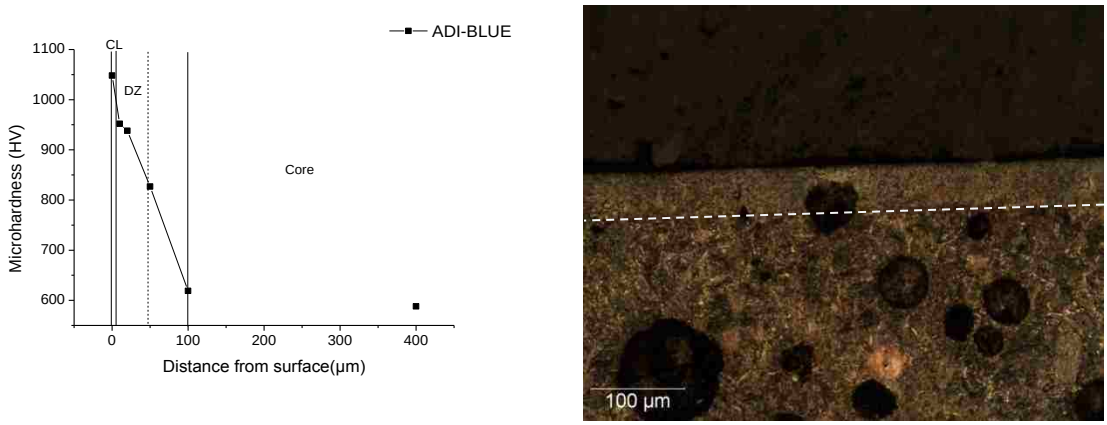


Microhardness gradient-ADI-BLUE　　ADI-BLUE(100X)

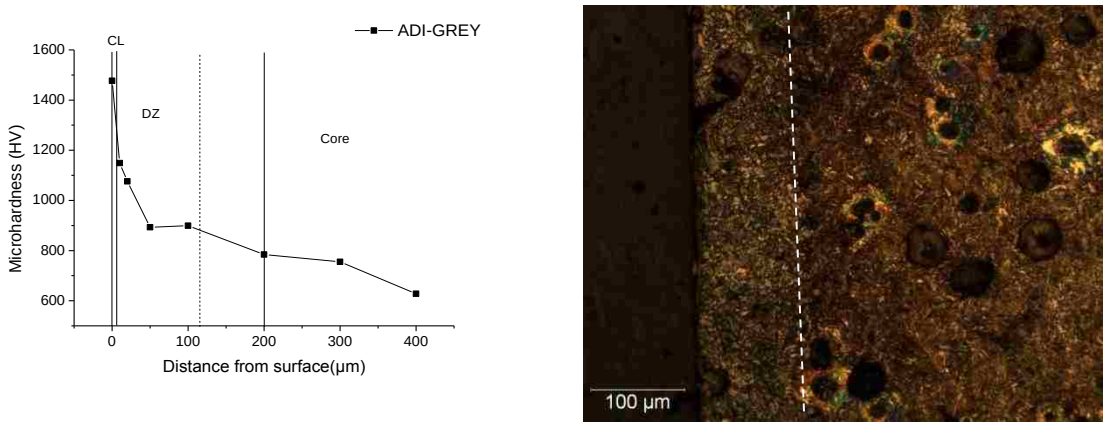


Microhardness gradient-ADI-Gray　　ADI-Gray(200X)

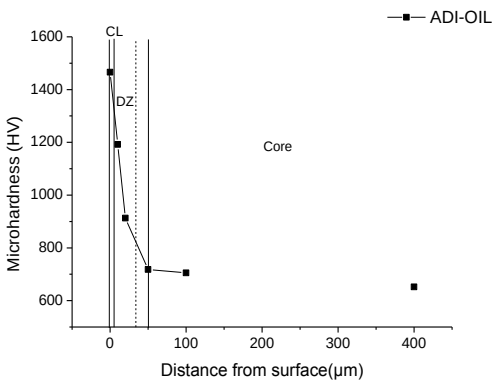


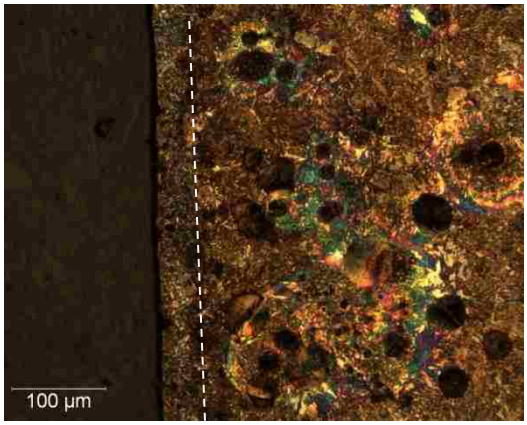


Microhardness gradient-ADI-OIL ADI-OIL(200X)

Figure 4.34 Relationship between microhardness and nitrided layer metallography-ADI

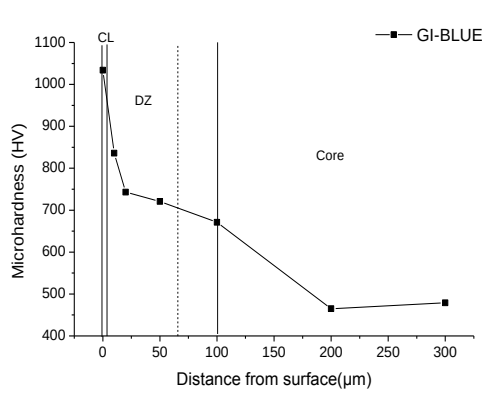


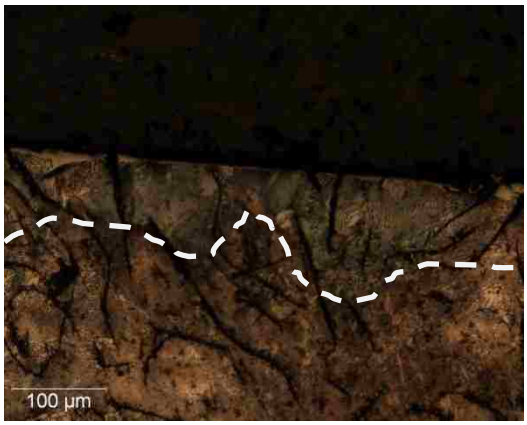


Microhardness gradient-GI-BLUE GI-BLUE(200X)

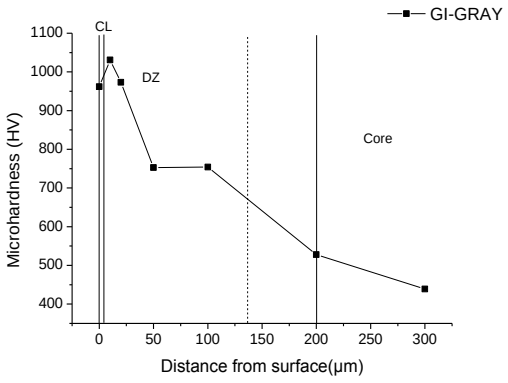



Microhardness gradient-GI-Gray GI-Gray(200X)

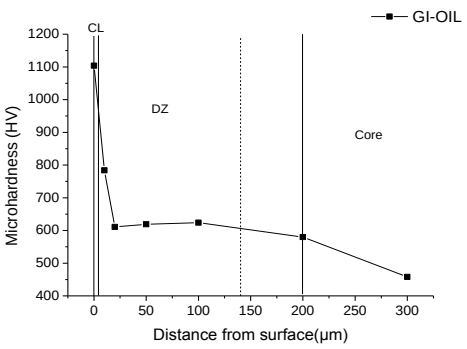


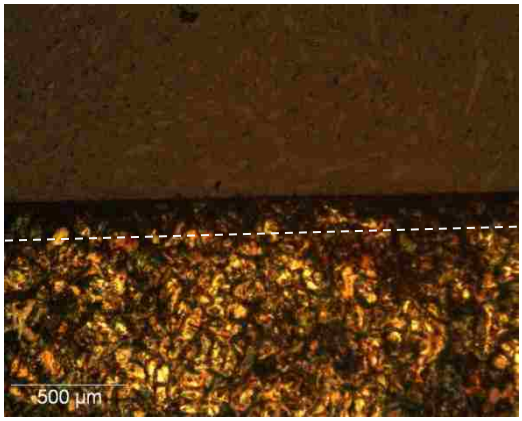


Microhardness gradient- GI-OIL GI-OIL(50X)

Figure 4.35 Relationship between microhardness and metallography of nitrided GI

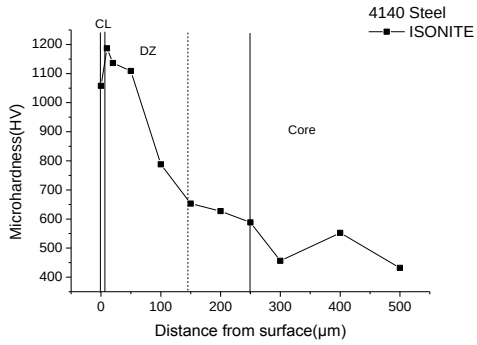


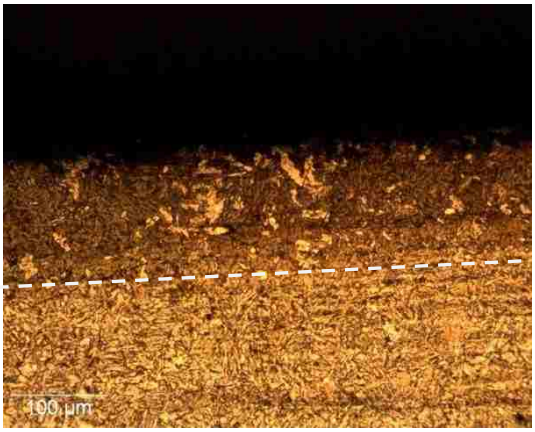


Microhardness gradient-4140 Isonite 4140 Isonite (200X)

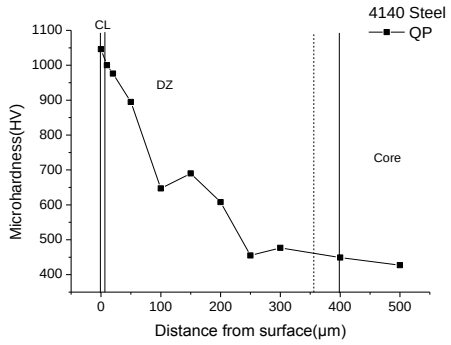


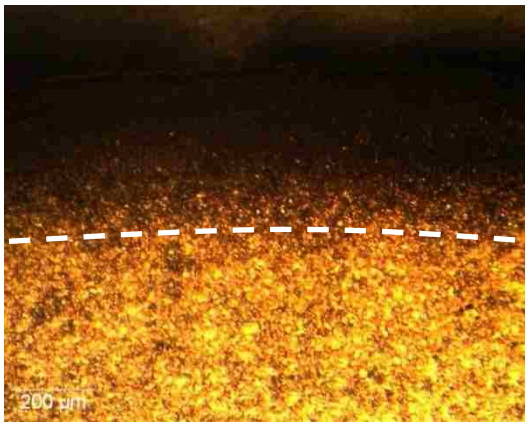


Microhardness gradient-4140 QP 4140 QP (100X)

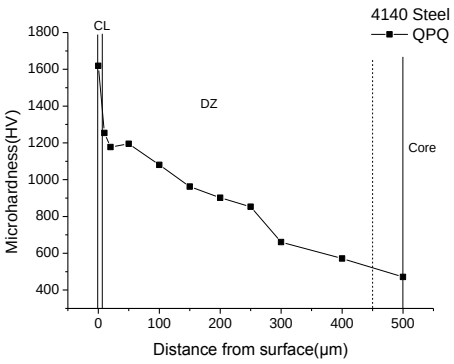


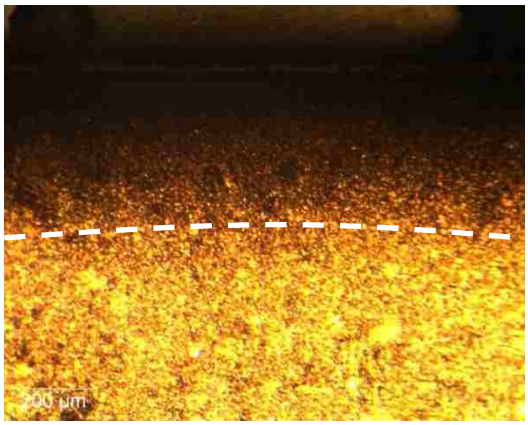


Microhardness gradient-4140 QPQ 4140 QPQ (100X)

Figure 4.36 Relationship between microhardness and DZ metallography-4140 steel

## 4.6. Wear test characterization

### 4.6.1 Coefficient of friction (COF)

The coefficient of friction was recorded continuously during the wear test. For every material/nitriding combination, 4 tests were performed (2 specimens ×2 flat surfaces). The COF is mainly related to the surface roughness, compound layer parameters and the lubricated condition. As shown in Figures 4.47 (a)-(l), the COF is always less than 0.045 indicating lubricated conditions. The COF either increased during the wear test because debris with hard particles accumulated in the wear track, e.g. DI-Gray, or decreased because the wear track was polished by the counterface ceramic ball and there was little or no debris, e.g. 4140 steel.

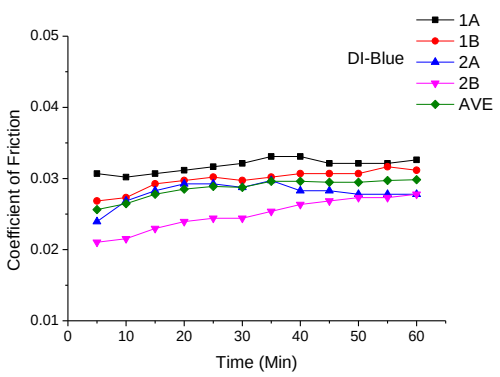


(a) COF of DI-Blue

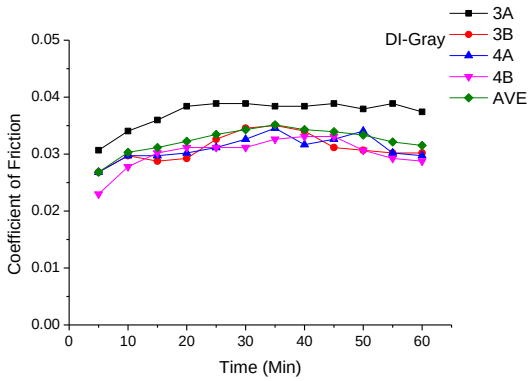


(b) COF of DI-Gray

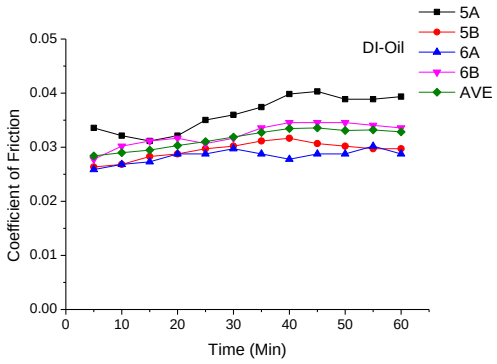


(c) COF of DI-Oil

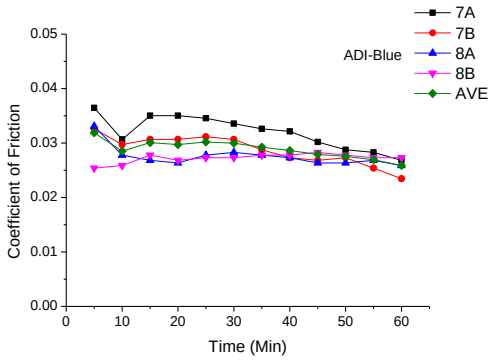


(d) COF of ADI-Blue

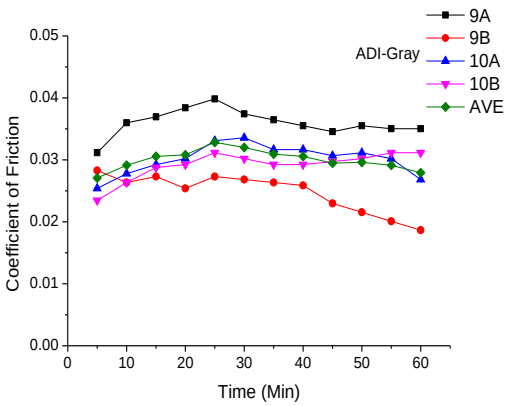


(e) COF of ADI-Gray

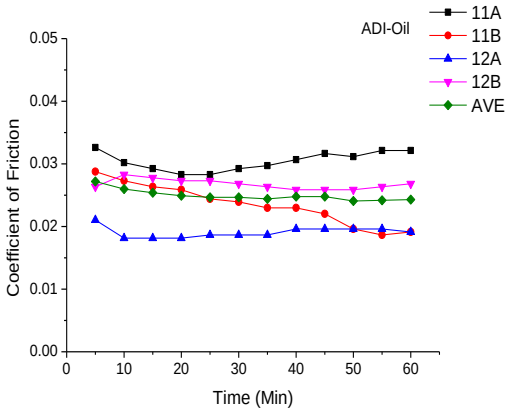


(f) COF of ADI-Oil

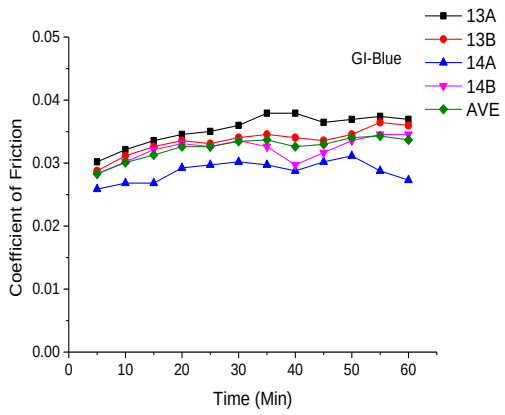


(g) COF of GI-Blue

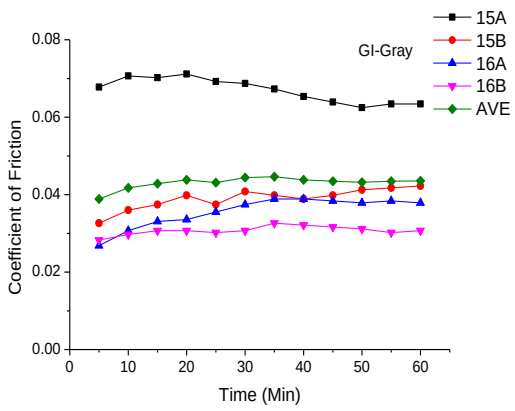


(h) COF of GI-Gray

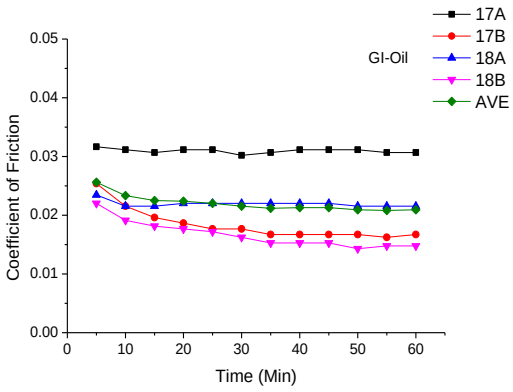


(i) COF of GI-Oil

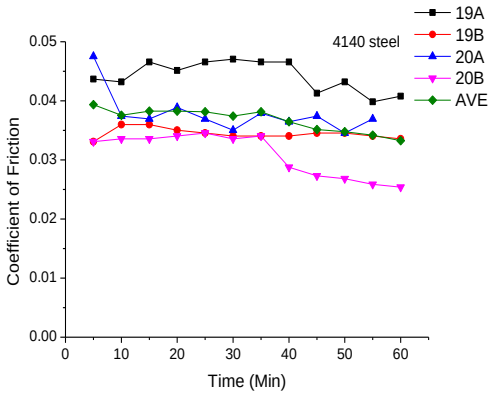


(j) COF of 4140-Isonite

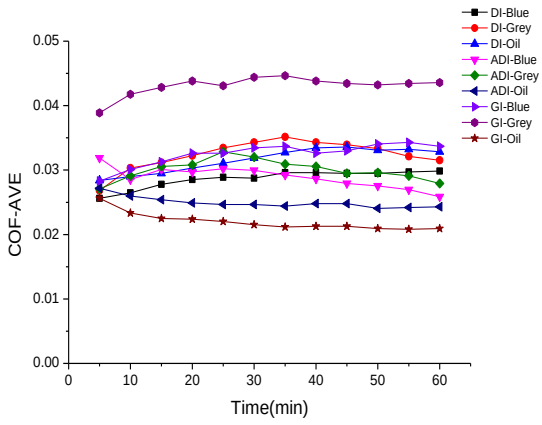


(k) The average of the COF of cast irons

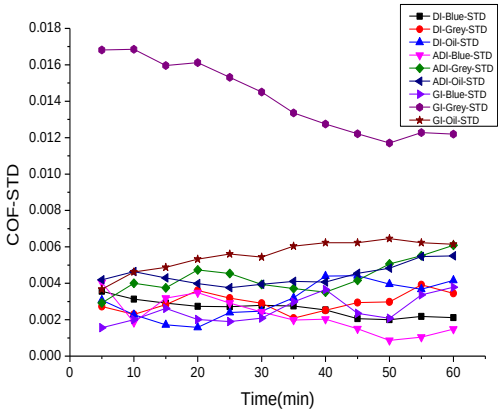


(l) The variability of the COF of cast irons

Figure 4.37 Coefficient of Friction VS time plots for nitrided cast irons and 4140 steel

4.6.2. Wear track width and depth measurements

The good tribological properties of nitrided materials are usually ascribed to the compound layer. To characterize the enhancement of wear resistance derived from the nitriding treatments, one of the simplest, but effective, methods is to measure the dimensions (width & depth) of the wear track. The width and depth of the wear tracks measured using a combination of SEM and image analysis software (Image J), are given in Figure 4.38 for wear track width (WTW), and Figure 4.39 for wear track depth (WTD).

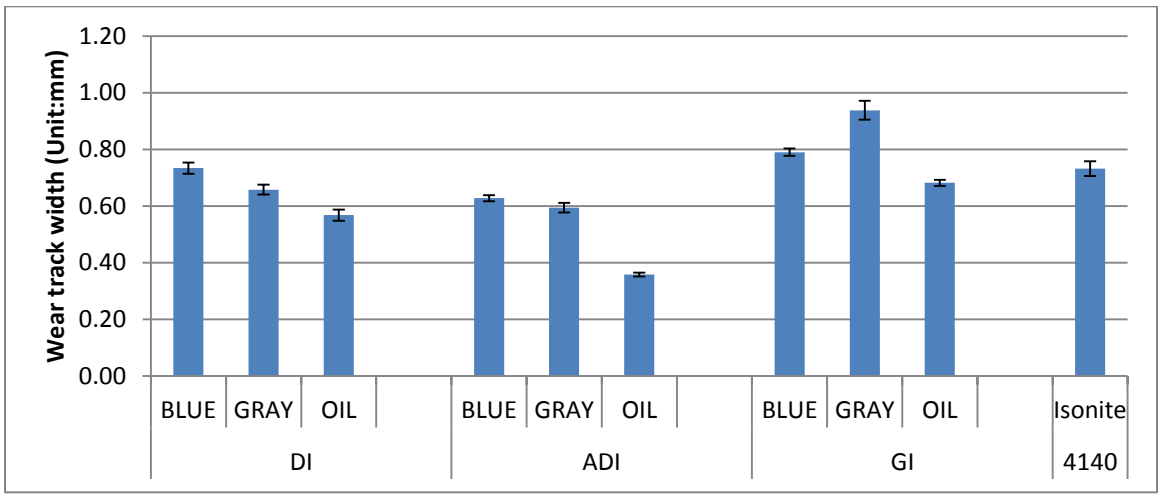


Figure 4.38: Average wear track width of nitrided cast irons and 4140 steel

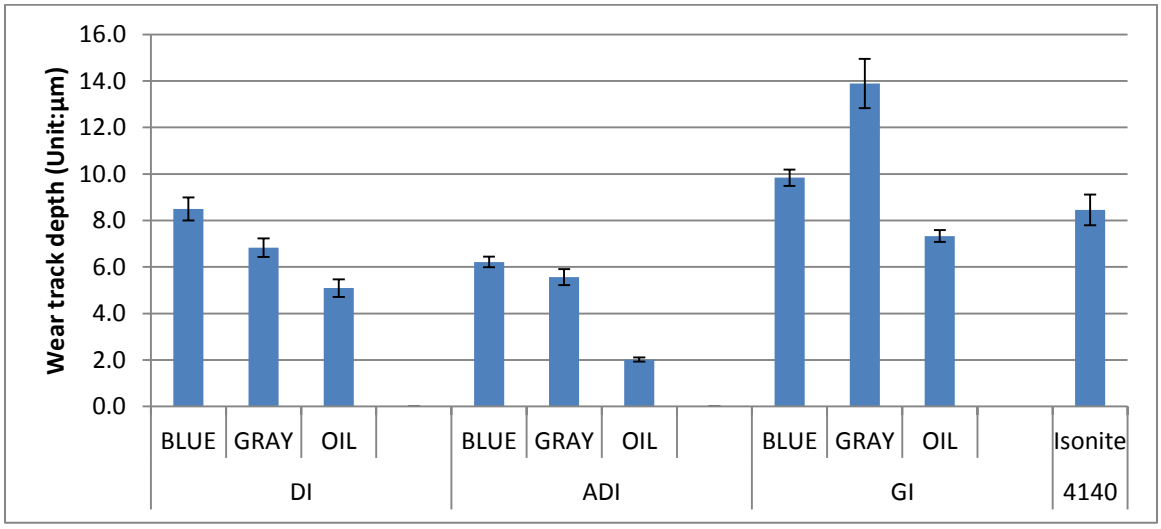


Figure 4.39: Average wear track depth of nitrided cast irons and 4140 steel

Given that the counterface is a ceramic ball, the wear track width increases as wear proceeds, i.e. as the ceramic ball penetrates the nitride layer. Figure 4.38 shows that ADI processed using Oil quench nitriding has the best wear resistance, while GI processed using Gray nitriding has the worst wear resistance. When compared with 4140 steel, DI processed using Gray and Oil nitriding process has better wear resistance, and DI processed using Blue has that equivalent wear capacity. ADI, regardless of nitriding treatment has better wear resistance than Isonited 4140 steel. The wear track depth results, Figure 4.39, lead one to similar conclusions.

To further investigate which material has the best wear resistance, and which nitriding treatment is the most effective in enhancing wear resistance, the results in Figures 4.38 and 4.39 have been re-plotted. The average of the wear track width for the three cast irons is plotted as a function of nitriding method in Figure 4.40. The average WTW for the three nitriding methods is plotted as a function of material in Figure 4.41. We can see that the Oil nitriding process gave the best wear resistance of the three cast irons, and nitrided ADI exhibited the best performance. Similar conclusions are drawn if WTD is plotted as a function of nitriding method, Figure 4.42, or material, Figure 4.43.

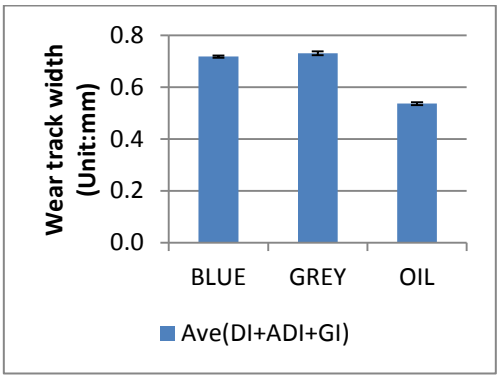


Figure 4.40: Wear track width with respect to nitriding method

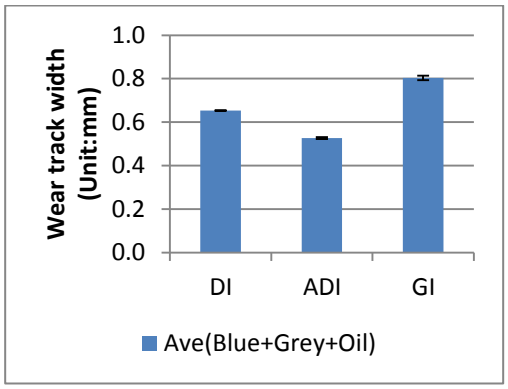


Figure 4.41: Wear track width with respect to material

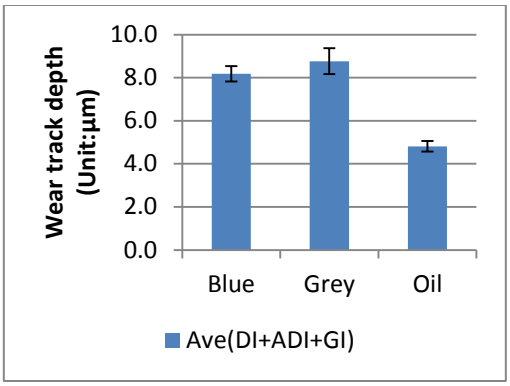


Figure 4.42: Wear track depth with respect to nitriding method

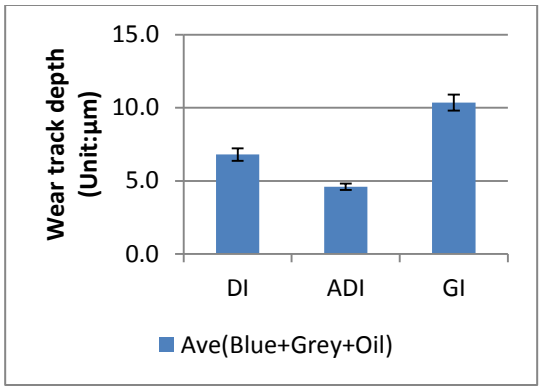


Figure 4.43: Wear track depth with respect to material

4.6.3 Comparison of wear track depth with CL thickness and DZ depth

In order to investigate whether the compound layer are still protective after the wear test, and to know how much of the nitrided layer has been worn away, the wear track widths have been compared with the CL thickness and DZ depth in Figure 4.44.

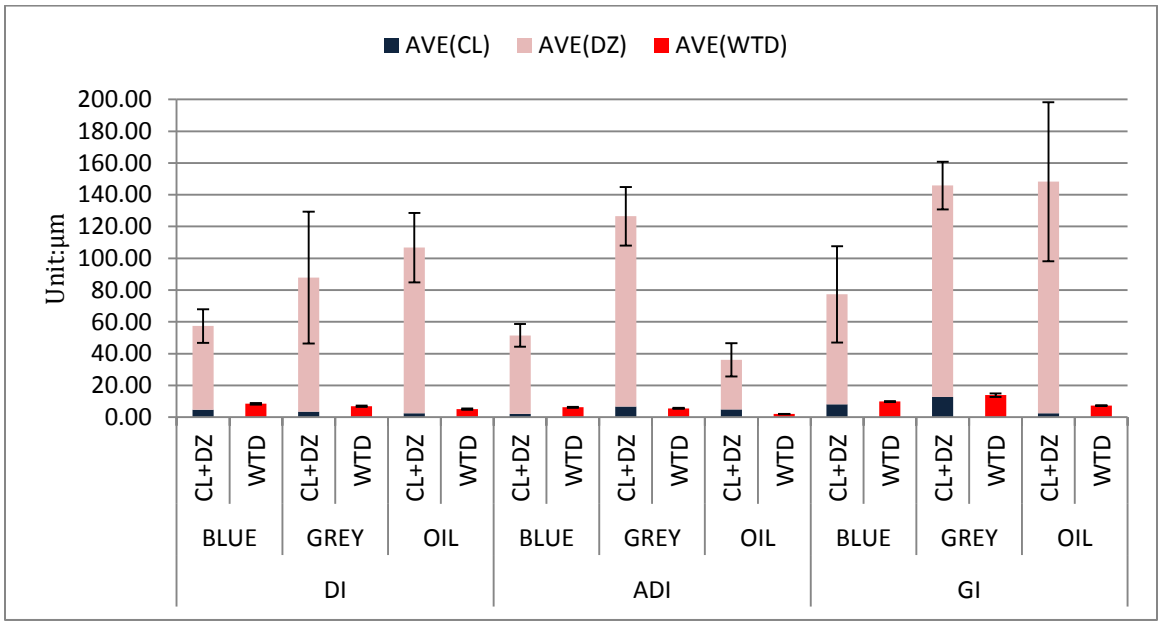


Figure 4.44: Comparisons of Diffusion Zone (DZ) depth, Compound Layer (CL) thickness and Wear Track Depth (WTD)

It can be seen from Figure 4.44 that wear track depths are similar to the values of the CL thickness, but are smaller than DZ depth. The difference between the CL thickness and wear track depth is given in Figure 4.45. For the duration of the wear test, the compound layers on ADI nitrided using either the Gray or Oil nitriding process was still protective. For all other material/nitriding process combinations, the CL was completely worn away. Thus the wear protection mechanisms switch from CL protection to DZ protection.

The thicknesses of the nitrided case remaining after wear testing, i.e. diffusion zone and compound layer if it was not totally worn away, are shown in Figure 4.46. This data is also replotted in Figure 4.47 as the percentage of nitrided case consumed during the wear test. The Oil nitriding process gave the best wear performance, i.e. lowest wear percentage, for all 3 cast irons.

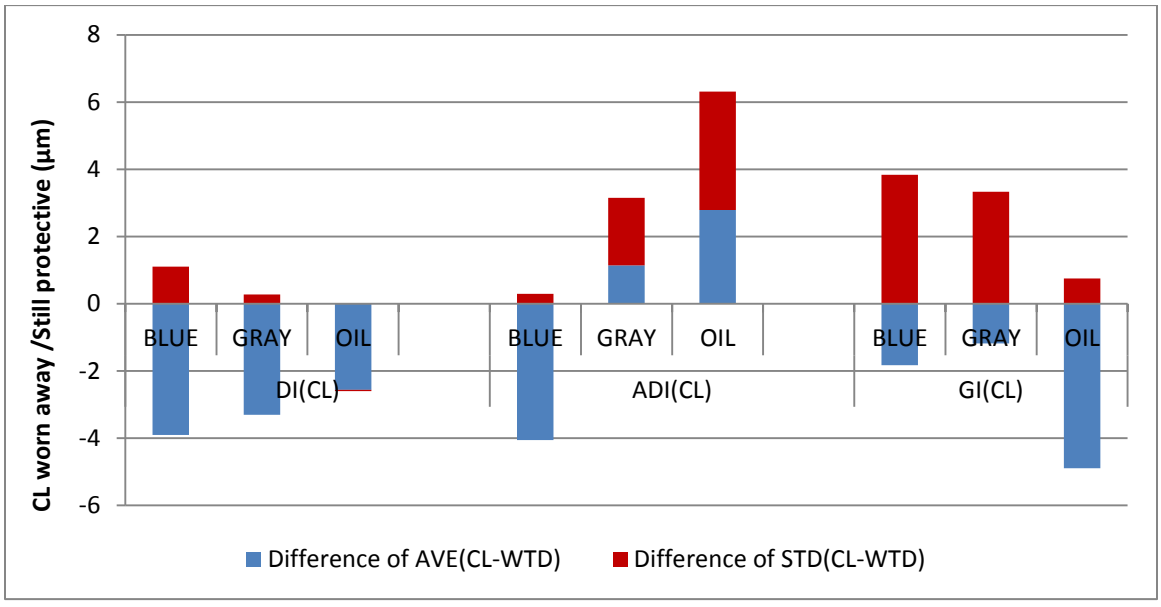


Figure 4.45: The difference between the CL thickness and wear track depth

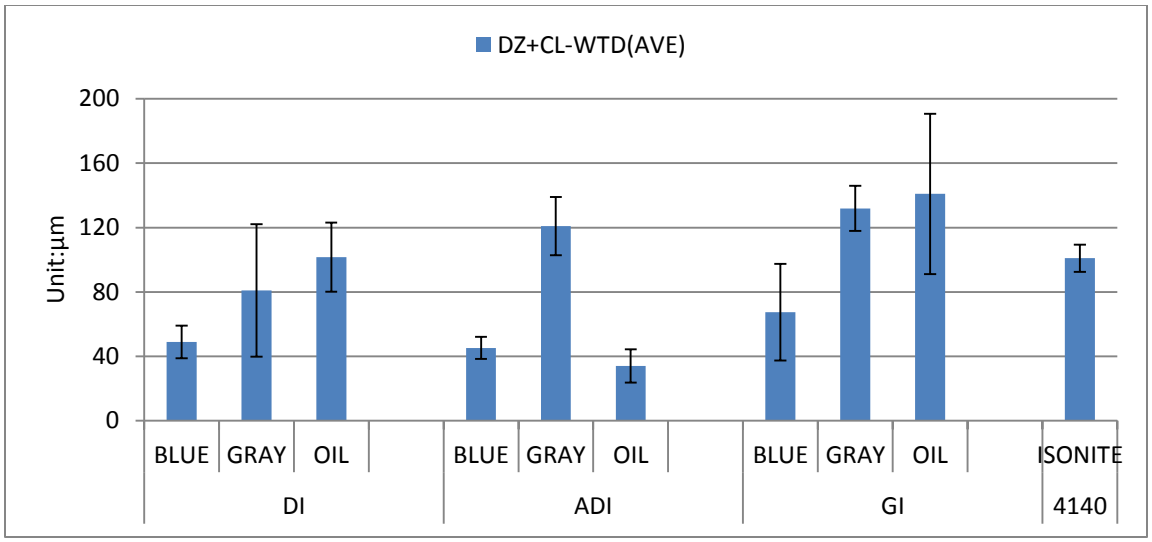


Figure 4.46: Compound layer plus diffusion zone thickness remaining after wear test

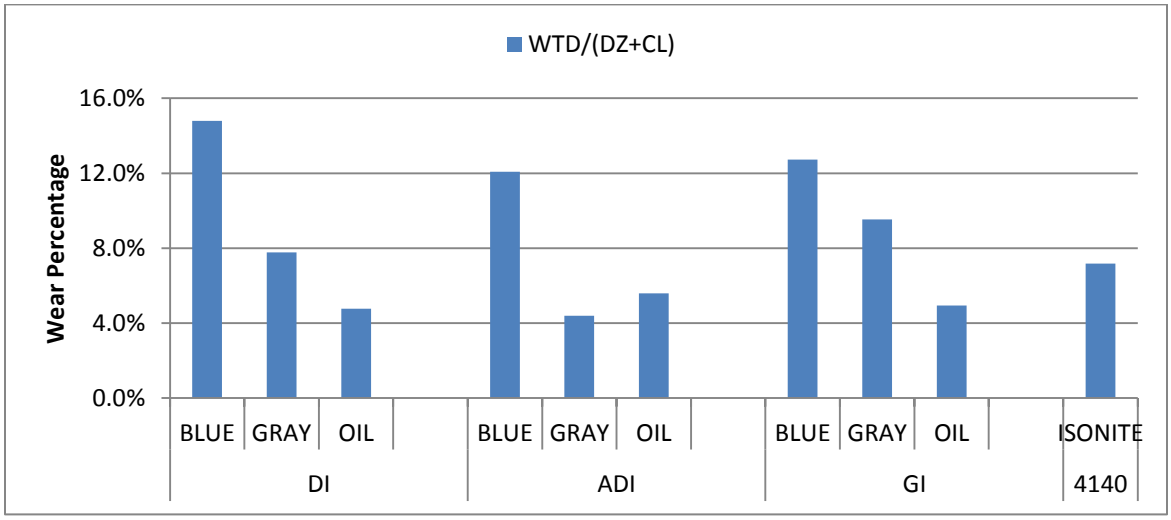


Figure 4.47: Percentages of nitrided case (CL+DZ) consumed during duration of wear test

4.6.4 SEM observations of wear tracks

Scanning electron microscopy (SEM) was used to characterize the wear track morphology and debris to help identity the wear mechanisms.

Figures 4.48-4.50 for DI indicate that wear track width decreases in the order, Blue>Gray>Oil. All tracks look polished. Figures 4.51-4.53 for ADI indicate that wear

track width decreases in the order, Blue>Gray>Oil. Tracks look polished, but there is less debris than for DI. New pits were not as easily formed as in DI, but some pits still formed at the graphite nodules.

Figures 4.54-4.56 for GI show that wear track width decreases in the order, Gray>Blue>Oil. The track looks polished. The amount of debris is more than that for DI or ADI. New pits are more easily formed at graphite flakes. Fewer pits were found for the oil quenched sample. This is consistent with the COF data for GI, Figure 4.37, where the COF for GI-Blue and GI-Gray increase with time (sliding distance) whereas GI-Oil shows a small decrease in COF with time.

Figure 4.57 indicates that wear track width for the Isonite-treated 4140 steel is at the same level of cast irons. The track also looks polished. More pits were found because more pits already existed before wear test (see area away from wear track in Figure 4.57), but less debris was accumulated. Because the matrix is uniform, there is no specific location for new pit formation.

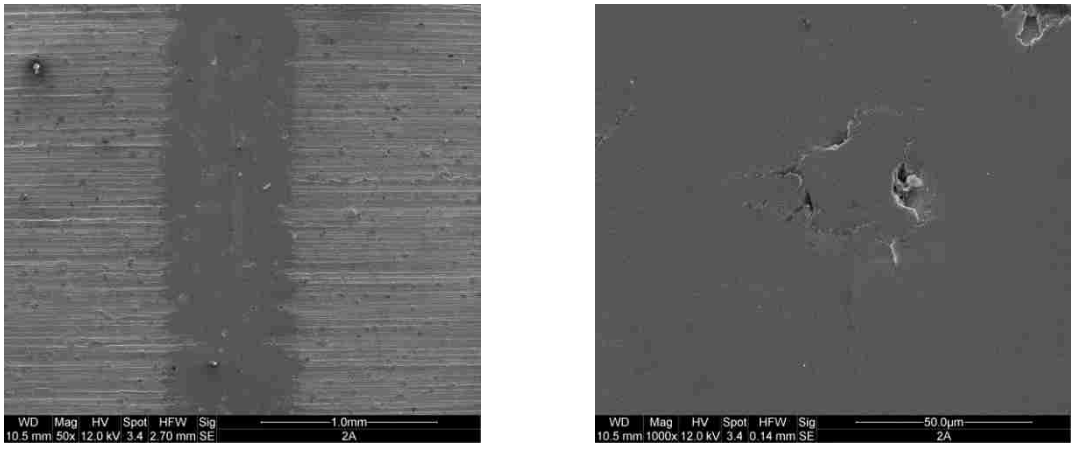


Figure 4.48: DI-Blue (50X, 1000X)

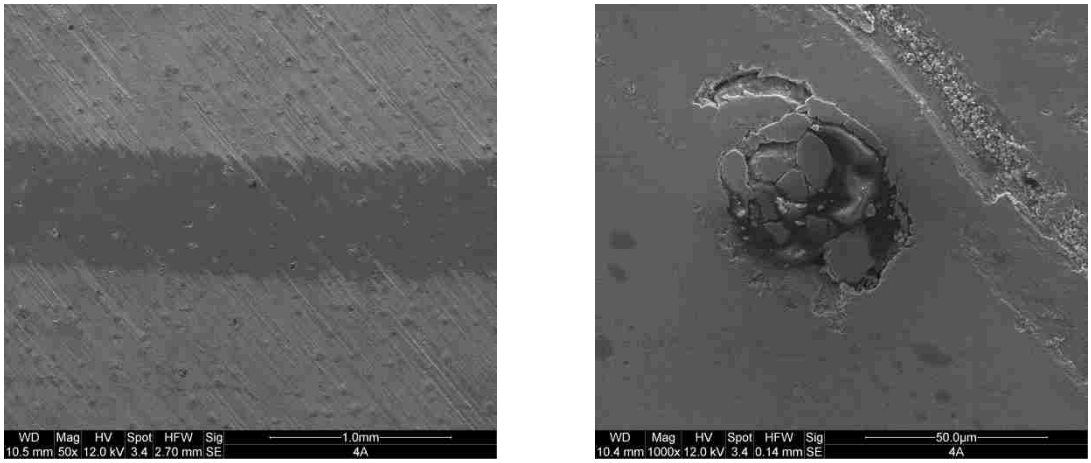


Figure 4.49: DI Gray (50X, 1000X)

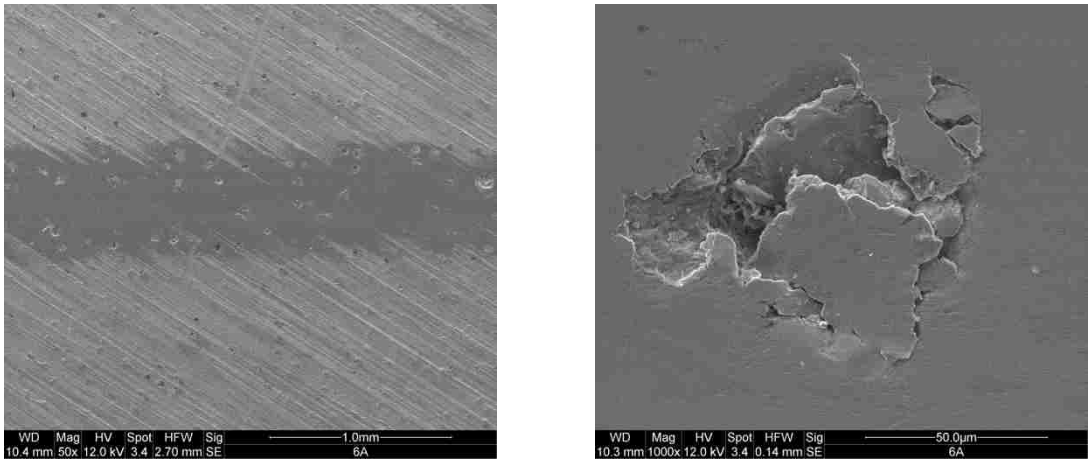


Figure 4.50: DI Oil (50X, 1000X)

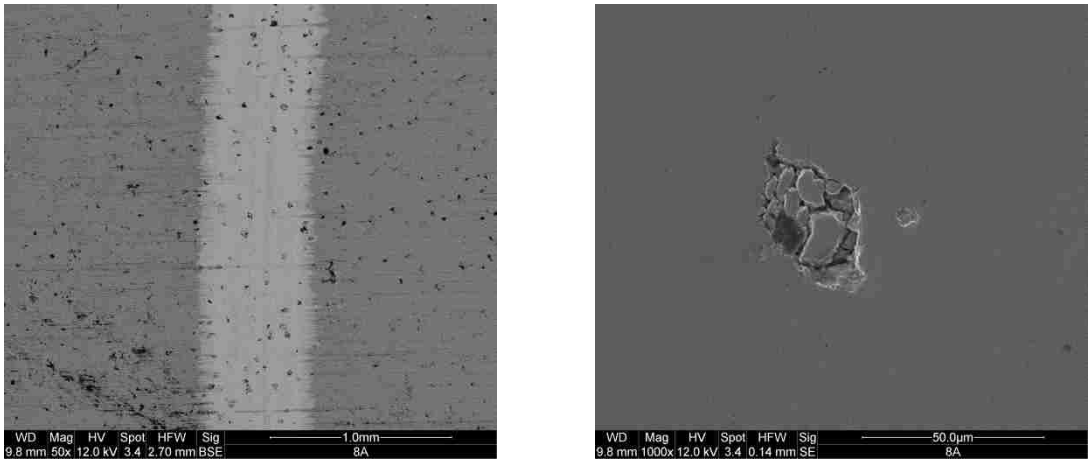


Figure 4.51: ADI-Blue (50X, 1000X)

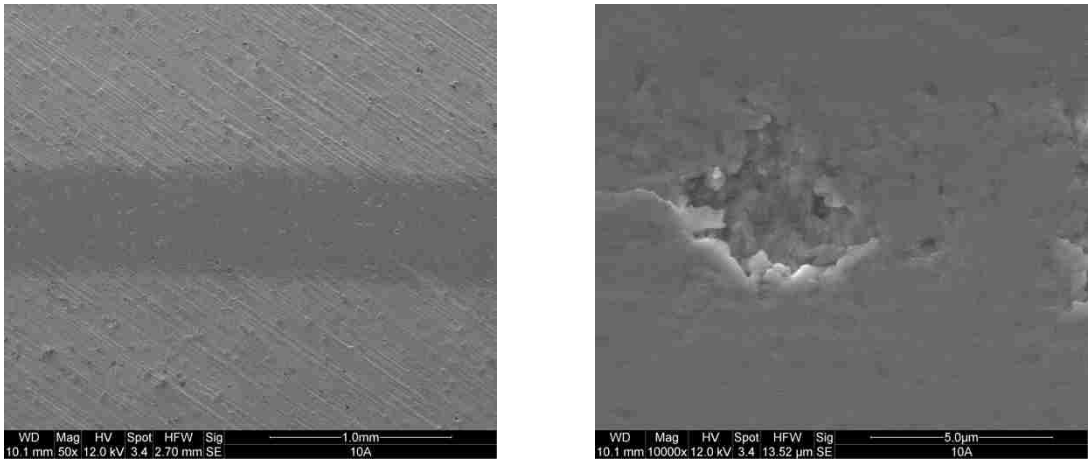


Figure 4.52: ADI-Gray (50X, 1000X)

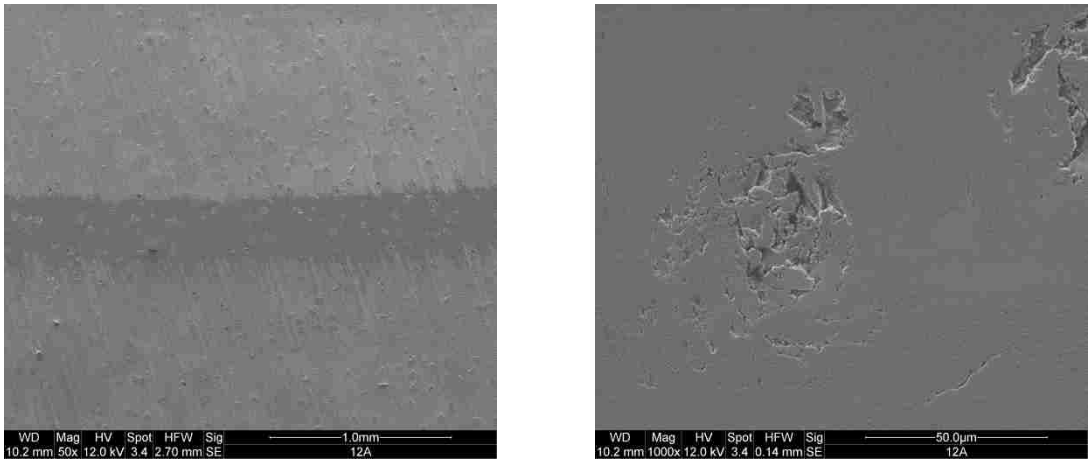


Figure 4.53: ADI-Oil (50X, 1000X)

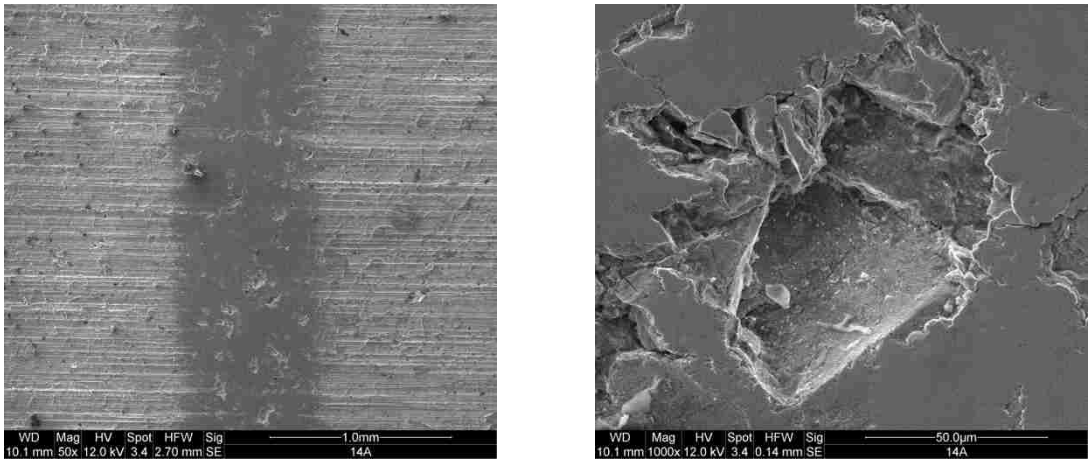


Figure 4.54: GI Blue (50X, 1000X)

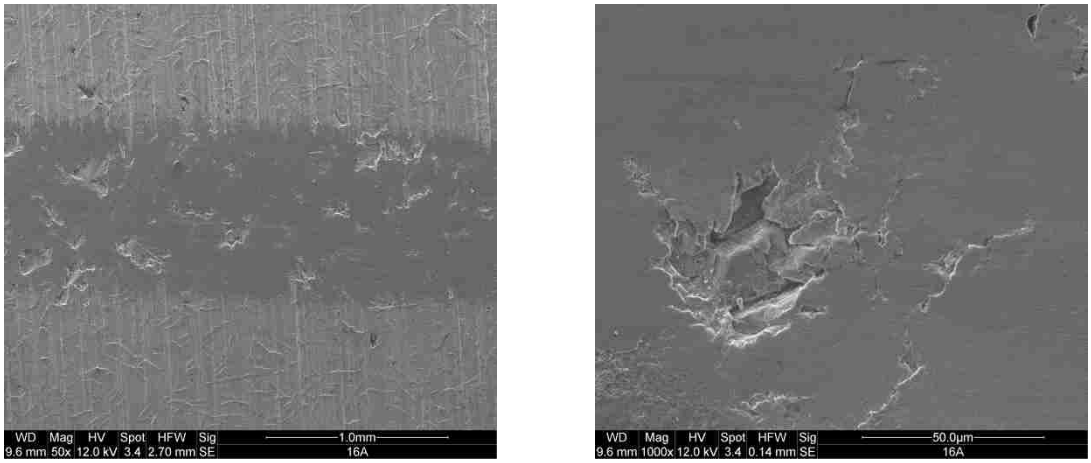


Figure 4.55: GI-Gray (50X, 1000X)

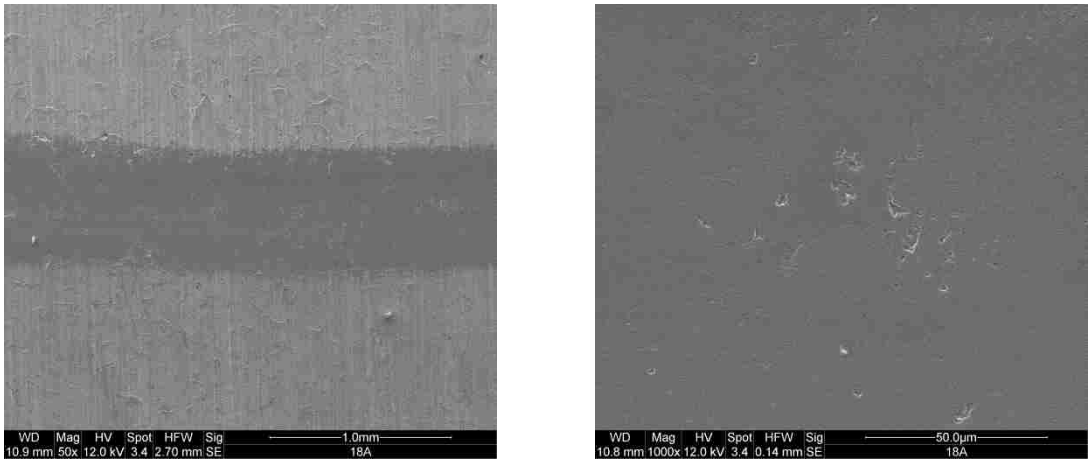


Figure 4.56: GI-Oil (50X, 1000X)

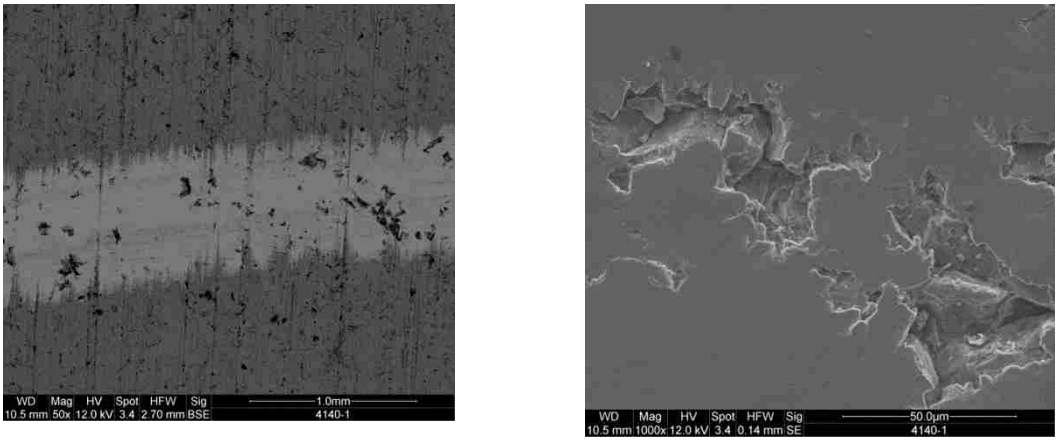


Figure 4.57: Isonite-treated 4140 steel (50X, 1000X)

4.6.5. Wear rate

Wear rate is commonly calculated using two main formulas, based either on weight loss[83]:

$$k = \Delta m/FS \quad (7)$$

or volume loss[140]

$$k = \Delta V/FS \quad (8)$$

Where k is the wear rate coefficient, Δm wear weight loss, ΔV wear volume loss, F the normal load, and S the total sliding distance. Equation (8) is more widely used and specifically more applicable to this study because of the different densities of the materials used in this study. In this study: F=44.45N(10lbs); S=6003.58m; FS=266871.6Nm.

The calculated wear rates of the nitrided cast irons and Isonited 4140 steel are shown in Figure 4.58.

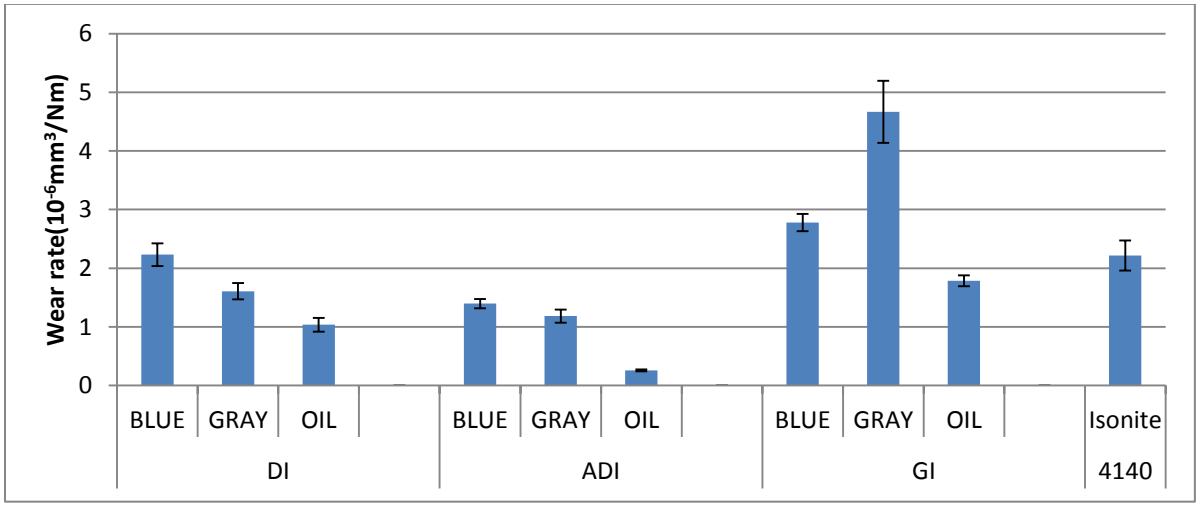


Figure 4.58: Average wear rate of the nitrided cast irons and Isonited 4140 steel

ADI treated using Oil nitriding process has the lowest wear rate. This is attributed to the optimum CL thickness, CL morphology, the adherence of the compound layer to the

substrate, high hardness, and low surface roughness. GI treated using Gray nitriding process has the highest wear rate. Although the compound layer is thicker, it is softer and less adherent and has a higher surface roughness. The properties of the CL on ADI (Oil) and GI (Gray) are compared in Table 4.5.

Table 4.5 Comparison of ADI (Oil), the best wear resistance, with GI (Gray), the poorest wear resistance

| | ADI (Oil) | GI (Gray) |
|---|---|---|
| Compound Layer Thickness | ~5μm, little variability | ~12μm, large variability |
| Morphology | CL could incorporate graphite nodules | Graphite flakes incorporated into CL |
| Adherent | Yes | Partially |
| Max. Surface Hardness(HV) | 2251 | 1017 |
| Surface Roughness (μm) | 0.93±0.13 | 2.03±0.60 |
| COF | 0.025-0.03 | 0.04 |

The relationship between wear rate and roughness and microhardness of nitrided surface are shown in Figure 5.59 and Figure 5.60. The linear fitting functions of wear rate against roughness and microhardness of nitrided surface are given in Equations (9) and (10). For Equation (9), the Residual Sum of Squares (RSS) is $7.27864^{-12}$, which indicates good linear relationship between wear rate and roughness. For Equation (10), the Residual Sum of Squares (RSS) is $3.5673^{-12}$, which also indicates good linear relationship between wear rate and microhardness.

$$\text{Wear rate}(10^{-6}\text{mm}^3/\text{Nm}) = 1.79Ra - 1.00 \quad (9)$$

$$\text{Wear rate}(10^{-6}\text{mm}^3/\text{Nm}) = 6.14 - 0.0024HV \quad (10)$$

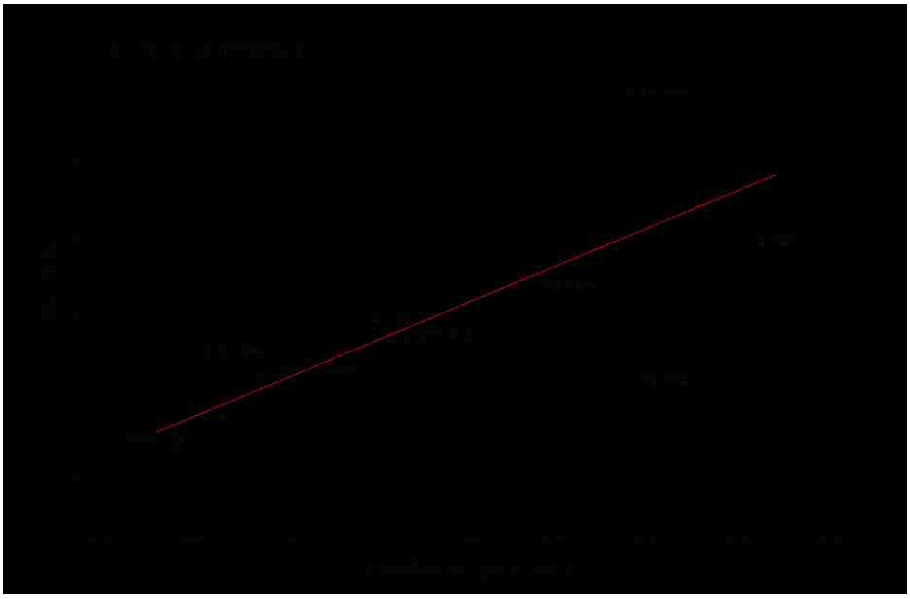

Figure 4.59: Function of wear rate against surface roughness

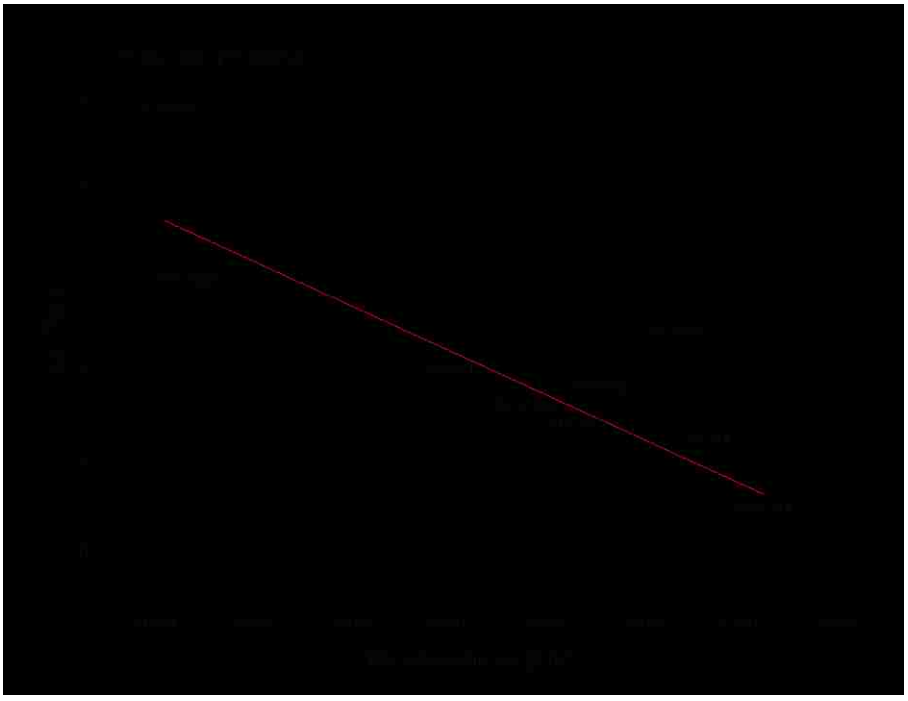

Figure 4.60: Function of wear rate against microhardness of nitrided surface

# CHAPTER V

# CONCLUSIONS

As noted in the Introduction, the primary purpose of this study was a "proof of concept" that nitriding could be used to enhance the wear resistance of cast irons and 4140 steel and to compare the effectiveness of different gas nitriding processes for cast irons and salt bath nitriding processes for 4140 steel. The wear performance was gauged using two main parameters, namely Coefficient of Friction (COF) and wear rate. The main conclusions were:

## 5.1 Cast irons

1. The COF for all cast irons in all nitrided conditions was small (<0.045), reflecting the lubricated test conditions (fully flooded or starved lubrication).

2. Small differences were seen in the variation of COF with time. A very small decrease in COF with time is interpreted as being related to polishing of the wear track. A small increase in COF with time is thought to be related to accumulation of debris in the wear track. When the COF stays essentially constant with time, it is considered that the polishing of the wear track is "balanced" by accumulation of some debris.

3. The overall wear rate is shown to be dependent on two parameters, namely the surface roughness and surface microhardness of the nitrided material. The wear rate decreased with increasing surface microhardness and decreasing surface roughness.

4. The best wear performance is shown when the wear track does not fully penetrate the compound layer. Such behaviour was seen for ADI processed using the Gray and Oil gas nitriding processes. These processes produced a compound layer thickness of 4-6μm, a low surface roughness (0.8-1.3 μm, Ra) and a high surface microhardness (1800-2200

HV) reflecting a dense and adherent compound layer. The compound layer thickness in GI was larger (up to 12μm) but it was not as hard (1000-1500 HV) and the surface roughness was higher (up to 2.5μm, Ra) and showed the greatest variability.

5.2 4140 Steel

1. The average compound layer thickness for the three nitriding processes (Isonite, QP, QPQ) were similar and varied from 8-10μm. However, the diffusion zone depth varied from 100 to 300μm with the ISONITE process having the thinnest diffusion zone (~100μm). The higher diffusion zone depths for QP and QPQ are attributed to the post salt bath nitriding processes, i.e. "-P" and "-PQ".

2. Only the ISONITE- processed steel was wear tested. The COF was similar to the cast irons (<0.045), and decreased with time indicating wear track polishing. The compound layer was almost fully worn away during wear testing. The surface microhardness of the ISONITE specimen was around 1400HV, which is softer than for cast irons. It is interesting that the QP and QPQ processes produce a surface microhardness of 2000-2200HV, which suggests that they may show improved wear behaviour compared to ISONITE- treated steels.

# CHAPTER VI

## RECOMMENDATIONS FOR FUTURE WORK

Based on this research, the following work is suggested to further understand the enhancement of wear resistance nitriding on the cast irons and steels.

1. All samples for nitriding and wear testing should be prepared with standard dimensions and surface finish. The surface finish should be polished to minimize surface roughness.

2. Wear tests should be done on the un-nitrided materials so as to gauge the improvements in wear resistance from nitriding.

3. Wear tests on 4140 steel processed using QP and QPQ methods should be carried out to confirm the postulated improvement in wear performance due to the high hardness of the nitrided case.

4. Other mechanical properties (fatigue, toughness) and corrosion resistance of the cast irons and steels treated using those nitriding processes should be studied. In many applications the component is subjected to both wear and a corrosive environment, i.e. tribocorrosion.

5. Since many automotive applications of nitrided cast irons and steels involve non-lubricated conditions, wear tests should be performed under dry conditions in order to determine the optimum nitride layer characteristics for enhanced wear resistance.

# REFERENCES

[1] Davis JR. Cast irons. Materials Park, OH: ASM International; 1996.

[2] Dhanapal P, Nazirudeen SSM. A Study of the Structure and Properties of High-Strength Bainite-Carbide Cast Iron with Globular Graphite. Metal Science and Heat Treatment. 2012;53:578-83.

[3] Martins R, Seabra J, Magalh ães L. Austempered ductile iron (ADI) gears: Power loss, pitting and micropitting. Wear. 2008;264:838-49.

[4] Sahin Y, Durak O. Abrasive wear behaviour of austempered ductile iron. Materials & Design. 2007;28:1844-50.

[5] Uma TR, Simha JB, Murthy KN. Influence of nickel on mechanical and slurry erosive wear behaviour of permanent moulded toughened austempered ductile iron. Wear. 2011;271:1378-84.

[6] Gulzar A, Akhter JI, Ahmad M, Ali G, Mahmood M, Ajmal M. Microstructure evolution during surface alloying of ductile iron and austempered ductile iron by electron beam melting. Applied Surface Science. 2009;255:8527-32.

[7] Shamanian M, Abarghouie SMRM, Pour SRM. Effects of surface alloying on microstructure and wear behavior of ductile iron. Materials & Design. 2010;31:2760-66.

[8] Arabi Jeshvaghani R, Harati E, Shamanian M. Effects of surface alloying on microstructure and wear behavior of ductile iron surface-modified with a nickel-based alloy using shielded metal arc welding. Materials & Design. 2011;32:1531-36.

[9] Nili Ahmadabadi M, Shamloo R. Control of austenitic transformation in ductile iron aided by calculation of Fe-C-Si-X phase boundaries. Journal of Phase Equilibria. 2001;22:194-98.

[10] Stefanescu DM. Solidification and modeling of cast iron—A short history of the defining moments. Materials Science and Engineering: A. 2005;413–414:322-33.

[11] Collini L, Nicoletto G, Konecna R. Microstructure and mechanical properties of pearlitic gray cast iron. Materials Science and Engineering a-Structural Materials Properties Microstructure and Processing. 2008;488:529-39.

[12] Jabbari Behnam MM, Davami P, Varahram N. Effect of cooling rate on microstructure and mechanical properties of gray cast iron. Materials Science and Engineering: A. 2010;528:583-88.

[13]http://www.globalmetals.com.au/_pdf/High_Tensile_Alloy/High_Tensile_Alloy_4140.pdf, access date: July 30. 2012.

[14] Singh R. Chapter 7 - Cast Iron. Applied Welding Engineering. Boston: Butterworth-Heinemann; 2012. p. 57-64.

[15] Prasad BK. Sliding wear response of a grey cast iron: Effects of some experimental parameters. Tribology International. 2011;44:660-67.

[16] Holmgren D, Diószegi A, Svensson IL. Effects of Carbon Content and Solidification Rate on the Thermal Conductivity of Grey Cast Iron. Tsinghua Science & Technology. 2008;13:170-76.

[17] Pouranvari M. On the weldability of grey cast iron using nickel based filler metal. Materials & Design. 2010;31:3253-58.

[18] Celis MM, Valle N, Lacaze J, Thorbjornsson IO, Johannesson B, Thorgrimsson JT. Microstructure of as cast reinforced ductile iron. International Journal of Cast Metals Research. 2011;24:76-82.

[19] Fatahalla N, Abuelezz A, Semeida M. C, Si and Ni as alloying elements to vary carbon equivalent of austenitic ductile cast iron: Microstructure and mechanical properties. Materials Science and Engineering a-Structural Materials Properties Microstructure and Processing. 2009;504:81-89.

[20] Peng YC, Jin HJ, Liu JH, Li GL. Effect of boron on the microstructure and mechanical properties of carbidic austempered ductile iron. Materials Science and Engineering a-Structural Materials Properties Microstructure and Processing. 2011;529:321-25.

[21] Imasogie BI, Afonja AA, Ali JA. Properties of ductile cast iron nodularised with multiple calcium-magnesium based master alloy. Materials Science and Technology. 2000;16:194-201.

[22] Hernandez-Rivera JL, Cambranis REC, de la Garza A. Study of microstructural evolution and mechanical properties exhibited by non alloyed ductile iron during conventional and stepped austempering heat treatment. Materials & Design. 2011;32:4756-62.

[23] http://www.ductile.org/didata/Section2/figures/pfig2_8.htm, access date: July 30. 2012.

[24] Benyounis KY, Fakron OMA, Abboud JH, Olabi AG, Hashmi MJS. Surface melting of nodular cast iron by Nd-YAG laser and TIG. Journal of Materials Processing Technology. 2005;170:127-32.

[25] Kiani-Rashid AR, Edmonds DV. Microstructural characteristics of Al-alloyed austempered ductile irons. Journal of Alloys and Compounds. 2009;477:391-98.

[26] Konecna R, Bubenko L, Nicoletto G. Microstructure vs. Near-threshold Fatigue Crack Growth Behavior of an Heat-treated Ductile Iron. Materials Science-Medziagotyra. 2012;18:23-27.

[27] Kiani-Rashid AR. The bainite transformation and the carbide precipitation of 4.88% aluminium austempered ductile iron investigated using electron microscopy. Journal of Alloys and Compounds. 2009;474:490-98.

[28] Cheng TW, Lui TS, Chen LH. Microstructural Features and Erosion Wear Resistance of Friction Stir Surface Hardened Spheroidal Graphite Cast Iron. Materials Transactions. 2012;53:167-72.

[29] Abedi A, Marashi SPH, Sohrabi K, Marvastian M, Mirbagheri SMH. The Effect of Heat Treatment Parameters on Microstructure and Toughness of Austempered Ductile Iron (Adi). Advances in Materials and Processing Technologies Ii, Pts 1 and 2. 2011;264-265:409-14.

[30] Hsu C-H, Lin K-T. A study on microstructure and toughness of copper alloyed and austempered ductile irons. Materials Science and Engineering: A. 2011;528:5706-12.

[31] Kilicli V, Erdogan M. The Nature of the Tensile Fracture in Austempered Ductile Iron with Dual Matrix Microstructure. Journal of Materials Engineering and Performance. 2010;19:142-49.

[32] Eric O, Rajnovic D, Zec S, Sidjanin L, Jovanovic MT. Microstructure and fracture of alloyed austempered ductile iron. Materials Characterization. 2006;57:211-17.

[33] Eric O, Sidjanin L, Miskovic Z, Zec S, Jovanovic MT. Microstructure and toughness of CuNiMo austempered ductile iron. Materials Letters. 2004;58:2707-11.

[34] Putatunda SK, Singar AV, Tackett R, Lawes G. Development of a high strength high toughness ausferritic steel. Materials Science and Engineering a-Structural Materials Properties Microstructure and Processing. 2009;513-14:329-39.

[35] Sahin Y, Kilicli V, Ozer M, Erdogan M. Comparison of abrasive wear behavior of ductile iron with different dual matrix structures. Wear. 2010;268:153-65.

[36] Liu JH, Li GL, Zhao XB, Hao XY, Zhang JJ. Effect of Austempering Temperature on Microstructure and Properties of Carbidic Austempered Ductile Iron. Materials and Design, Pts 1-3. 2011;284-286:1085-88.

[37] Holzapfel H, Schulze V, Vohringer O, Macherauch E. Residual stress relaxation in an AISI 4140 steel due to quasistatic and cyclic loading at higher temperatures. Materials Science and Engineering a-Structural Materials Properties Microstructure and Processing. 1998;248:9-18.

[38] Chuang JH, Tsay LW, Chen C. Crack growth behaviour of heat-treated 4140 steel in air and gaseous hydrogen. International Journal of Fatigue. 1998;20:531-36.

[39] Meysami AH, Ghasemzadeh R, Seyedein SH, Aboutalebi MR. An investigation on the microstructure and mechanical properties of direct-quenched and tempered AISI 4140 steel. Materials & Design. 2010;31:1570-75.

[40] Starke P, Walther F, Eifler D. New fatigue life calculation method for quenched and tempered steel SAE 4140. Materials Science and Engineering a-Structural Materials Properties Microstructure and Processing. 2009;523:246-52.

[41] Xie KY, Breen AJ, Yao L, Moody MP, Gault B, Cairney JM, Ringer SP. Overcoming challenges in the study of nitrided microalloyed steels using atom probe. Ultramicroscopy. 2012;112:32-38.

[42] DST-Technologies. http://dsttechnologies.net/applications/applications-of-nitriding, Access date: July 20; 2012.

[43] Podgornik B, Vizintin J, Wanstrand O, Larsson M, Hogmark S, Ronkainen H, Holmberg K. Tribological properties of plasma nitrided and hard coated AISI 4140 steel. Wear. 2001;249:254-59.

[44] Abisset S, Maury F, Feurer R, Ducarroir M, Nadal M, Andrieux M. Gas and plasma nitriding pretreatments of steel substrates before CVD growth of hard refractory coatings. Thin Solid Films. 1998;315:179-85.

[45] Pye D. Practical Nitriding and Ferritic Nitrocarburizing: ASM International; 2003.

[46] Gerasimov SA, Golikov VA, Gress MA, Mukhin GG, Snop VI. High-pressure gas nitriding of steels. Metal Science and Heat Treatment. 2004;46:227-29.

[47] Lee DB, Kim MJ, Chen L, Bak SH, Yaskiv O, Pohrelyuk I, Fedirko V. Oxidation of nitride layers formed on Ti-6Al-4V alloys by gas nitriding. Metals and Materials International. 2011;17:471-77.

[48] Lee DB, Pohrelyuk I, Yaskiv O, Lee JC. Gas nitriding and subsequent oxidation of Ti-6Al-4V alloys. Nanoscale Research Letters. 2012;7:1-5.

[49] Januszewicz B, Klimek L. Nitriding of titanium and Ti6Al4V alloy in ammonia gas under low pressure. Materials Science and Technology. 2010;26:586-90.

[50] Lee S, Kim W, Suh CY, Cho SW, Ryu T, Park JS, Shon IJ. Preparation of Titanium-Chromium Nitride by Gas Nitriding of the Explosion Products of Cr-Coated Ti Wire. Materials Transactions. 2011;52:261-64.

[51] Spies HJ, Reinhold B, Wilsdorf K. Gas nitriding - Process control and nitriding non-ferrous alloys. Surface Engineering. 2001;17:41-54.

[52] Khan KK, Mehmood M, ul Hassan M, Ahmad J, Iqbal Z, Muddasser T. Gas Nitriding of Electrodeposited Ni-W Alloys. Metal Science and Heat Treatment. 2011;53:87-90.

[53] Zinchenko VM, Syropyatov VY. New possibilities of gas nitriding as a method for anticorrosion treatment of machine parts. Metal Science and Heat Treatment. 1998;40:261-65.

[54] Piccilli MR, Balestrassi PP, Paiva AP, Ferreira JR, Garcia-Diaz A. Crack avoidance in steel piston rings through the optimization of process and gas nitriding parameters. International Journal of Advanced Manufacturing Technology. 2011;56:397-409.

[55] Arif AFM, Akhtar SS, Yilbas BS. Effect of process variables on gas nitriding of H13 tool steel with controlled nitriding potential. International Journal of Surface Science and Engineering. 2010;4:396-415.

[56] Rida M, Tout H. Simultaneous numerical simulation of gas phase nitriding (NH3-H-2) and of the nitrogen transfer in alpha-iron (550 degrees C and 1 atm) (Part I). Revue De Metallurgie-Cahiers D Informations Techniques. 2010;107:117-24.

[57] Garzon CM, Tschiptschin AP. New high temperature gas nitriding cycle that enhances the wear resistance of duplex stainless steels. Journal of Materials Science. 2004;39:7101-05.

[58] Vershinin DS, Smolyakova MY. Study of gas-mixture composition influence on structure and properties of titanium alloy VT6 at low-temperature nitriding. Journal of Surface Investigation-X-Ray Synchrotron and Neutron Techniques. 2012;6:159-64.

[59] Hussain K, Tauqir A, ul Haq A, Khan AQ. Effect of retained austenite on gas nitriding of high strength steel. Materials Science and Technology. 1998;14:1218-20.

[60] Fare S, Lecis N, Brescia E, Mazzola N. Role of Grain Boundaries in diffusional Phenomena during Gas Nitriding of Pure Iron. 11th International Conference on the Mechanical Behavior of Materials (Icm11). 2011;10.

[61] Yilbas B, Arif AFM, Karatas C, Aleem BJA, Tabet N. Laser gas-assisted nitriding of steel residual stress analysis. Industrial Lubrication and Tribology. 2010;62:214-23.

[62] Ratajski J, Olik R, Suszko T, Dobrodziej J, Michalski J. Design, Control and in Situ Visualization of Gas Nitriding Processes. Sensors. 2010;10:218-40.

[63] Limodin N, Verreman Y. Fatigue strength improvement of a 4140 steel by gas nitriding: Influence of notch severity. Materials Science and Engineering a-Structural Materials Properties Microstructure and Processing. 2006;435:460-67.

[64] Roy A, Kumar KS, Raghunath A, Sharma RC, Shekhar R. Feasibility and kinetics of nitriding of pure titanium and Ti-6Al-4V in molten salt bath of potassium nitrate. Surface Engineering. 2012;28:458-63.

[65] Shen YZ, Oh KH, Lee DN. Nitriding of steel in potassium nitrate salt bath. Scripta Materialia. 2005;53:1345-49.

[66] Wang J, Lin YH, Yan J, Zen DZ, Zhang Q, Huang RB, Fan HY. Influence of time on the microstructure of AISI 321 austenitic stainless steel in salt bath nitriding. Surface & Coatings Technology. 2012;206:3399-404.

[67] Funatani K. Low-temperature salt bath nitriding of steels. Metal Science and Heat Treatment. 2004;46:277-81.

[68] Li GJ, Peng Q, Wang J, Li C, Wang Y, Gao J, Chen SY, Shen BL. Surface microstructure of 316L austenitic stainless steel by the salt bath nitrocarburizing and post-oxidation process known as QPQ. Surface & Coatings Technology. 2008;202:2865-70.

[69] Li HY, Luo DF, Yeung CF, Lau KH. Microstructural studies of QPQ complex salt bath heat-treated steels. Journal of Materials Processing Technology. 1997;69:45-49.

[70] Yu YX, He BL, Shi JP. The effect of QPQ salt-bath nitriding on microstructure and wear resistance of 4Cr5MoSiV1 steel. Materials Processing Technologies, Pts 1 and 2. 2011;154-155:57-60.

[71] Li GJ, Peng Q, Li C, Wang Y, Gao J, Chen SY, Wang J, Shen BL. Microstructure analysis of 304L austenitic stainless steel by QPQ complex salt bath treatment. Materials Characterization. 2008;59:1359-63.

[72] Taylor E. Qpq - Salt Treatment That Prevents Corrosion. Metal Progress. 1983;124:21-25.

[73] Wahl G, Etchells IV. Qpq - Surface Heat-Treatment for Corrosion-Resistance. Heat Treatment of Metals. 1984;11:64-64.

[74] Yeung CF, Lau KH, Li HY, Luo DF. Advanced QPQ complex salt bath heat treatment. Journal of Materials Processing Technology. 1997;66:249-52.

[75] Li YH, Luo DF, Wu SX. Effect of QPQ salt bath oxidation on corrosion resistance. Heat Treatment of Materials. 2006;118:209-14.

[76] Luo DF, Li S. Effect of cryogenic and QPQ compound treatment on the microstructures and performance of high speed steel. Chinese Journal of Mechanical Engineering. 2012;25:184-89.

[77] Soleimani SMY, Mashreghi AR, Ghasemi SS, Moshrefifar M. The effect of plasma nitriding on the fatigue behavior of DIN 1.2210 cold work tool steel. Materials & Design. 2012;35:87-92.

[78] Hosseini SR, Ashrafizadeh F. Accurate measurement and evaluation of the nitrogen depth profile in plasma nitrided iron. Vacuum. 2009;83:1174-78.

[79] Mirjani M, Mazrooei J, Karimzadeh N, Ashrafizadeh F. Investigation of the effects of time and temperature of oxidation on corrosion behavior of plasma nitrided AISI 4140 steel. Surface & Coatings Technology. 2012;206:4389-93.

[80] Li Y, Wang L, Xu J, Zhang D. Plasma nitriding of AISI 316L austenitic stainless steels at anodic potential. Surface & Coatings Technology. 2012;206:2430-37.

[81] Ichiki R, Nagamatsu H, Yasumatsu Y, Iwao T, Akamine S, Kanazawa S. Nitriding of steel surface by spraying pulsed-arc plasma jet under atmospheric pressure. Materials Letters. 2012;71:134-36.

[82] Koval NN, Schanin PM, Akhmadeev YK, Lopatin IV, Kolobov YR, Vershinin DS, Smolyakova MY. Influence of the composition of a plasma-forming gas on nitriding in a non-self-maintained glow discharge with a large hollow cathode. Journal of Surface Investigation-X-Ray Synchrotron and Neutron Techniques. 2012;6:154-58.

[83] Wang QL, Huang CH, Zhang L. Microstructure and Tribological Properties of Plasma Nitriding Cast CoCrMo Alloy. Journal of Materials Science & Technology. 2012;28:60-66.

[84] Halling J. Principles of tribology. London: Macmillan; 1975.

[85] Gohar R, Rahnejat H. Fundamentals of tribology. London: Imperial College Press; 2008.

[86] Bhushan B, Israelachvili JN, Landman U. Nanotribology - Friction, Wear and Lubrication at the Atomic-Scale. Nature. 1995;374:607-16.

[87] Stachowiak GW, Batchelor AW. Engineering tribology. 3rd ed. Amsterdam ; Boston: Elsevier Butterworth-Heinemann; 2005.

[88] Yin X, Komvopoulos K. A slip-line plasticity analysis of abrasive wear of a smooth and soft surface sliding against a rough (fractal) and hard surface. International Journal of Solids and Structures. 2012;49:121-31.

[89] Khonsari MM, Booser ER. Applied tribology : bearing design and lubrication. 2nd ed. Chichester, England ; Hoboken, NJ: Wiley; 2008.

[90] Shrestha SB. http://www.ku.edu.np/mech/Tutorials/Lubrication.pdf Accessed on 20 July.: Kathmandu University; 2012.

[91] Colangelo VJ, Heiser FA. Analysis of metallurgical failures. 2nd ed. New York: Wiley; 1987.

[92] Bucholz EW, Zhao XY, Sinnott SB, Perry SS. Friction and Wear of Pyrophyllite on the Atomic Scale. Tribology Letters. 2012;46:159-65.

[93] Karlsson P, Gaard A, Krakhmalev P, Bergstrom J. Galling resistance and wear mechanisms for cold-work tool steels in lubricated sliding against high strength stainless steel sheets. Wear. 2012;286:92-97.

[94] Koval' AD, Efremenko VG, Brykov MN, Andrushchenko MI, Kulikovskii RA, Efremenko AV. Principles for developing grinding media with increased wear resistance. Part 1. Abrasive wear resistance of iron-based alloys. Journal of Friction and Wear. 2012;33:39-46.

[95] Reizer R, Pawlus P, Galda L, Grabon W, Dzierwa A. Modeling of worn surface topography formed in a low wear process. Wear. 2012;278–279:94-100.

[96] Mahzoon F, Behgozin SA, Bahrololoom ME, Javadpour S. Study the Fatigue-Wear Behavior of a Plasma Electrolytic Nitrocarburized (PEN/C) 316L Stainless Steel. Journal of Materials Engineering and Performance. 2012;21:1751-56.

[97] Goryacheva IG, Torskaya EV. Modeling of fatigue wear of a two-layered elastic half-space in contact with periodic system of indenters. Wear. 2010;268:1417-22.

[98] Ding HY, Dai ZD, Zhang Y, Zhou GH. Corrosive Fretting Wear Behavior of a Titanium Alloy TC11 in Artificial Seawater. Advanced Tribology. 2009:322-26.

[99] Kanchanomai C, Saengwichian B, Manonukul A. Delamination wear of metal injection moulded 316L stainless steel. Wear. 2009;267:1665-72.

[100] Qin F, Hu J, Chou YK, Thompson RG. Delamination wear of nano-diamond coated cutting tools in composite machining. Wear. 2009;267:991-95.

[101] Zhao YT, Wang SQ, Yang ZR, Wei MX. A new delamination pattern in elevated-temperature oxidative wear. Journal of Materials Science. 2010;45:227-32.

[102] Micele L, Palombarini G, Guicciardi S, Silvestroni L. Tribological behaviour and wear resistance of a SiC-MoSi2 composite dry sliding against Al2O3. Wear. 2010;269:368-75.

[103] Gou LQ, Shi XL, Zhao XM, Bai Y, Qiao LJ. Composite diamond-DLC coated nanoprobe tips for wear resistance and adhesion reduction. Surface & Coatings Technology. 2012;206:4099-105.

[104] Barrau O, Boher C, Gras R, Rezai-Aria E. Analysis of the friction and wear behaviour of hot work tool steel for forging. Wear. 2003;255:1444-54.

[105] Shi W, Dong H, Bell T. Tribological behaviour and microscopic wear mechanisms of UHMWPE sliding against thermal oxidation-treated Ti6Al4V. Materials Science and Engineering a-Structural Materials Properties Microstructure and Processing. 2000;291:27-36.

[106] Dubrujeaud B, Vardavoulias M, Jeandin M. The Role of Porosity in the Dry Sliding Wear of a Sintered Ferrous Alloy. Wear. 1994;174:155-61.

[107] Corral IB, Calvet JV, Salcedo MC. Use of roughness probability parameters to quantify the material removed in plateau-honing. International Journal of Machine Tools & Manufacture. 2010;50:621-29.

[108] Tochil'nikov DG, Kupchin AN, Shepelevskii AA, Shiyan PA, Ginzburg BM, Ponimatkin VP. Effect of wear debris on antifriction and antiwear properties of industrial oils I-20A and I-40A in friction of steel surfaces. Journal of Friction and Wear. 2011;32:221-26.

[109] Nie X, Wang L, Yao ZC, Zhang L, Cheng F. Sliding wear behaviour of electrolytic plasma nitrided cast iron and steel. Surface & Coatings Technology. 2005;200:1745-50.

[110] Riahi AR, Alpas AT. Wear map for grey cast iron. Wear. 2003;255:401-09.

[111] Xie JP, Wang AQ, Wang WY, Li LL. Study on Erosion Wear Property of Nickel-Chromium Cast Iron. Materials and Computational Mechanics, Pts 1-3. 2012;117-119:1084-87.

[112] Wei MX, Wang SQ, Cui XH. Comparative research on wear characteristics of spheroidal graphite cast iron and carbon steel. Wear. 2012;274:84-93.

[113] Wesley SB, Goyal HS, Harsha AP. Investigation on three-body abrasive wear of ferritic steels, austenitic steel, and low-carbon steel. Proceedings of the Institution of Mechanical Engineers Part J-Journal of Engineering Tribology. 2012;226:163-73.

[114] Podgornik B, Vizintin J, Thorbjornsson I, Johannesson B, Thorgrimsson JT, Celis MM, Valle N. Improvement of ductile iron wear resistance through local surface reinforcement. Wear. 2012;274:267-73.

[115] Sarjas H, Goljandin D, Kulu P, Mikli V, Surzenkov A, Vuoristo P. Wear Resistant Thermal Sprayed Composite Coatings Based on Iron Self-Fluxing Alloy and Recycled Cermet Powders. Materials Science-Medziagotyra. 2012;18:34-39.

[116] Tillmann W, Luo W, Tekkaya AE, Franzen V. Wear analysis of rolled and ground iron-based-alloy-coatings with and without hard material reinforcement. Materialwissenschaft Und Werkstofftechnik. 2012;43:485-94.

[117] Maranho O, Rodrigues D, Boccalini M, Sinatora A. Mass loss and wear mechanisms of HVOF-sprayed multi-component white cast iron coatings. Wear. 2012;274:162-67.

[118] Prince M, Thanu AJ, Gopalakrishnan P. Improvement in wear and corrosion resistance of AISI 1020 steel by high velocity oxy-fuel spray coating containing Ni-Cr-B-Si-Fe-C. High Temperature Materials and Processes. 2012;31:149-55.

[119] Pang GX, Li ZL, Chen ZY, Wang YJ. Electron Brush-plating Technique of Cr12MoV Die Steel and Its Wear Resistance. Rare Metal Materials and Engineering. 2012;41:180-82.

[120] Lu LH, Zhang JW, Shen DJ, Wu LL, Jiang GR, Li L. TEM analysis and wear resistance of the ceramic coatings on Q235 steel prepared by hybrid method of hot-dipping aluminum and plasma electrolytic oxidation. Journal of Alloys and Compounds. 2012;512:57-62.

[121] Siva RS, Jaswin MA, Lal DM. Enhancing the Wear Resistance of 100Cr6 Bearing Steel Using Cryogenic Treatment. Tribology Transactions. 2012;55:387-93.

[122] Akhbarizadeh A, Amini K, Javadpour S. Effects of applying an external magnetic field during the deep cryogenic heat treatment on the corrosion resistance and wear behavior of 1.2080 tool steel. Materials & Design. 2012;41:114-23.

[123] Fernandes FAP, Heck SC, Picon CA, Totten GE, Casteletti LC. Wear and corrosion resistance of pack chromised carbon steel. Surface Engineering. 2012;28:313-17.

[124] Chang SH, Huang KT, Wang YH. Effects of Thermal Erosion and Wear Resistance on AISI H13 Tool Steel by Various Surface Treatments. Materials Transactions. 2012;53:745-51.

[125] Calik A, Karakas S, Ucar N. Wear Behaviour of Boronised and Induction Hardened Spheroidal Graphite Cast Iron. Journal of the Balkan Tribological Association. 2012;18:44-50.

[126] Gurevich YG. Wear-Resistant Coatings of White Cast Iron on Powder Steels. Powder Metallurgy and Metal Ceramics. 2012;50:619-24.

[127] Wang AQ, Xie JP, Wang WY, Li JW. Study on the Microstructures and Wear Resistance of ZG30 Steel Surface Layer. Materials and Computational Mechanics, Pts 1-3. 2012;117-119:1271-75.

[128] Fan XS, Yang ZG, Zhang C. High Temperature Oxidation and Wear Resistance of Y-modified Hot Dipping Aluminized Coating on SCH12 Steel. Rare Metal Materials and Engineering. 2012;41:231-35.

[129] Quaeyhaegens C, Kerkhofs M, Stals LM, VanStappen M. Promising developments for new applications. Surface & Coatings Technology. 1996;80:181-84.

[130] Navinsek B, Panjan P, Milosev I. Industrial applications of CrN (PVD) coatings, deposited at high and low temperatures. Surface & Coatings Technology. 1997;97:182-91.

[131] Aouadi S. Characterization of titanium chromium nitride nanocomposite protective coatings. Applied Surface Science. 2004;229:387-94.

[132] Warcholinski B, Gilewicz a, Kuklinski Z, Myslinski P. Hard CrCN/CrN multilayer coatings for tribological applications. Surface and Coatings Technology. 2010;204:2289-93.

[133] Wiecinski P, Smolik J, Garbacz H, Kurzydlowski KJ. Microstructure and mechanical properties of nanostructure multilayer CrN/Cr coatings on titanium alloy. Thin Solid Films. 2011;519:4069-73.

[134] Lin J, Sproul WD, Moore JJ, Lee S, Myers S. High rate deposition of thick CrN and Cr2N coatings using modulated pulse power (MPP) magnetron sputtering. Surface and Coatings Technology. 2011;205:3226-34.

[135] Khamseh S, Nose M, Kawabata T, Matsuda K, Ikeno S. Influence of total gas pressure on the microstructure and properties of CrAlN films deposited by a pulsed DC balanced magnetron sputtering system. Journal of Alloys and Compounds. 2010;503:389-91.

[136] Chim YC, Ding XZ, Zeng XT, Zhang S. Oxidation resistance of TiN, CrN, TiAlN and CrAlN coatings deposited by lateral rotating cathode arc. Thin Solid Films. 2009;517:4845-49.

[137] Pulugurtha SR, Bhat DG, Gordon MH, Shultz J, Staia M, Joshi SV, Govindarajan S. Mechanical and tribological properties of compositionally graded CrAlN films deposited by AC reactive magnetron sputtering. Surface & Coatings Technology. 2007;202:1160-66.

[138] Tlili B, Mustapha N, Nouveau C, Benlatreche Y, Guillemot G, Lambertin M. Correlation between thermal properties and aluminum fractions in CrAlN layers deposited by PVD technique. Vacuum. 2010;84:1067-74.

[139] Tong X, Li FH, Kuang M, Ma WY, Chen XC, Liu M. Effects of WC particle size on the wear resistance of laser surface alloyed medium carbon steel. Applied Surface Science. 2012;258:3214-20.

[140] Singh K, Krishnamurthy N, Suri AK. Adhesion and wear studies of magnetron sputtered NbN films. Tribology International. 2012;50:16-25.

[141] Parthasarathi NL, Duraiselvam M, Borah U. Effect of plasma spraying parameter on wear resistance of NiCrBSiCFe plasma coatings on austenitic stainless steel at elevated temperatures at various loads. Materials & Design. 2012;36:141-51.

[142] Liyanage T, Fisher G, Gerlich AP. Microstructures and abrasive wear performance of PTAW deposited Ni-WC overlays using different Ni-alloy chemistries. Wear. 2012;274:345-54.

[143] Yang J, Wang TS, Zhang B, Zhang FC. Sliding wear resistance and worn surface microstructure of nanostructured bainitic steel. Wear. 2012;282:81-84.

[144] Abedi HR, Fareghi A, Saghafian H, Kheirandish SH. Sliding wear behavior of a ferritic-pearlitic ductile cast iron with different nodule count. Wear. 2010;268:622-28.

[145] Khorsand H, Habibi M, Ashtari M, Yoozbashizadeh H. The role of heat treatment on wear behavior of powder metallurgy low alloy steels. Powder Metallurgy in Automotive Applications-Ii. 2002:197-201.

[146] Koszela W, Dzierwa A, Galda L, Pawlus P. Experimental investigation of oil pockets effect on abrasive wear resistance. Tribology International. 2012;46:145-53.

[147] Zhong LS, Xu YH, Ye FX. In Situ NbC Particulate-Reinforced Iron Matrix Composite: Microstructure and Abrasive Wear Characteristics. Tribology Letters. 2012;47:253-59.

[148] ASTM. G190-06 Standard Guide for Developing and Selecting Wear Tests. 2007.

[149] ASTM. G133-05(2010) Standard Test Method for Linearly Reciprocating Ball-on-Flat Sliding Wear. 2010.

[150] http://www.mcmaster.com/#ceramic-balls/=jovcqe, access date: Oct. 10. 2012.

[151] ASTM. E768-99(2010) Standard Guide for Preparing and Evaluating Specimens for Automatic Inclusion Assessment of Steel. 2010.

[152] ASTM. E384-11e1 Standard Test Method for Knoop and Vickers Hardness of Materials. 2012.

[153] ASTM. B946-11 Standard Test Method for Surface Finish of Powder Metallurgy (P/M) Products. 2011.

[154] ASTM. A247-10 Standard Test Method for Evaluating the Microstructure of Graphite in Iron Castings. 2010.

[155] ASTM. E1245-03(2008) Standard Practice for Determining the Inclusion or Second-Phase Constituent Content of Metals by Automatic Image Analysis. 2008.

# APPENDICES

Table A: CL thickness of DI, ADI and GI treated using the gas nitriding processes

| Material | Nitriding Process | CL thickness (μm) |
|---|---|---|
| DI | Blue | 4.59 ±1.59 |
| | Gray | 3.52 ±0.68 |
| | Oil | 2.53 ±0.34 |
| ADI | Blue | 2.16 ±0.52 |
| | Gray | 6.70 ±2.36 |
| | Oil | 4.81 ±3.61 |
| GI | Blue | 8.01 ±4.19 |
| | Gray | 12.70 ±4.38 |
| | Oil | 2.43 ±1.00 |

Table B: DZ depth of DI, ADI and GI treated using the gas nitriding processes

| Material | Nitriding Process | CL thickness (μm) |
|---|---|---|
| DI | Blue | 52.83 ±8.99 |
| | Gray | 84.27 ±40.83 |
| | Oil | 104.24 ±21.52 |
| ADI | Blue | 49.29 ±6.61 |
| | Gray | 119.77 ±16.01 |
| | Oil | 31.32 ±6.82 |
| GI | Blue | 69.30 ±26.17 |
| | Gray | 133.08 ±10.64 |
| | Oil | 145.83 ±49.03 |

# VITA AUCTORIS

NAME Zaidao Yang

DATE OF BIRTH 1986

PLACE OF BIRTH Henan, China

EDUCATION First High School of Yanjin

Henan, China

2006

Bachelor of Materials Science and Engineering

Changchun University of Technology

Changchun, China

2006-2010

Masters of Applied Science

Engineering Materials

University of Windsor

Windsor, ON, Canada

2010-2012